US Army Corps
of Engineers
Construction Engineering
Research Laboratory

USACERL Technical Report M-91/11
December 1990
Electromagnetic Pulse (EMP) Validation and
Design Recommendations for C^3I Facilities

A Study of the Parallel-Plate EMP Simulator and the Simulator-Obstacle Interaction

by
Stephen D. Gedney

The Parallel-Plate Bounded-Wave EMP Simulator is typically used to test the vulnerability of electronic systems to the electromagnetic pulse (EMP) produced by a high altitude nuclear burst by subjecting the systems to a simulated EMP environment. However, when large test objects are placed within the simulator for investigation, the desired EMP environment may be affected by the interaction between the simulator and the test object. This "simulator/obstacle" interaction can be attributed to the following phenomena: (1) mutual coupling between the test object and the simulator, (2) fringing effects due to the finite width of the conducting plates of the simulator, and (3) multiple reflections between the object and the simulator's tapered end-sections. When the interaction is significant, the measurement of currents coupled into the system may not accurately represent those induced by an actual EMP.

To better understand the problem of simulator/obstacle interaction, a dynamic analysis of the fields within the parallel-plate simulator is presented. The fields are computed using a moment method solution based on a wire mesh approximation of the conducting surfaces of the simulator. The fields within an empty simulator are found to be predominately transverse electromagnetic (TEM) for frequencies within the simulator's bandwidth, properly simulating the properties of the EMP propagating in free space. However, when a large test object is placed within the simulator, it is found that the currents induced on the object can be quite different from those on an object situated in free space. A comprehensive study of the mechanisms contributing to this deviation is presented.

The contents of this report are not to be used for advertising, publication, or promotional purposes. Citation of trade names does not constitute an official indorsement or approval of the use of such commercial products. The findings of this report are not to be construed as an official Department of the Army position, unless so designated by other authorized documents.

DESTROY THIS REPORT WHEN IT IS NO LONGER NEEDED

DO NOT RETURN IT TO THE ORIGINATOR

CONTENTS

FIGURES

REPORT DOCUMENTATION PAGE

Form Approved
OMB No. 0704-0188

1. AGENCY USE ONLY (Leave Blank)	2. REPORT DATE	3. REPORT TYPE AND DATES COVERED
	December 1990	Final

4. TITLE AND SUBTITLE
A Study of the Parallel-Plate EMP Simulator and the Simulator-Obstacle Interaction

5. FUNDING NUMBERS
PE 4A162734
PR AT41
TA C59
WU MA

6. AUTHOR(S)
Stephen D. Gedney

7. PERFORMING ORGANIZATION NAME(S) AND ADDRESS(ES)
U.S. Army Construction Engineering Research Laboratory (USACERL)
2902 Newmark Drive, PO Box 4005
Champaign, IL 61824-4005

8. PERFORMING ORGANIZATION REPORT NUMBER
TR M-91/11

9. SPONSORING/MONITORING AGENCY NAME(S) AND ADDRESS(ES)
HQUSACE
ATTN: CEMP-EE
20 Massachusetts Avenue, NW.
Washington, DC 20314-1000

10. SPONSORING/MONITORING AGENCY REPORT NUMBER

11. SUPPLEMENTARY NOTES
Copies are available from the National Technical Information Service, 5285 Port Royal Road, Springfield, VA 22161

12a. DISTRIBUTION/AVAILABILITY STATEMENT
Approved for public release; distribution is unlimited.

12b. DISTRIBUTION CODE

13. ABSTRACT (Maximum 200 words)

The Parallel-Plate Bounded-Wave EMP Simulator is typically used to test the vulnerability of electronic systems to the electromagnetic pulse (EMP) produced by a high altitude nuclear burst by subjecting the systems to a simulated EMP environment. However, when large test objects are placed within the simulator for investigation, the desired EMP environment may be affected by the interaction between the simulator and the test object. This "simulator/obstacle" interaction can be attributed to the following phenomena: (1) mutual coupling between the test object and the simulator, (2) fringing effects due to the finite width of the conducting plates of the simulator, and (3) multiple reflections between the object and the simulator's tapered end-sections. When the interaction is significant, the measurement of currents coupled into the system may not accurately represent those induced by an actual EMP.

To better understand the problem of simulator/obstacle interaction, a dynamic analysis of the fields within the parallel-plate simulator is presented. The fields are computed using a moment method solution based on a wire mesh approximation of the conducting surfaces of the simulator. The fields within an empty simulator are found to be predominately transverse electromagnetic (TEM) for frequencies within the simulator's bandwidth, properly simulating the properties of the EMP propagating in free space. However, when a large test object is placed within the simulator, it is found that the currents induced on the object can be quite different from those on an object situated in free space. A comprehensive study of the mechanisms contributing to this deviation is presented.

14. SUBJECT TERMS
Parallel-plate
vulnerability
EMP simulator
electromagnetic pulses

15. NUMBER OF PAGES
110

16. PRICE CODE

17. SECURITY CLASSIFICATION OF REPORT	18. SECURITY CLASSIFICATION OF THIS PAGE	19. SECURITY CLASSIFICATION OF ABSTRACT	20. LIMITATION OF ABSTRACT
Unclassified	Unclassified	Unclassified	SAR

FOREWORD

This study was performed for the Directorate of Military Programs (CEMP), Headquarters, U.S. Army Corps of Engineers (HQUSACE), under Project 4A162734AT41, "Military Facilities Engineering Technology," Work Unit MA, Task C59, "Electromagnetic Pulse (EMP) Validation and Design Recommendations for C^3I Facilities." The technical monitor was Mr. Leslie Horvath, CEMP-EE.

This research was performed for the U.S. Army Construction Engineering Research Laboratory (USACERL), Engineering and Materials Division (EM) under Contract No. DACA88-88-M-0663 by Mr. Stephen G. Gedney, of the University of Illinois at Urbana. Mr. Ray G. McCormack was the principal investigator. Dr. Paul A. Howdyshell is Acting Chief of USACERL-EM. The USACERL technical editor was Mr. William J. Wolfe, Information Management Office.

COL Everett R. Thomas is Commander and Director of USACERL, and Dr. L.R. Shaffer is Technical Director.

FIGURES (Cont'd)

FIGURES (Cont'd)

FIGURES (Cont'd)

FIGURES (Cont'd)

TABLES

A STUDY OF THE PARALLEL-PLATE EMP SIMULATOR AND THE SIMULATOR-OBSTACLE INTERACTION

1 INTRODUCTION

Background

The Electromagnetic Pulse (EMP) produced by a high altitude nuclear burst can couple large transient currents into electronic systems, burning out sensitive electronic circuitry or equipment. Of great significance is the potentially affected range of severe EMP exposure. A nuclear burst at an altitude of 50 to 120 miles, centered over the United States, would expose the entire continental United States to EMP,[1] exposing both military and civilian electronic systems to an EMP threat.

EMP "hardening" is the shielding or protection of a system from EMP. The methods used for hardening are dependent upon the system and its environment and are the topic of much research. Hardening of a system is not limited to the initial development, but must also be maintained over time. For example, a conducting gasket used to seal a door may degrade over time without detection, causing sensitive equipment thought to have been shielded to become vulnerable to EMP exposure. Unfortunately, most systems of interest, such as an airplane, satellite, or a ground-based shelter, are much too complex to study analytically, or even numerically. Therefore, EMP hardening evaluation must be performed experimentally. EMP simulators have been developed to produce the threat level environment of the EMP to provide experimental evaluation of the system hardening, and to monitor its deterioration over time.

Objectives

The objectives of this study were: (1) to analyze a parallel-plate bounded-wave EMP simulator, (2) to analyze and model the simulator-obstacle interaction, and (3) to determine effects of simulator/obstacle interaction on the currents induced on objects placed within the simulator.

Approach

A literature search into the physical and theoretical interpretations of the parallel-plate bounded-wave EMP simulator was performed. A dynamic field solution was derived to study the field distribution within the parallel-plate region of the finite-length EMP simulator. A moment method solution, based on a wire-mesh approximation of the conducting surfaces, was used to approximate the near fields within the EMP simulator. The field distribution of an asymmetric EMP parallel-plate simulator was presented (Chapter 2).

The phenomena contributing to the simulator/obstacle interaction is studied using a dynamic field analysis (Chapter 4) based on the method of moment solution discussed in Chapter 3.

---

[1] L.W. Ricketts, J.E. Bridges, and J. Miletta, *EMP Radiation and Protective Techniques* (John Wiley and Sons, New York, 1976).

Mode of Technology Transfer

It is recommended that the results of this research be incorporated into Technical Manual (TM) 5-855-5, *Electromagnetic Pulse Protection*, which is currently under revision.

2 THE PARALLEL-PLATE EMP SIMULATOR

The purpose of an EMP simulator is to provide an approximation of the EMP environment. The characteristics of an EMP environment are dependent upon the altitude of the nuclear burst and the locality of the electronic system with respect to the source region and ground.[2] A number of EMP simulators have been designed and are currently in use to provide the proper EMP excitation for specific conditions.[3] This report will consider the EMP environment produced by a high altitude nuclear burst by assuming a transient pulse propagating away from the source region in free space, without any ground reflections. The EMP in this environment can be represented as a uniform transverse electromagnetic (TEM) plane wave. The EMP waveform is generally assumed to be doubly exponential in nature with a rise time of about a nanosecond and a fall time of about a microsecond. Furthermore, the peak magnitude of the electric field is of about 100,000 V/m. The simulator typically used to approximate this environment is the parallel-plate bounded-wave EMP simulator, consisting of a finite-width parallel-plate waveguide. This wave-guiding structure supports a TEM mode that is generally uniform through its cross section. It would normally be difficult to excite the waveguide with a TEM wave, but in this case, excitation is accomplished by launching a quasi-spherical TEM wave from a conical, tapered end-section. If the end-section is gradually tapered, the wavefront will assume the form of a nearly uniform TEM wave.

The parallel-plate waveguide must also be truncated by a reflectionless load. This is achieved by constructing the simulator with a second conical tapered end-section that is typically matched to the parallel-plate waveguide by loading it with the characteristic impedance of the waveguide. Figure 1 illustrates an example of the parallel-plate EMP simulator.* The parallel-plate EMP simulator is an open waveguiding structure. The fields guided within it can be represented by a superposition of discrete and continuous modes. However, at sufficiently low frequencies, where the plate separation is much shorter than a wavelength, only the TEM mode will propagate. The characteristics of the TEM mode propagating in a finite-width, infinite-length, parallel-plate waveguide can be derived from a quasi-static approximation.[4] Also, the quasi-static characteristics of the conical tapered end-sections can be determined with the use of a stereographic projection and conformal-mapping techniques.[5]

Under a transient pulse excitation of the parallel-plate simulator, there will be significant energy distributed throughout a very broad band, extending into the high frequency region. Unfortunately, for practical purposes, the plate separation is quite large and the bandwidth of single-mode operation is much smaller than that of interest under pulse excitation. As a result, higher-order transverse electric (TE) and

---

[2] For a more complete discussion of the mechanisms that generate EMP environments, see C.L. Longmire, "On the Electromagnetic Pulse Produced by Nuclear Explosions," *IEEE Transactions on Antennas and Propagation*, vol. AP-27 (January 1978), pp. 3-13.

[3] Carl E. Baum, "EMP Simulators for Various Types of Nuclear EMP Environments: An Interim Categorization," *IEEE Transactions on Antennas and Propagation*, vol. AP-27 (January 1978), pp. 35-53.

* All figures are located at the end of each chapter.

[4] Carl E. Baum, *General Principles for the Design of Atlas I and II, Part III: Additional Considerations for the Design of the Terminations*, Sensor and Simulation Note 145 (Air Force Weapons Laboratory, Kirtland AFB, Albuquerque, NM, 3 January 1972); Carl E. Baum, D.V. Giri, and R.D. Gonzalez, *Electromagnetic Field Distribution of the TEM Mode in a Symmetrical Two-Parallel-Plate Transmission Line*, Sensor and Simulation Note 219 (Air Force Weapons Laboratory, 1 April 1976); T.L. Brown and K.D. Granszow, *A Parameter Study of Two Parallel-Plate Transmission Line Simulators of EMP Sensor and Simulation Note 21*, Sensor and Simulation Note 52 (Air Force Weapons Laboratory, Kirtland AFB, NM, 19 April 1968).

[5] F.C. Yang and K.S.H. Lee, *Impedance of a Two-Conical-Plate Transmission Line*, Sensor and Simulation Note 221 (Air Force Weapons Laboratory, November 1976); F.C. Yang and L. Marin, *Field Distributions of a Two-Conical-Plate and Curved Cylindrical-Plate Transmission Line*, Sensor and Simulation Note 229 (Air Force Weapons Laboratory, September 1977).

transverse magnetic (TM) modes will propagate along the waveguide. Furthermore, in the high-frequency region, the open simulator will act as a radiator and will no longer support purely guided modes.

To develop an accurate approximation of the field distribution within the simulator, non-TEM modes must be studied. Initially, one can assume the parallel-plate section to be infinitely wide and long. In this case, the modes can be thought of as those existing in a rectangular waveguide whose width goes to infinity.[6] For lower frequencies, it has been shown that a detailed field mapping, carried out at a single CW frequency, can be well approximated with the superposition of propagating modes when using the rectangular waveguide approximation. However, if further accuracy is desired, a more complete analysis can be derived by computing the discrete modes of a very long, finite-width parallel-plate waveguide. This problem was first approached by assuming either narrow plates[7] or wide plates.[8] Marin (1974) found that for narrow plates (width << separation), the TE modes suffer greater attenuation as they propagate than do the TM modes. It was also found that, for wide plates (width >> separation), the TM modes have a greater attenuation than the TE modes. Therefore, for the case of an arbitrary width, one should expect the existence of both propagating TE and TM modes inside the parallel-plate region.

A more complete analysis[9] was performed at the University of Illinois on the study of the source excitation of the finite-width parallel-plate waveguide. This analysis involved the computation of the total E-field, as a superposition of the discrete and continuous spectrum. The results of Rushdi et al., and of Krichevski are valid for waveguides whose cross sections are large compared to a wavelength, whereas the results of Tsao et al. are valid for a small-to-moderate cross section.

It is important to understand that these techniques approximate the fields for an infinitely long parallel-plate waveguide. However, the parallel-plate region of the simulator is finite in length and is excited and terminated by conical transmission lines. Unfortunately, the previous quasi-static analyses do not account for the generation of spurious modes due to the mismatch at the interface of the two waveguides. An analytic expression has been developed[10] for the TEM modes of a semi-infinite, finite-width, parallel-plate waveguide, excited by a conical transmission line. Although the formulation does not include the effects of any reflected fields, it does yield insight into the excitation process of the parallel-plate section. It should be realized that interfacing the two waveguides requires the matching of a spherical wavefront, which has E_θ and H_ϕ components, into a planar wavefront supported by the parallel-plate region. Along the vertical plane y = a constant, the fields are matched across the transition as $E_z = -E_\theta \sin\theta$, $E_y = E_\theta \cos\theta$, $H_x = -H_\phi \cos\phi$, and $H_y = -H_\phi \sin\phi$; ϕ represents the angle between the center axis and the observation point, and θ its elevation where the origin is at the apex of the conical

---

[6] N. Marcuvitz, *Waveguide Handbook* (McGraw-Hill, 1951).

[7] L. Marin, *Modes on a Finite-Width, Parallel-Plate Simulator I. Narrow Plates*, Sensor and Simulation Note 201 (Air Force Weapons Laboratory, September 1974).

[8] T. Itoh and R. Mittra, *Analysis of Modes in a Finite-Width Parallel-Plate Waveguide*, Sensor and Simulation Note 208 (Air Force Weapons Laboratory, January 1975); L. Marin, *Modes on a Finite-Width, Parallel-Plate Simulator, II. Wide Plates*, Sensor and Simulation Note 223 (Air Force Weapons Laboratory, November 1977); L. Marin and G.C. Lewis, Jr., *Modes on a Finite-Width Parallel-Plate Simulator III. Numerical Results for Modes on Wide Plates*, Sensor and Simulation Note 227 (Air Force Weapons Laboratory, September 1977).

[9] V. Krichevsky, *Source Excitation of an Open, Parallel-Plate Waveguide, Numerical Results*, Sensor and Simulation Note 254 (Air Force Weapons Laboratory, August 1978); A.M. Rushdi, R.C. Menendez, R. Mittra, and S.W. Lee, "Leaky Modes in Parallel-Plate EMP Simulators," *IEEE Transactions on Electromagnetic Compatibility*, vol. EMC-20 (August 1978), pp. 443-451; C-H Tsao, E. Yung, and R. Mittra, *The Source Excitation of a Finite-Width Parallel-Plate Waveguide*, Sensor and Simulation Note 255 (Air Force Weapons Laboratory, February 1979).

[10] J. Lam, *Excitation of the Parallel-Plate Section of a Bounded-Wave EMP Simulator by a Conical Transmission Line*, Sensor and Simulation Note 263 (Air Force Weapons Laboratory, 31 May 1979).

waveguide. As a result, there will exist both transversal and longitudinal electric and magnetic fields at the interface, contributing to a superposition of TEM, TE, and TM modes. However, for gradually tapered end-sections, the mismatch is relatively small and the higher order modes are quite small for low frequencies.

Furthermore, at the transition, there exists a certain time dispersion in matching the spherical wave into a plane wave[11] since the cross section is not a plane of constant phase. Figure 2 shows that a dispersion distance is defined and is related to the time dispersion as:

$$\Delta = \Delta\rho + \Delta\gamma. \qquad \text{[Eq 1]}$$

When the wavelength is less than or equal to four times the dispersion distance, the higher-order modes produced become significant in amplitude, leading to a large distortion of the waveform. Therefore, the dispersion distance determines the "band-width" of the simulator.

The analyses that have been reviewed thus far in this chapter all offer excellent physical and theoretical interpretations of the parallel-plate bounded-wave EMP simulator by considering ideal situations. Such modal analyses have led to the explanation of notches in the magnetic field,[12] the design of optimum loads, and the development of other standards in design.[13] Furthermore, accurate field mappings have been generated, although such generation requires the use of experimental data. This is quite efficient for the simulators that have been constructed, and for frequencies well within the simulator bandwidth. However, as one approaches the simulator's cutoff frequency, the presence of higher order modes will greatly distort the uniformity of the simulator fields. Additionally, the uniformity of the fields will be greatly distorted due to field fringing and mismatches between the conical tapered end-sections and the parallel-plate region. To study the field distribution within the parallel-plate region of the finite-length EMP simulator, a dynamic field solution is presented. A wire mesh approximation of the surface of the conducting plate is devised, and a moment method solution is obtained with the use of the Numerical Electromagnetics Code (NEC), a user-oriented computer code developed at Lawrence Livermore National Laboratory.[14] With the use of this approximation, the near fields within the EMP simulator have been obtained. In Chapter 3, the field distribution of an asymmetric EMP parallel-plate simulator is presented. It is shown that for sufficiently low frequencies, the field is predominantly TEM. Field distributions in the mid-frequency range are presented and their nonuniformity is discussed. A field solution near the simulator cutoff frequency is also presented, and the phenomena contributing to this cutoff is illustrated. The purpose of the parallel-plate EMP simulator is to approximate the electromagnetic environment produced away from the source region of a high altitude nuclear burst, providing a means to perform a hardening evaluation of various electronic systems. For the simulator to provide an effective means of experimental evaluation, there should be negligible interaction between the test object and the simulator. To achieve this, the test object must be sufficiently small in comparison to the plate separation

---

[11] C.E. Baum, *The Conical Transmission Line as a Wave Launcher and Terminator for a Cylindrical Transmission Line*, Sensor and Simulation Note 31 (Air Force Weapons Laboratory, 16 January 1967).

[12] R.W.P. King and D.J. Blejer, "The Electromagnetic Field in an EMP Simulator at High Frequency," *IEEE Transactions on Electromagnetic Compatibility*, vol. EMC-21 (August 1979), pp. 263-269.

[13] D.V. Giri, T.K. Liu, F.M. Tesche, and R.W.P. King, *Parallel-Plate Transmission Line Type of EMP Simulators: A Systematic Review and Recommendations*, Sensor and Simulation Note 261 (Air Force Weapons Laboratory, 1 April 1980).

[14] G.J. Burke and A.J. Poggio, *Numerical Electromagnetics Code (NEC) – Method of Moments*, Technical Document 116, vols. I and II (Naval Ocean Systems Center [NOSC], January 1981).

(less than 40 percent of the distance between plates) and the object must be located more than a wavelength away from the conducting plates. For objects that are not sufficiently small, there will be interaction between the simulator and the test object, greatly distorting the desired electromagnetic environment. As a result, the currents coupled into the system could be produced by the interaction and not by the EMP, leading to a misinterpretation of the experimental results. This could have serious consequences on the EMP hardening evaluation. Chapter 4 focuses on this problem of "simulator-obstacle" interaction and provides an in-depth study of the phenomena contributing to it. A numerical analysis of the interaction is presented by placing a test object in the parallel-plate region of the simulator and using the method of moment solution discussed in Chapter 3 to provide a dynamic solution to the problem.

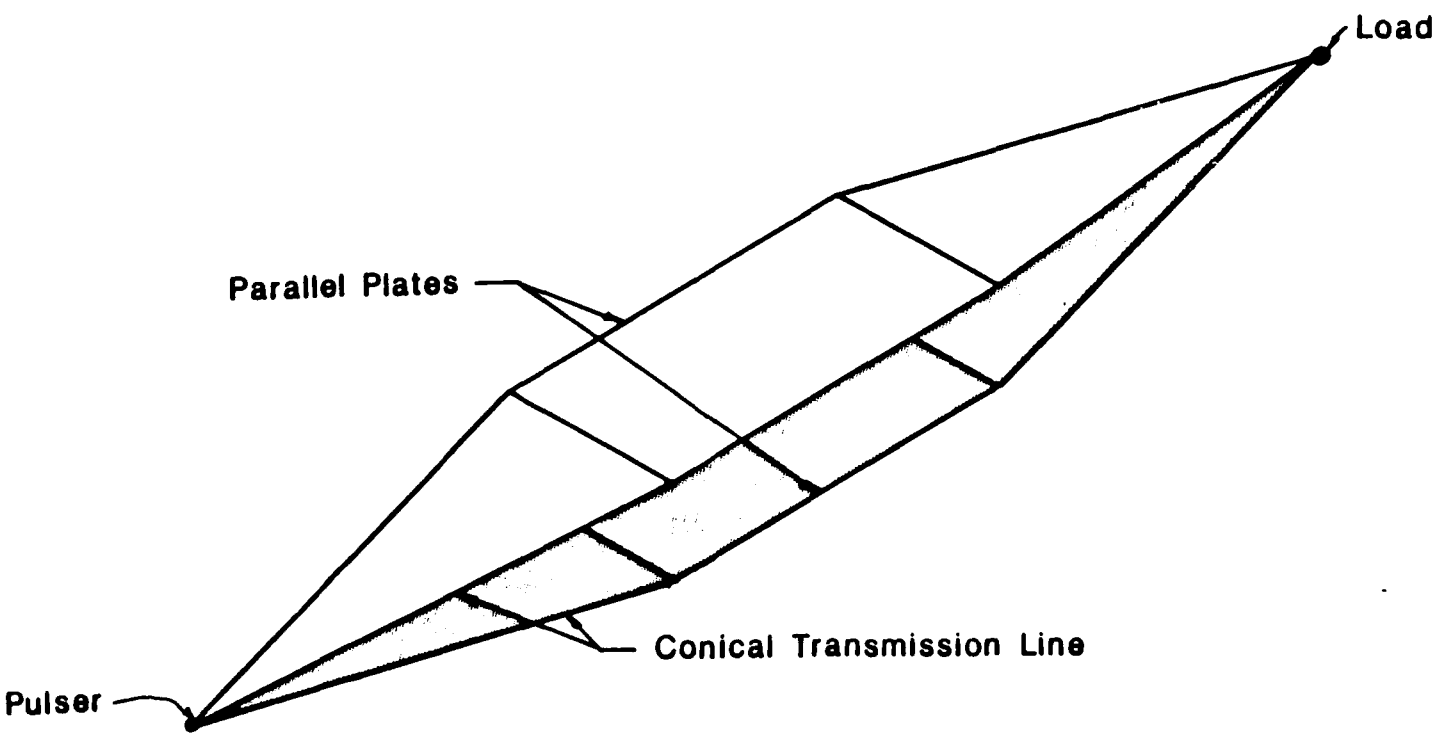

Figure 1. Symmetric parallel-plate bounded-wave EMP simulator.

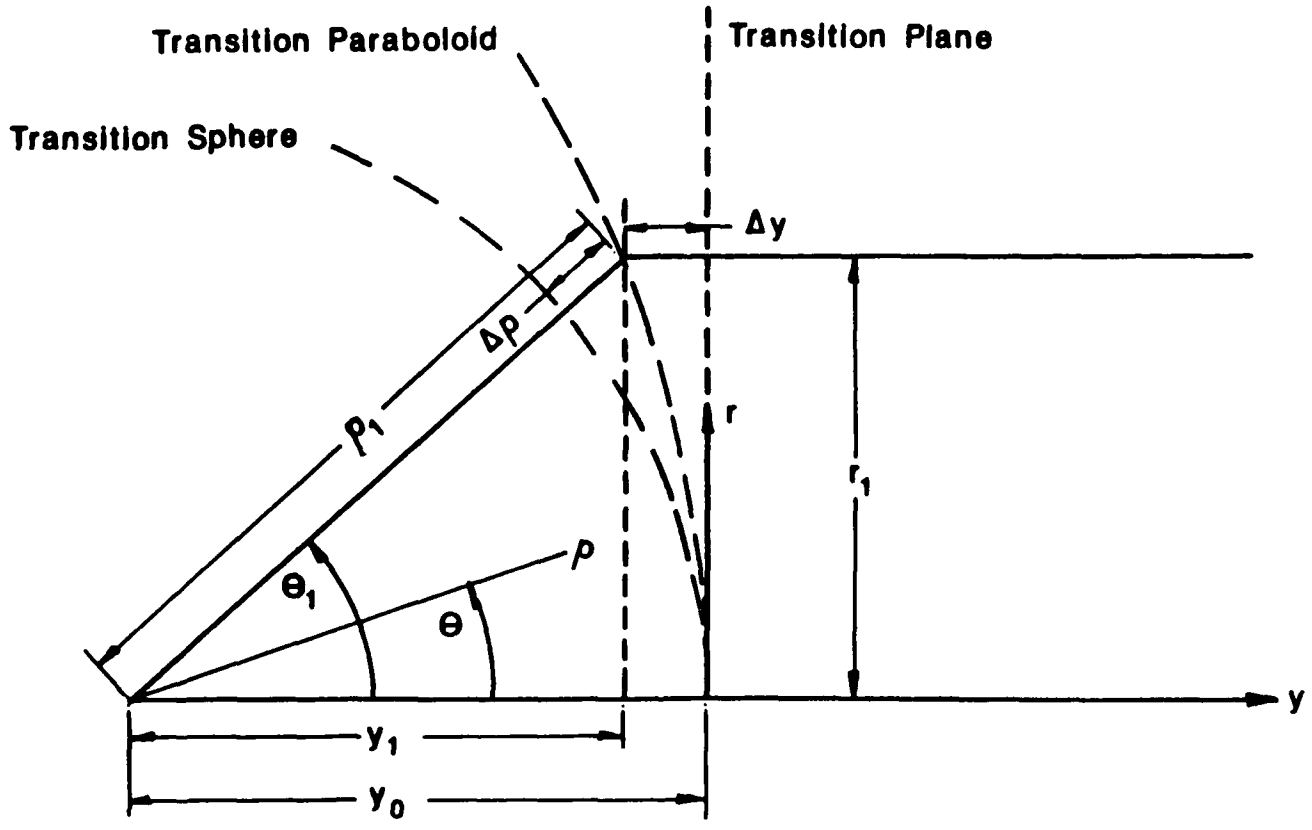

Figure 2. Matching of the conical tapered end-section and the associated dispersion distance of the spherical wavefront.

3 DYNAMIC FIELD ANALYSIS OF THE PARALLEL-PLATE BOUNDED-WAVE EMP SIMULATOR

Introduction

The parallel-plate EMP simulator is characterized as a transmission-line type of simulator. Chapter 2 presented a number of analogies for approximating the field distribution within the parallel-plate region of the simulator. These approximations were all limited to the case of a parallel-plate transmission line either semi-infinite or infinite in length. However, the bounded-wave simulator consists of a finite-length parallel-plate transmission line that is excited and terminated by conically tapered end-sections. This chapter presents a dynamic field solution of the bounded-wave parallel-plate EMP simulator using a moment method solution. The conducting surfaces of the simulator are approximated by a thin-wire mesh model, and the incident field is treated as an applied voltage source distributed across the source gap region. The following section discusses this thin-wire mesh model of the simulator.

Developing the Problem

In this report, NEC is used to analyze the thin-wire-scattering problem.[15] NEC is particularly useful in this application since it provides the capability of modeling multiple-wire junctions. The unknown electric current distributed over the wire mesh is expanded into subdomain basis functions defined by a three-term spline function, in which two terms are eliminated by enforcing charge and current continuity across each multiple wire junction, and the third is eliminated by satisfying the surface boundary condition on the tangential E-field by point matching the Electric Field Integral Equation (EFIE).

A preliminary study of the plane-wave scattering from a finite-dimensional conducting plate, modeled by a thin-wire mesh has verified that the NEC code provides a valid approximation to such a scattering geometry.[16] To minimize the number of unknowns as well as to best approximate the surface currents, a rectangular mesh was used to model the plate, with segment lengths no greater than one tenth of a wavelength. Additionally, the area of the mesh openings was kept constant. This model provided a good approximation of the edge singularities. The conducting surface of the EMP simulator was modeled in the same manner, with the inclusion of an edge wire and continuous wires along the longitudinal direction. A sample model is illustrated in Figure 3.

NEC has been used to wire-model conducting surfaces for a large number of problems in which the principal area of interest was the far field. However, in the EMP simulator problem, one is interested in the near field characteristics, viz., the field distribution in the central region of the simulator. NEC enforces Kirchoff's current law across each multiple wire junction to satisfy total current continuity. Yet the discontinuity in the vector currents at a wire bend or at a wire junction of more than two wires, leads

[15] For a complete description of the NEC-2 code, see Burke and Poggio.

[16] Stephen D. Gedney, *A Dynamic Analysis of the Parallel-Plate EMP Simulator Using a Wire Mesh Approximation and the Numerical Electromagnetics Code*, Technical Manuscript M-87/15/ADA187535 (U.S. Army Construction Engineering Research Laboratory [USACERL], September 1987).

to nonphysical singularities in the near field that could produce errors in the results. It was found through numerical solution that the singularities are negligible when sampling the electric field at distances of at least one-twelfth of a wavelength from the wire mesh.

An accurate source model is extremely important to establish the proper excitation of the transmission-line type of EMP simulator. The excitation must be distributed across the source gap region, and must provide the dominant TEM mode. Similarly, the load model must properly terminate the waveguide, minimizing reflections due to model limitations. The Applied E-Field (AEF) source was to distribute a constant E-field over the source-gap region. The wire model used is illustrated in Figure 4, where the AEF is applied across the vertical wires. Figure 5 (a) and (b) illustrate the scattered E-field computed along the surface of the source wire segment for a 1-volt excitation. The amplitude, as expected, is constant and has a phase of −180 degrees. There is a noticeable singularity in the pulse due to the sharp wire bend of the model; nevertheless, it was found that the error due to this singularity in the fields in the central region of the simulator is negligible.

An accurate model of the terminating load impedance is equally important to minimize reflections of the propagating field back into the parallel-plate region. In practice, when the simulator is terminated by its characteristic impedance, a large amount of the available energy is dissipated by the load and very little reflection is encountered. Since the load is to be matched to the dominant TEM mode, which contains only a vertical E-field component, the loading wire segments have been placed vertically across the load gap region. However, at higher frequencies, where TE and TM modes will propagate, the line is no longer matched; less energy will be dissipated by the load and more energy has the potential of being reflected back into the simulator. A common technique used to minimize reflections is to use a sloped distributed load. This will not only match the vertical E-field, but will dissipate the longitudinal fields of the TM modes as well. Furthermore, the load is made to be slightly inductive to account for the change in characteristic impedance at higher frequencies. Another advantage of sloping the load is that the required current in the termination will reach its late time value much faster during pulse excitation. This can be explained in a simplified manner by the fact that the currents entering the load from the conducting plates will reach a position on the terminating load much faster after the arrival of the incident wave. In doing so, the load becomes better matched in its quasi-static characteristic impedance. Furthermore, since the incident wave arrives at different times along the surface of the load, the reflections encountered are dispersed in time, and the incident wave is reflected back at an oblique angle, and not directly back into the simulator.[17] The analysis with NEC will not be able to consider sloped terminations due to the limitations of the gap model. The model used with NEC consists of purely resistive loads that are distributed over thin vertical wires. Figure 6 illustrates the thin-wire approximation of the load gap model.

The source and load models of the parallel-plate simulator were developed through the analysis of the transmission-line type rhombic EMP simulator.[18] The models described above provided an excellent approximation of the desired distributed source and load and reproduced both the theoretical and

---

[17] For a detailed study of sloped terminations of parallel-plate simulators, see: Carl E. Baum, *A Sloped Admittance Sheet Plus Coplanar Conducting Flanges as a Matched Termination of a Two-Dimensional Parallel-Plate Transmission Line*, Sensor and Simulation Note 95 (Air Force Weapons Laboratory, 31 December 1969); Carl E. Baum, *General Principles for the Design of Atlas I and II, Part III: Additional Considerations for the Design of the Terminations*, Sensor and Simulation Note 145 (Air Force Weapons Laboratory, 3 January 1972); David L. Wright, *Sloped Parallel Resistive Rod Terminations for Two-Dimensional Parallel-Plate Transmission Lines*, Sensor and Simulation Note 103 (Air Force Weapons Laboratory, 7 May 1970).

[18] Gedney.

experimental results reported by Shen and King.[19] It should be noted that error was encountered in the characteristic impedance of the simulator, computed with the use of NEC, when the source and load gap heights were on the order of one-fourth of a wavelength. This was due to the phase shift in the current inherent to the model limitations. Despite the error in the matched impedance value, the simulator fields and the conductor currents compared extremely well under matched conditions.

Numerical Results

This study considers the case of an asymmetrical parallel-plate simulator with conical tapered end-sections. The dimensions are modeled after the ACHATES simulator, designed by the Air Force Weapons Laboratory.[20] The ACHATES simulator has a height to width ratio of

$$\frac{h}{a} = 1.2335 \qquad \text{[Eq 2]}$$

This aspect ratio is chosen such that the simulator has a quasi-static characteristic impedance of 100 Ω. It can be shown that V of input voltage across the source gap of ACHATES will produce a field of V/m at the center of the ground plane (at x=0). As discussed in Chapter 1, the bandwidth of a parallel-plate simulator is determined by the dispersion distance associated with the spherical wavefront that is launched into the parallel-plate region from the conical tapered end-section. The more gradual the taper, the higher the bandwidth of the simulator. The design of the ACHATES initially considered is one with very long tapered end-sections, which result in a bandwidth of 450 MHz. The dimensions of the simulator are shown in Figure 7, and the wire mesh approximation generated for NEC, in Figure 3.

Initially three different operating frequencies are chosen for this example, excitations of: (1) 75 MHz (2) 100 MHz, and (3) 125 MHz. For each case, the characteristic impedance of the simulator is computed by determining the load resistance that minimizes the current standing wave ratio and also minimizes the radiation efficiency, which is determined as the power radiated over the input power. Then the distribution of E-fields in the central parallel-plate region often referred to as the "Working Volume," is analyzed.

Table 1 illustrates the characteristics of the simulator for various terminating loads. The computed characteristic impedance is 120 Ω for a 75 MHz excitation, 120 Ω for a 100 MHz excitation, and 95 Ω for a 125 MHz excitation. In comparison to the rhombic EMP simulator, the characteristic impedance seems to be much more stable over a broad frequency range.

The E-field distribution in the parallel-plate region due to a 1-V continuous wave excitation across the source gap is illustrated in Figures 8 through 16. The vertical E-field, E_z, along the y-direction, is

---

[19] H.M. Shen and R.W.P. King, "The Rhombic EMP Simulator," *IEEE Transactions on Electromagnetic Compatibility*, vol. EMC-24 (May 1982), pp. 255-265; H.M. Shen and R.W.P. King, "The Rhombic EMP Simulator," *IEEE Transactions on Electromagnetic Compatibility*, vol. EMC-24 (May 1982), pp. 255-265.

[20] K. Chen, CAPT G. Michaelidis, Carl E. Baum, and D.V. Giri, *ACHATES Design*, ACHATES Memo 1 (Air Force Weapons Laboratory, 5 November 1976).

illustrated in Figures 8 to 10 for the three cases considered. The fields are quite uniform and have a linearly progressive phase shift throughout the working volume. It should also be noted that the phase has little change along the vertical direction since the propagating waves have planar equiphase fronts. Recall that the design of ACHATES is such that 1 V of input produced 1 V/m at the ground plane (at x=0), in the quasi-static case. This is true for all three cases. The deviation is due to the existence of non-TEM modes, which become more significant as the frequency is increased.

Figures 11 to 13 illustrate the vertical E-field as a function of the vertical direction. The fields are quite uniform throughout the height of the simulator. However it is apparent that there is error in the computed field close to the thin-wire mesh. Figures 14 to 16 illustrate the longitudinal component (E_y) in the x=0 plane, which is representative of the propagating TM field. The longitudinal field is on the order of a magnitude smaller than the vertical E-field. However, it becomes more significant in the higher-frequency regions.

Table 1 shows that, at lower frequencies, a larger amount of energy is dissipated by the load impedance and larger reflections occur due to an impedance mismatch. As a result, the standing wave ratio (SWR) of the fields in the parallel-plate region is much more sensitive to the load impedance at low frequencies. Therefore, the simulator is typically loaded in its quasi-static characteristic impedance. The computed characteristic impedance of the model currently under study is 120 Ω. Therefore in the following examples, the field distribution in the mid-frequency region is illustrated when the simulator is terminated by a 120 Ω load.

Higher order TE and TM modes will propagate in the parallel-plate region when the height of the top plate above the ground plane is greater than $\frac{\lambda}{2}$. For the model illustrated in Figure 7, this occurs at approximately 159 MHz. Figures 17 and 18 illustrate the vertical E-field in the x=0 plane of the parallel-plate region due to a 158.6 MHz excitation, which is very close to this resonant frequency of the waveguide. The SWR of the vertical E-field in the parallel-plate region is computed as 1.23. The vertical E-field is less uniform along the z-direction as compared to the lower frequency excitations. This is due to the presence of higher order modes. At the interface with the source end-section, the field has the characteristics of a spherical wavefront, although the field is still somewhat uniform since the radius of the wavefront is quite large. As the observation point is moved through the parallel-plate region the wavefront becomes linear with a progressive shift in phase. Figures 19 and 20 represent the TM component of the field in the working volume along the x=0 plane.

Figures 21 and 22 illustrate the vertical E-field in the x=0 plane of the parallel-plate region for a 203 MHz excitation, when the simulator is terminated by a 120 Ω load. The SWR of the vertical E-field is found to be 1.3. The field again is quite uniform near the interface between the parallel-plate region and the source end-section, yet it deviates substantially as one moves through the working volume. Figure 23 illustrates the longitudinal component of the E-field, representing the TM component of the field. As the frequency approaches that of the cutoff of the simulator bandwidth, the magnitude of the TM modes become much more significant because a "quasi-spherical" wavefront propagates from the wave-launching conical tapered end-section into the parallel-plate region. Along the ground plane, the incident E-field is vertical and there is no longitudinal component. Moving above the ground plane in the x=0 plane, the field consists of both TM and TEM modes. Then, getting closer to the top plate, the TM component becomes more significant since E_y is larger due to the characteristics of the incident wavefront. Consequently, at higher frequencies, the trailing edge of the spherical wavefront will become comparable to a wavelength and significant TM modes will be generated. This happens at the upper frequency cutoff of the simulator, which, for this example, is 450 MHz.

Figures 24 through 33 illustrate the field distribution in the simulator along the transverse direction. Figures 24 through 28 illustrate the field distribution due to a 158.6 MHz excitation. The vertical and longitudinal components of the E-field are very uniform along the transverse directions, illustrating little effects due to field fringing. Figures 27 and 28 illustrate the TE component of the field. The TE field is largest near the edge of the waveguide due to the spherical wavefront being matched into the parallel-plate region.

Figures 29 through 33 illustrate the field distribution along the transverse direction caused by a 203 MHz excitation. The vertical and longitudinal components of the E-field are much less uniform than that of the previous case. It is illustrated that field fringing has a much larger effect on the fields in the parallel-plate region at this frequency. In addition, the aberration of the wavefront is more significant and a larger amount of energy is coupled into higher order TE and TM modes. In the following section, an analysis of the generation of the TE and TM modes is presented, and their determination of the simulator cutoff frequency is discussed.

In order to develop a better understanding of the mechanism contributing to the large aberration in the planar wavefront of the parallel-plate region, the field distribution within the simulator is analyzed near its cutoff. By shortening the conical tapered end-sections from 44 m to 1.95 m, the bandwidth of the simulator is reduced from 450 MHz to 200 MHz.[21] In doing so, the simulator has a computed characteristic impedance of 110 Ω for a 100 MHz excitation, and a corresponding current SWR of 1.125. Furthermore, at 175 MHz, (very near cutoff) the simulator is matched when loaded by 95 Ω, and has a corresponding current SWR of 1.08. It should also be noted that the radiation efficiency for the 175 MHz case is 80.19 percent. Therefore, very little energy is dissipated by the load resistance, and most of the energy is either being reflected or radiated. Figures 34 to 39 illustrate the E-field distribution in the working volume due to a 1-volt excitation across the source gap.

The vertical E-field as a function of y is illustrated in Figures 34 and 35. At 100 MHz, the field is uniform and has a linearly progressive phase shift. However, close to the simulator cutoff frequency, there is a large contribution from higher-order TM and continuous modes. The vertical field deviates significantly from its uniformity and in fact has a 1/R contribution, where R is the distance from the source. Furthermore, the phase shift is no longer linear. It should be noted, although it is not illustrated, that away from the x=0 plane, there is a large contribution to the field from higher-order TE modes. The distribution of the vertical E-field in the vertical direction is illustrated in Figures 36 and 37. At 100 MHz, the field is relatively uniform, and the phase is approximately constant over the height of the parallel-plate. However, at 175 MHz, the field is no longer uniform. Furthermore, the phase indicates that the modes contributing to the spherical wavefront propagate with little attenuation into the working volume. At y = –0.25 m, there is a 45 degree phase lag from z = 0 to z equals 0.94 m. A rough computation shows the maximum deviation of the spherical wavefront at the planar interface to be 2.165 × 1.95, or 0.215 m (where 2.165 is the length the wavefront has to travel along the top plate of the conical taper). At 175 MHz, this corresponds to a $\frac{2\pi}{\lambda} \times 0.215$ phase shift of 45.15 degrees. The wavefront becomes planar as the wave propagates with y, although it loses a considerable amount of energy.

Figures 38 and 39 illustrate the longitudinal E-field along the vertical direction. In comparison to Figure 15, Figure 38 shows the longitudinal component of the E-field to be much larger towards the waveguide interface at y=–.50 m. However, at 175 MHz, there is a significant increase in the amplitude of E_y throughout the parallel-plate region. An interesting observation in Figure 39 is that the location of

[21]Chen et al.

the peak amplitude of E_y along the vertical occurs at shorter distances from the ground as the wavefront travels from one end of the parallel-plate region to the other. This can be explained by ray optics. The incident field is a diverging wavefront, bounded by the conical tapered end-section. Near the ground plane, the waves propagate directly into the parallel-plate region. However, for larger angles of incidence, the waves are reflected by the surface of the top parallel-plate. The maximum angle is determined by the angle of the tapered end-section. Once reflected, this ray determines the reflected shadow boundary, which is propagating in the negative z direction as it progresses in y. Therefore, due to the constructive interference of the longitudinal component of the E-field, the peak field progressively occurs at shorter distances from the ground.

Table 1 (a)

NEC Model of the ACHATES EMP Simulator; 75 MHz

Z_L (Ω)	$Re(Z_{in})$ (Ω)	$IM(Z_{in})$ (Ω)	η_{eff} (%)	SWR
0.0	33.07	100.50	100.0	15.920
50.0	83.25	60.03	18.34	2.350
75.0	93.09	38.09	12.17	1.685
95.0	96.42	22.69	10.09	1.384
100.0	96.82	19.19	9.80	1.326
110.0	97.20	12.60	9.41	1.225
120.0	97.15	6.54	9.23	1.141
150.0	95.32	-8.74	9.54	1.248
200.0	89.76	-26.75	11.53	1.331
500.0	63.27	-62.78	28.55	2.602
1000.0	48.11	-73.36	47.85	3.805
10000.0	31.96	-82.45	90.74	6.757

Table 1 (b)

NEC Model of the ACHATES EMP Simulator; 100 MHz

Z_L (Ω)	$Re(Z_{in})$ (Ω)	$IM(Z_{in})$ (Ω)	η_{eff} (%)	SWR
0.0	20.49	16.82	100.00	8.830
50.0	56.23	15.90	28.51	1.980
75.0	71.89	15.45	22.88	1.475
90.0	80.67	15.19	21.49	1.292
100.0	86.31	15.02	20.99	1.196
110.0	91.76	14.85	20.78	1.137
120.0	97.04	14.68	20.77	1.129
150.0	112.00	14.20	21.54	1.218
200.0	134.10	23.44	24.20	1.502
300.0	170.20	12.12	42.41	2.710
1000.0	288.20	8.18	60.18	3.250
10000.0	408.60	22.87	93.56	5.200

Table 1 (c)

NEC Model of the ACHATES EMP Simulator; 125 MHz

Z_L (Ω)	$Re(Z_{in})$ (Ω)	$IM(Z_{in})$ (Ω)	η_{eff} (%)	SWR
0.0	63.61	-99.67	100.00	6.143
50.0	90.78	-23.66	39.00	1.480
75.0	88.57	-4.20	33.39	1.164
95.0	85.35	6.80	32.56	1.126
100.0	84.49	9.07	32.55	1.139
110.0	82.76	13.18	32.63	1.163
120.0	81.04	16.76	33.01	1.373
150.0	76.24	25.12	34.58	1.474
200.0	69.65	34.03	38.13	1.837
500.0	51.73	50.27	56.81	3.504
1000.0	43.67	55.02	71.86	5.115
10000.0	35.84	57.66	92.16	8.380

Figure 3. Wire Mesh Approximation of the conducting surface of the asymmetric Parallel-Plate EMP Simulator.

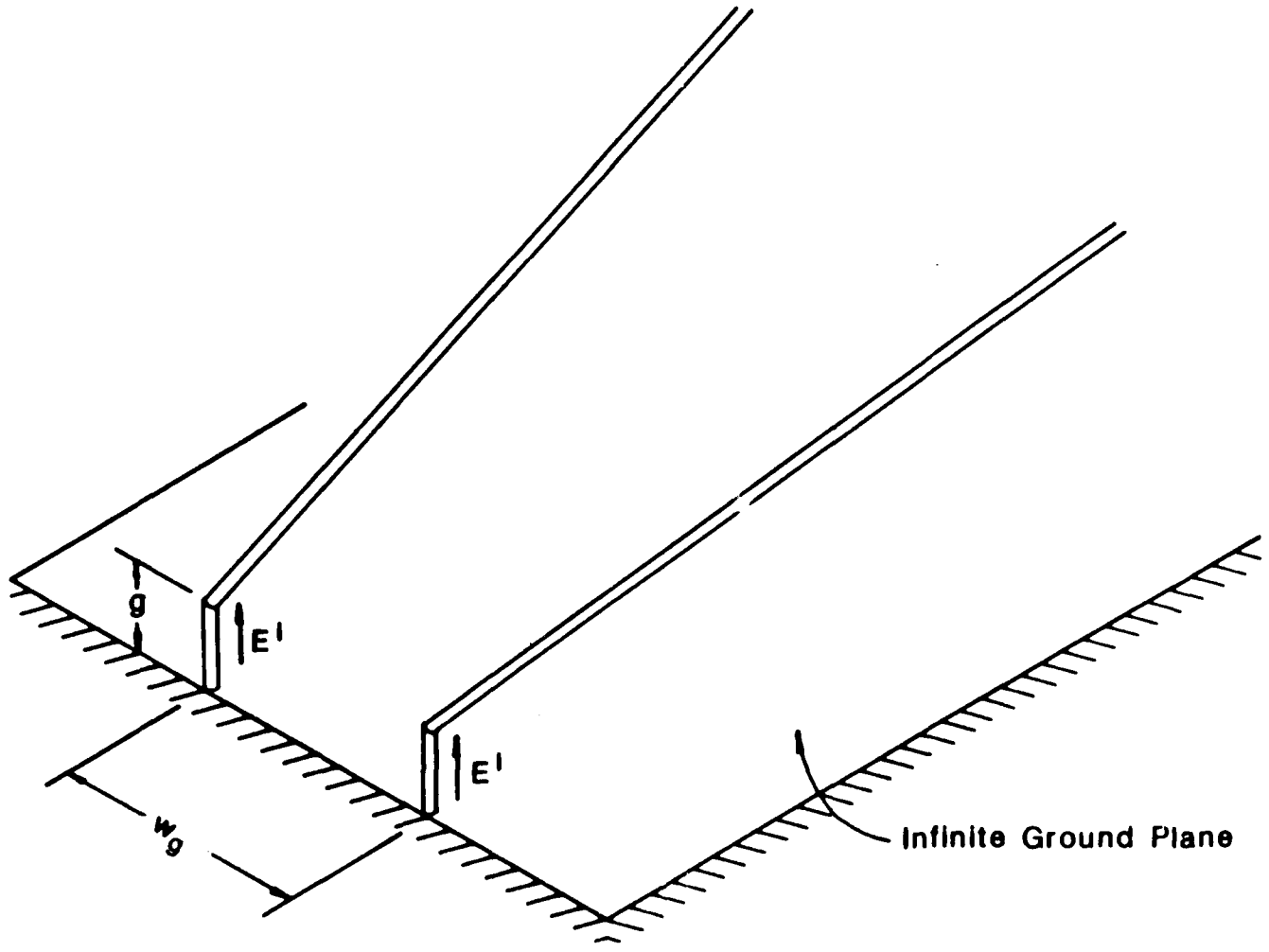

Figure 4. Thin-wire model of the source gap region of the EMP Simulator.

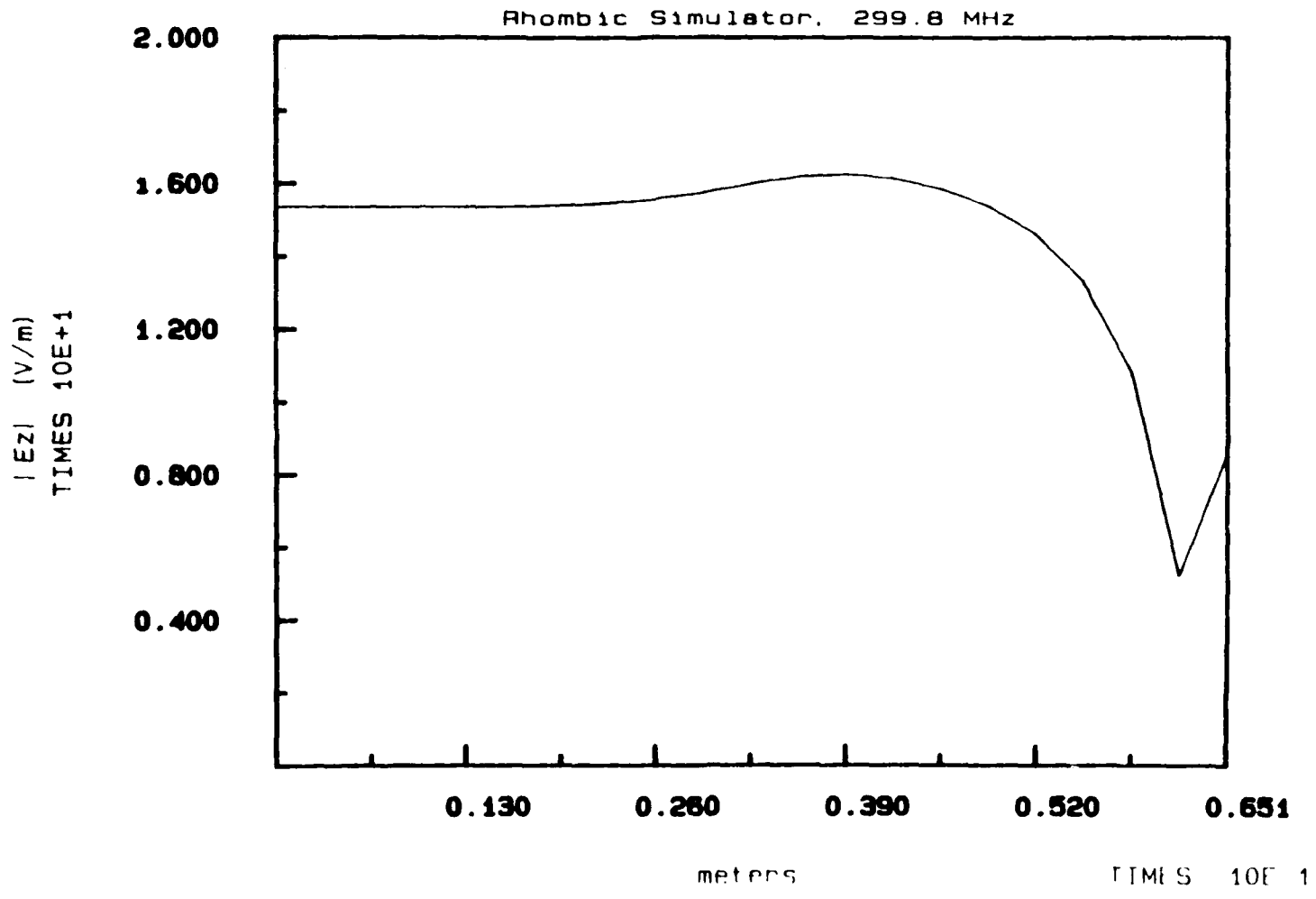

(a) Scattered axial E-field.

Figure 5. Scattered axial E-field due to an AEF on the surface of the source segment.

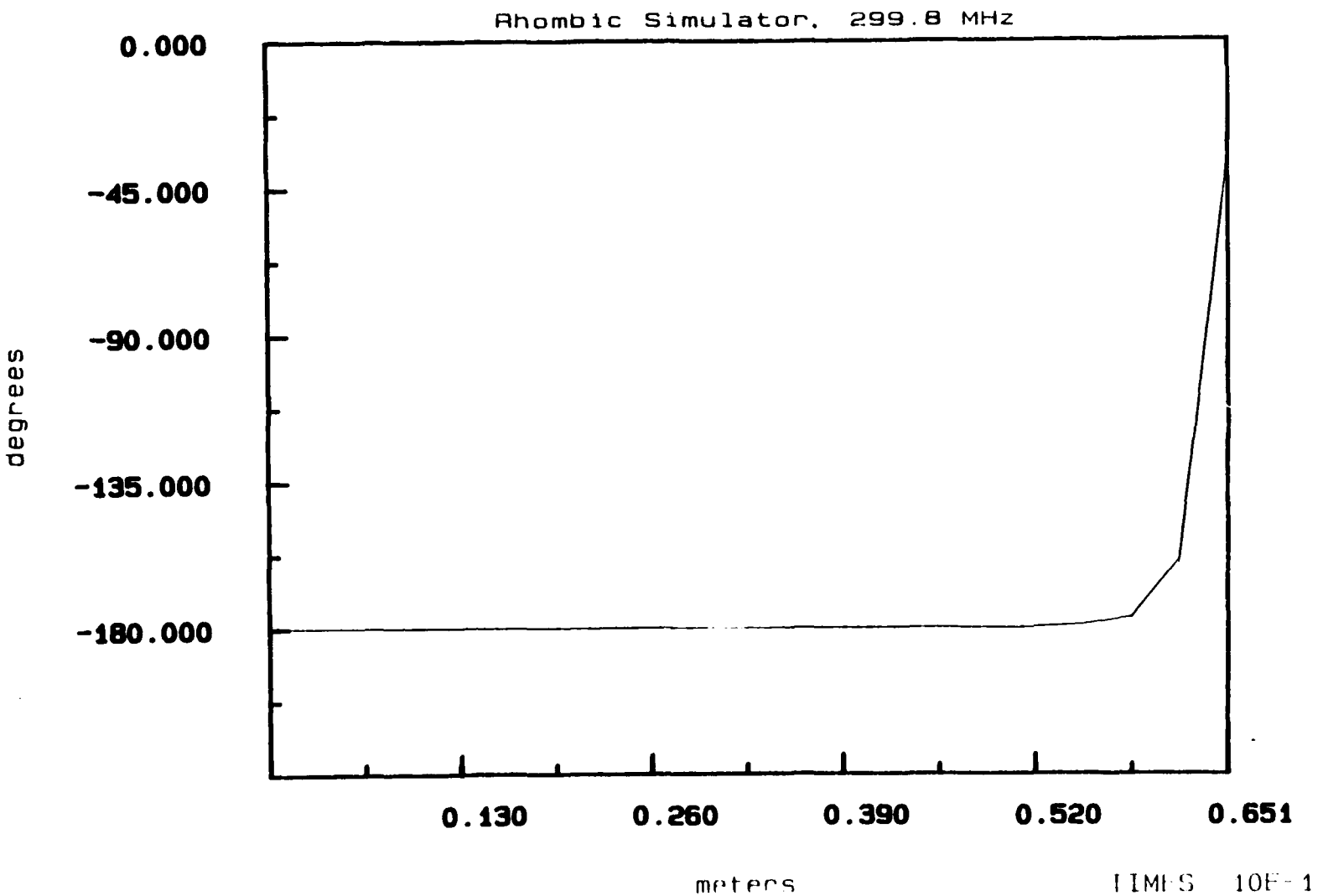

(b) Phase of axial E-field.

Figure 5. (Cont').

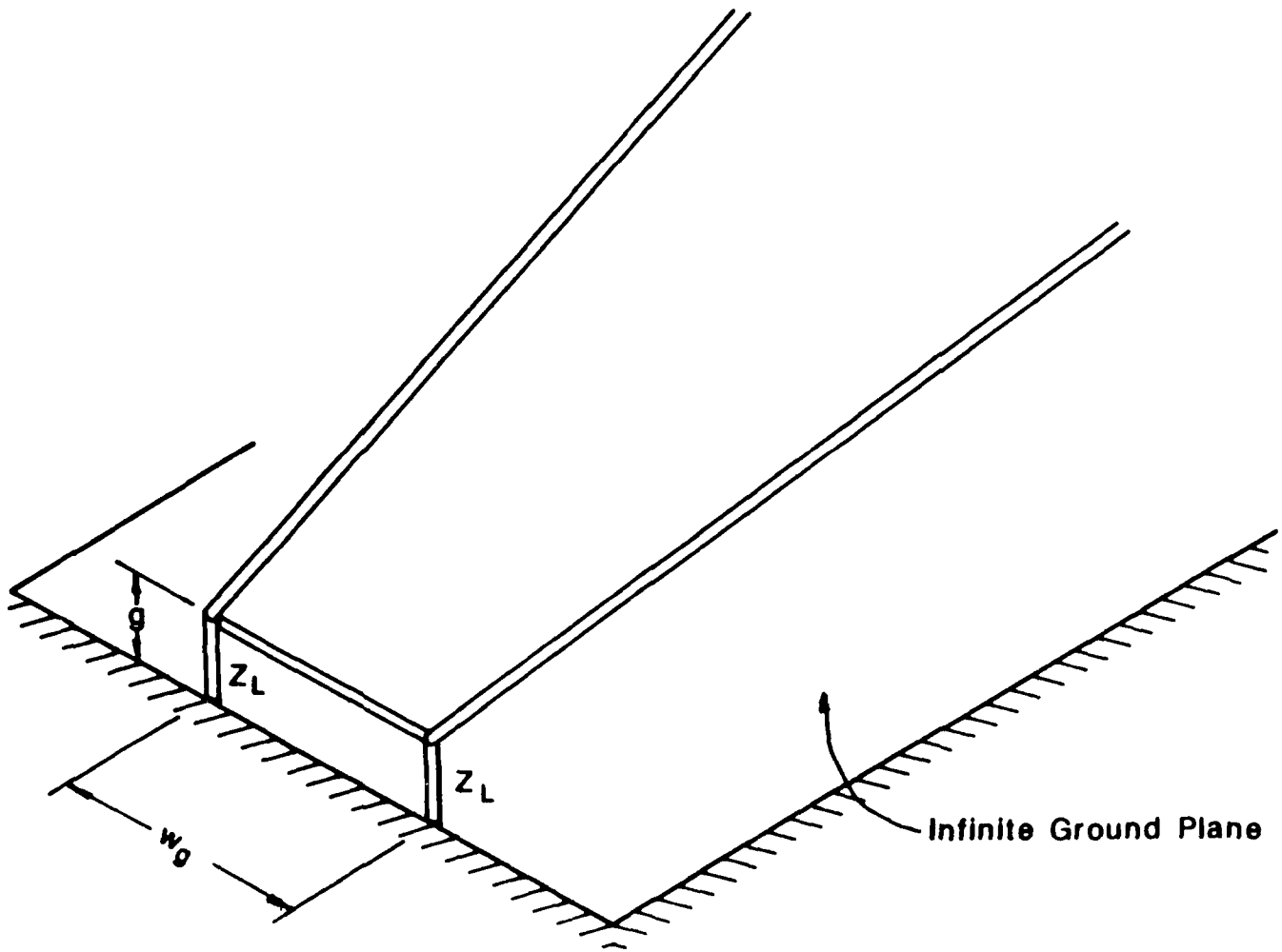

Figure 6. Thin-wire model of the terminating load gap region of the EMP Simulator.

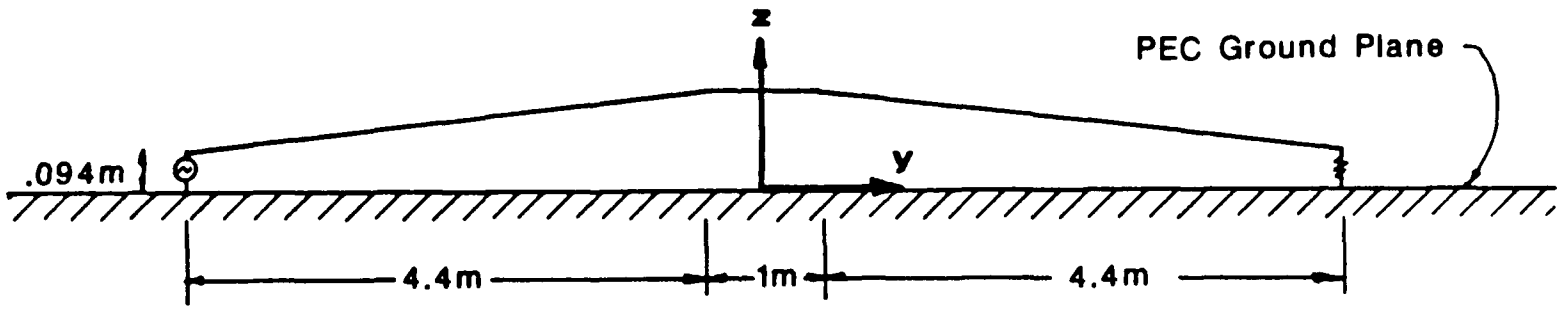

(a) Side view.

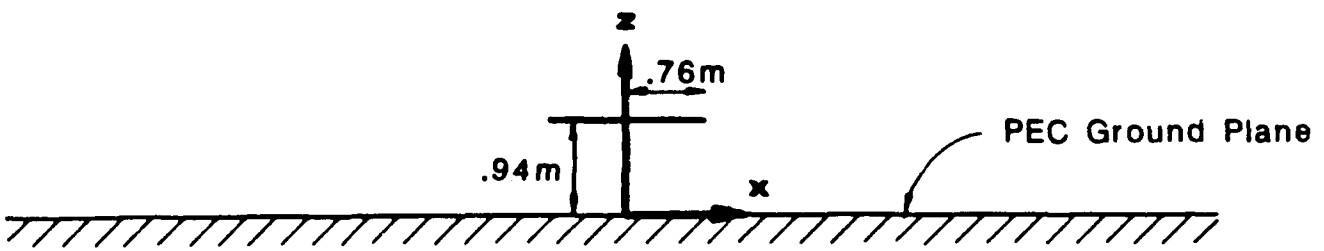

(b) Cross section; inside of parallel-plate region.

Figure 7. Dimensions of the ACHATES asymmetric parallel-plate bounded-wave EMP simulator with a 450 MHz bandwidth.

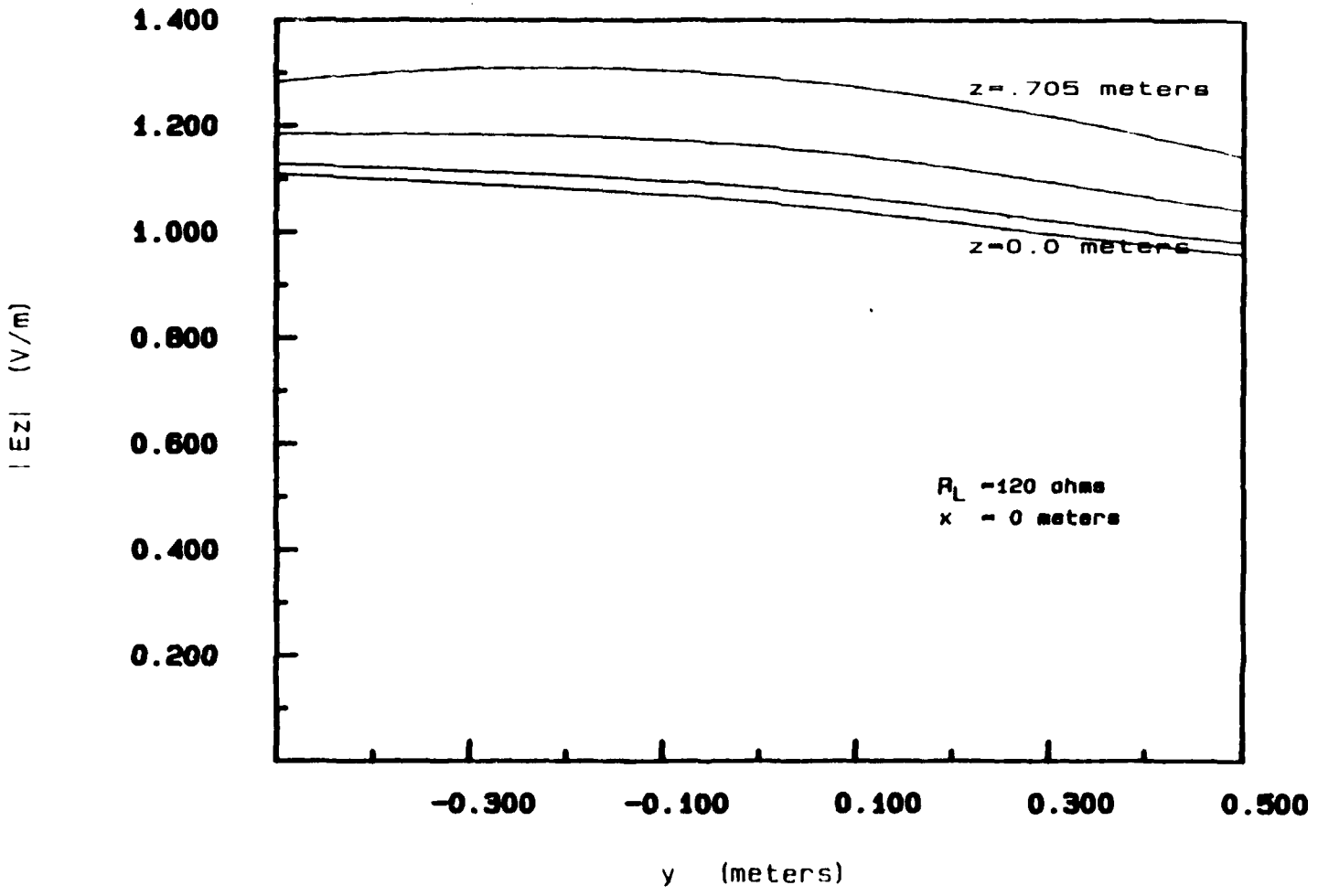

(a) Magnitude of E_z

Figure 8. Vertical E-field computed along the longitudinal direction in the parallel-plate region of the 450 MHz bandwidth ACHATES EMP simulator due to a 75 MHz unit-amplitude excitation.

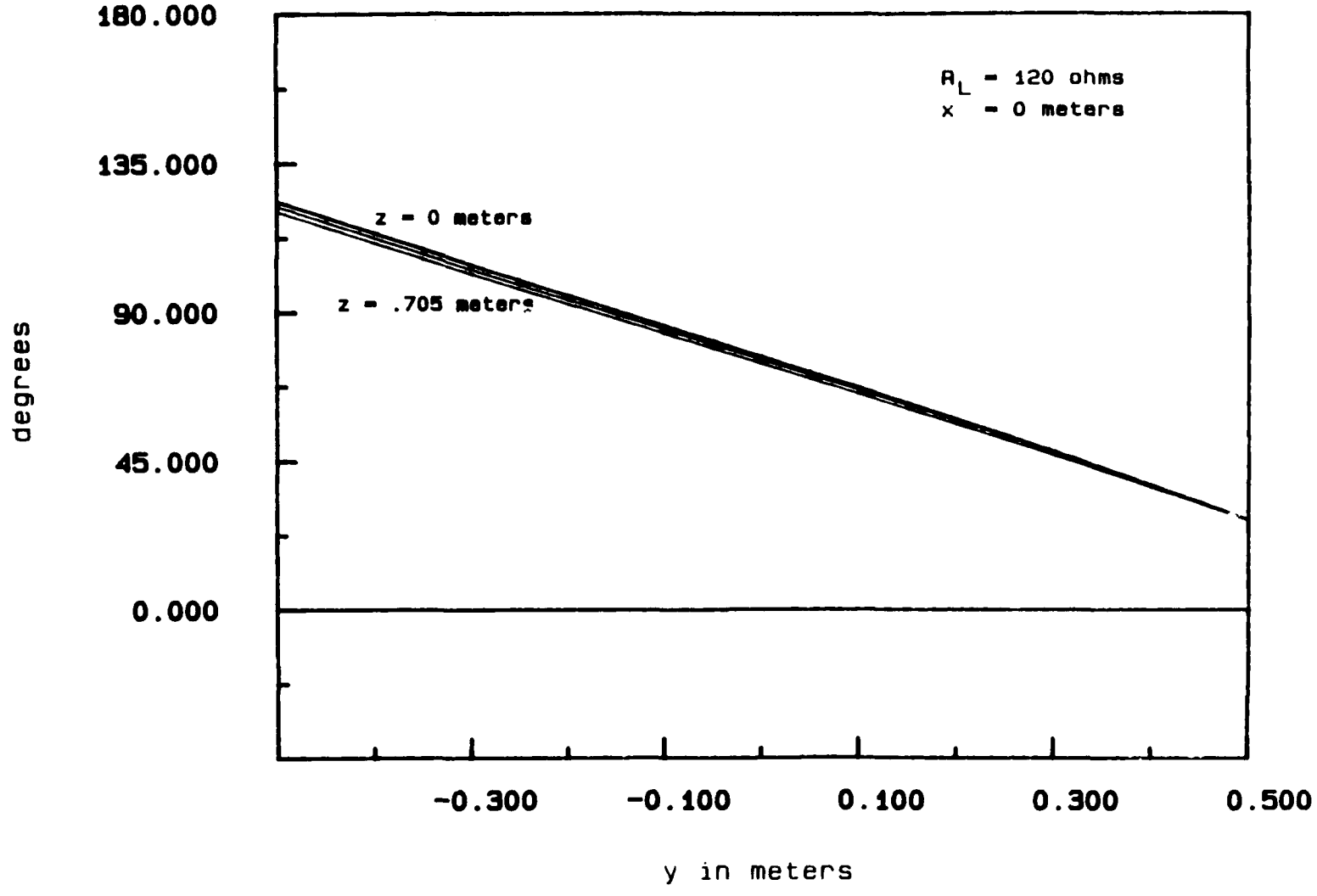

(b) Phase of E_z.

Figure 8. (Cont'd)

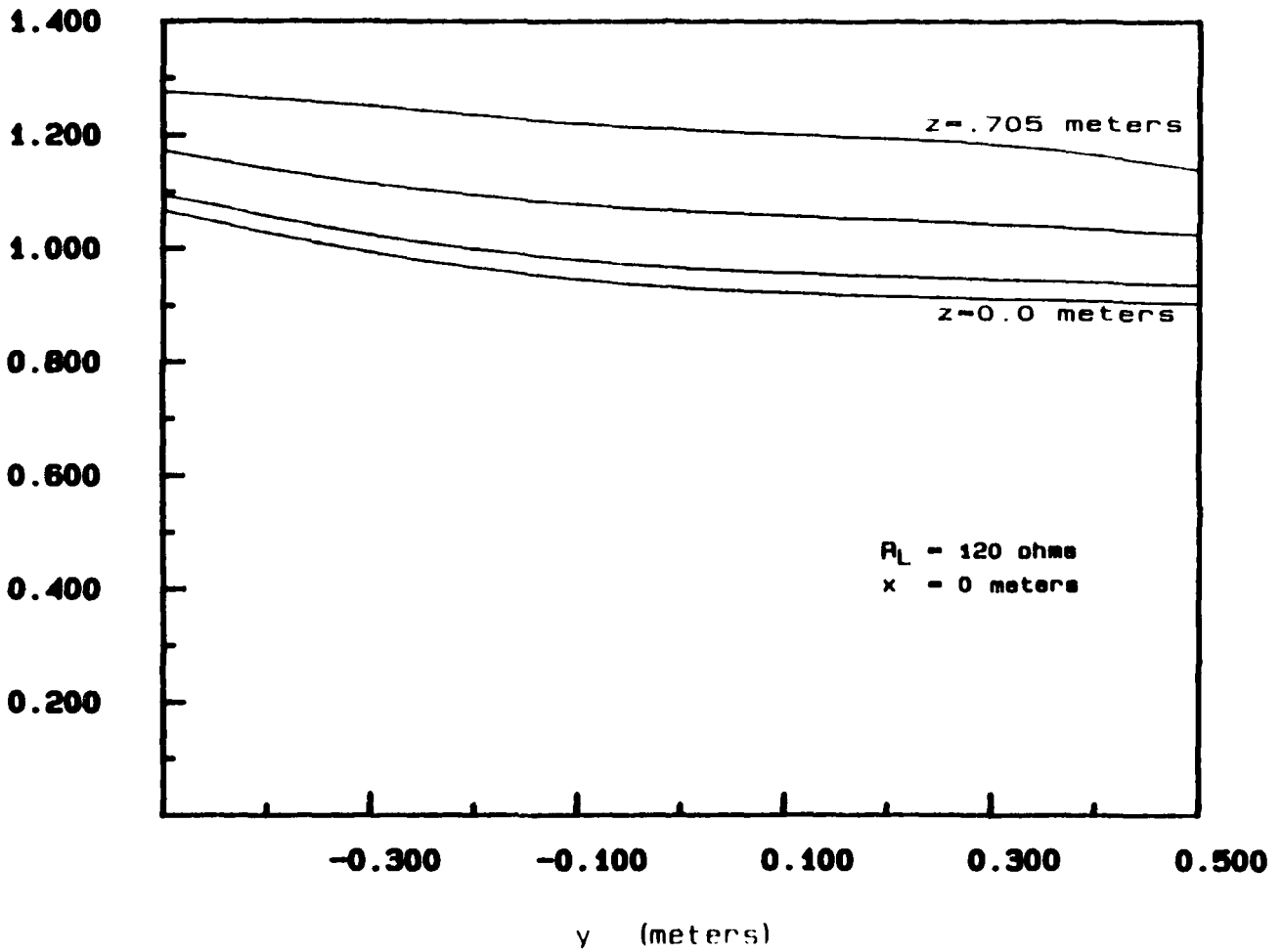

(a) Magnitude of E_t

Figure 9. Vertical E-field computed along the longitudinal direction in the parallel-plate region of the 450 MHz bandwidth ACHATES EMP simulator due to a 100 MHz unit-amplitude excitation.

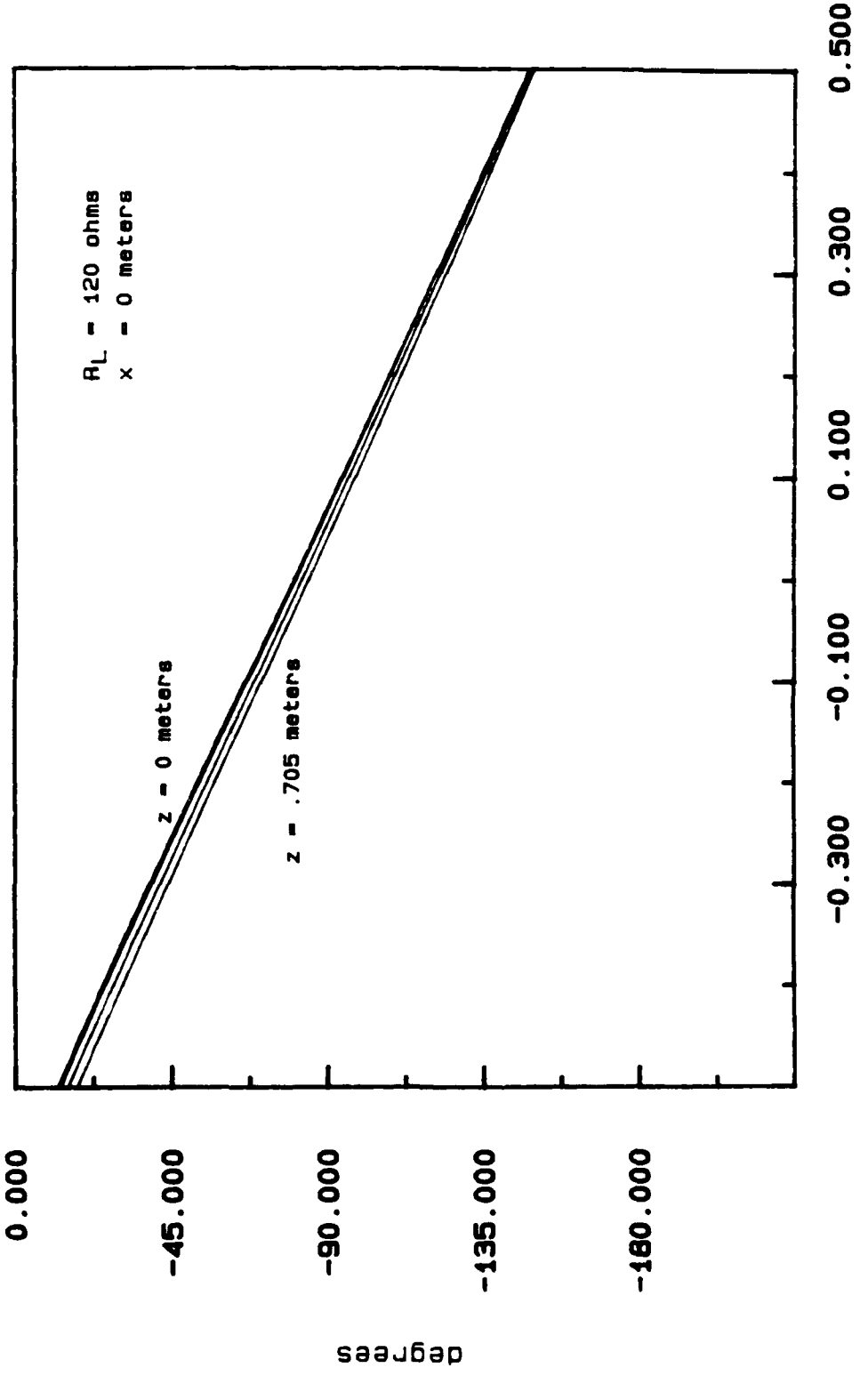

(b) Phase of E_z.

Figure 9. (Cont'd).

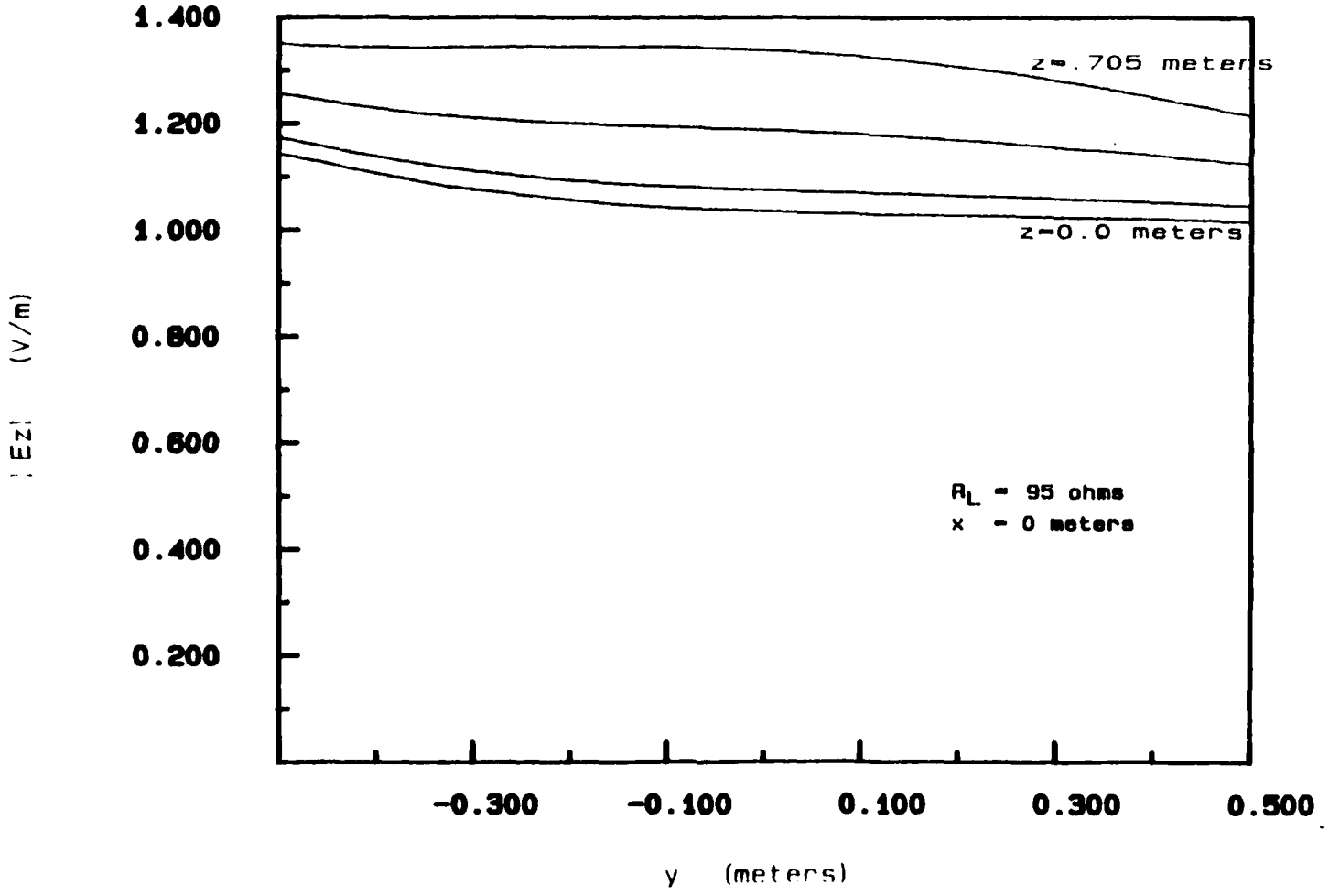

(a) Magnitude of E_z

Figure 10. Vertical E-field computed along the longitudinal direction in the parallel-plate region of the 450 MHz bandwidth ACHATES EMP simulator due to a 125 MHz unit-amplitude excitation.

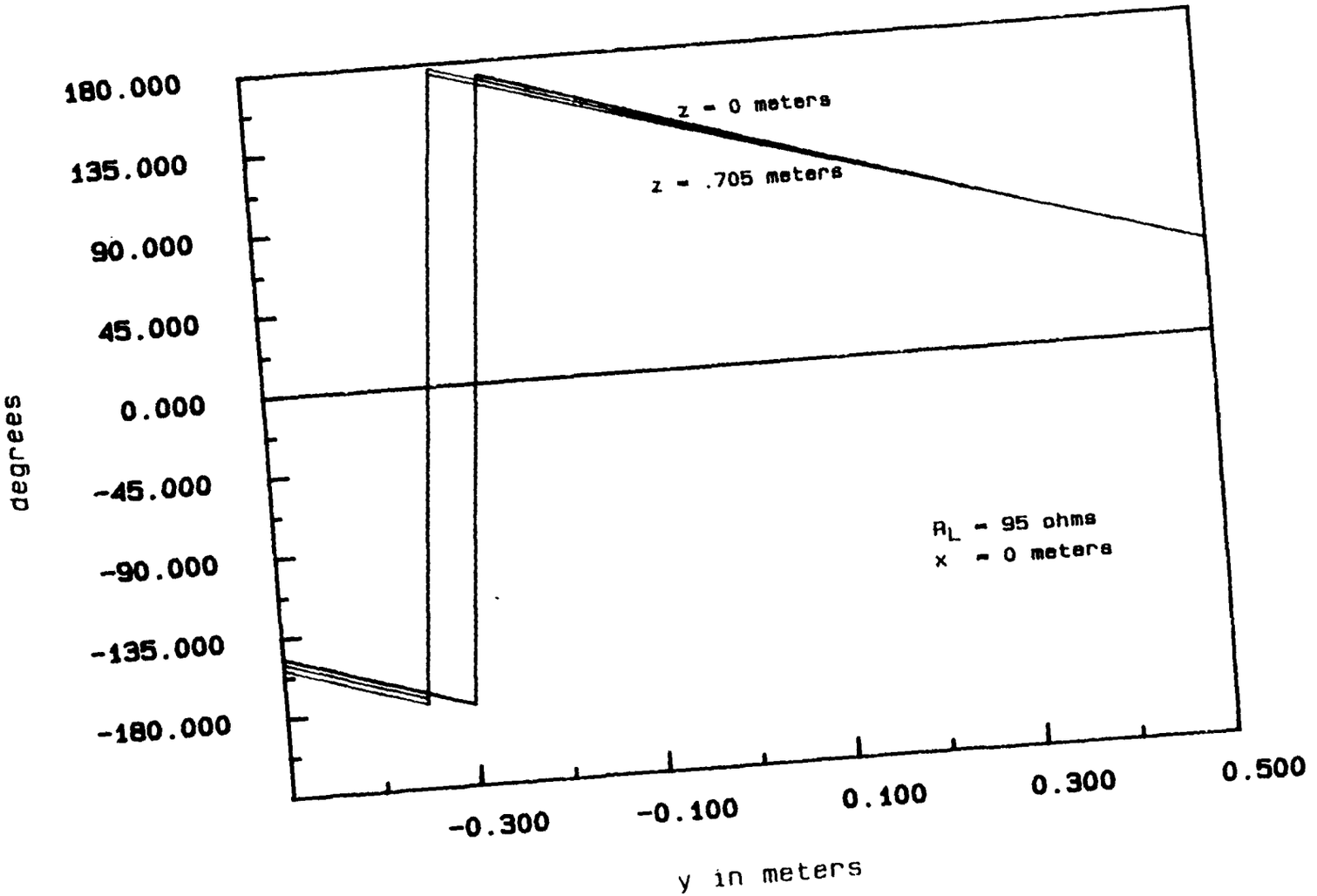

(b) Phase of E_r

Figure 10. (Cont'd).

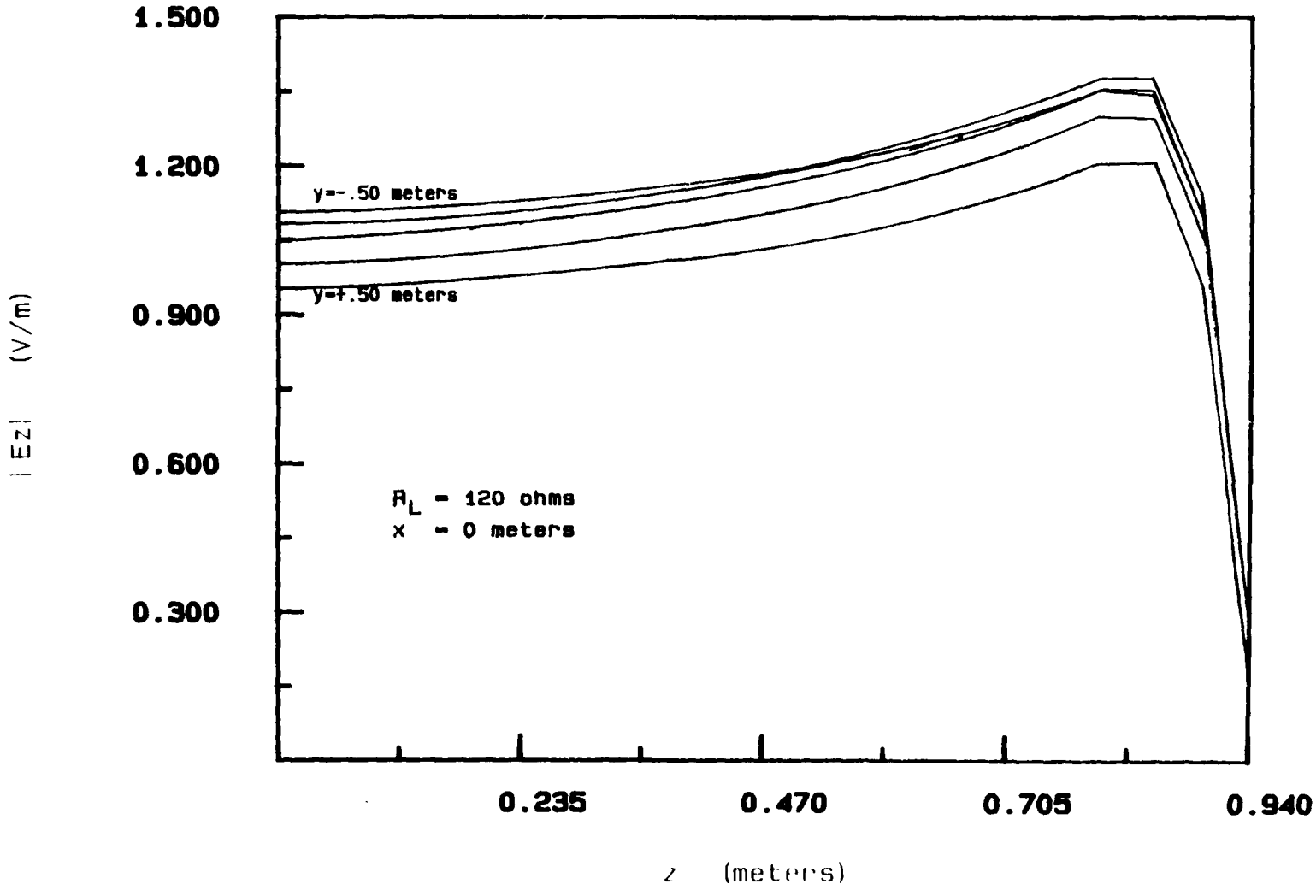

Figure 11. Magnitude of the vertical E-field computed along the vertical direction at various longitudinal positions (y=0.5, -0.25, 0.0, 0.25m) due to a 75 MHz unit-amplitude excitation.

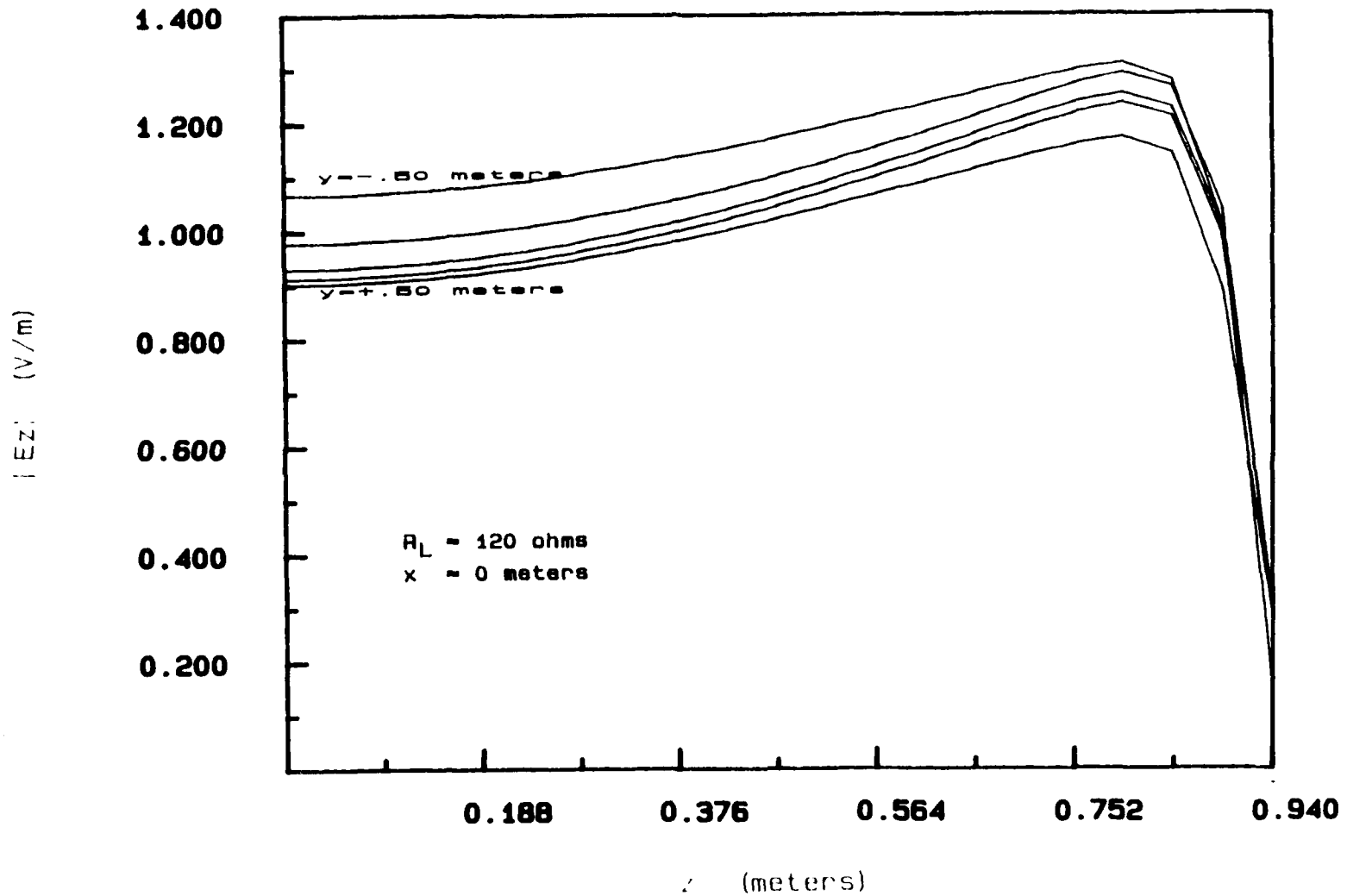

Figure 12. **Magnitude of the vertical E-field computed along the vertical direction at various longitudinal positions due to a 100 MHz unit-amplitude excitation.**

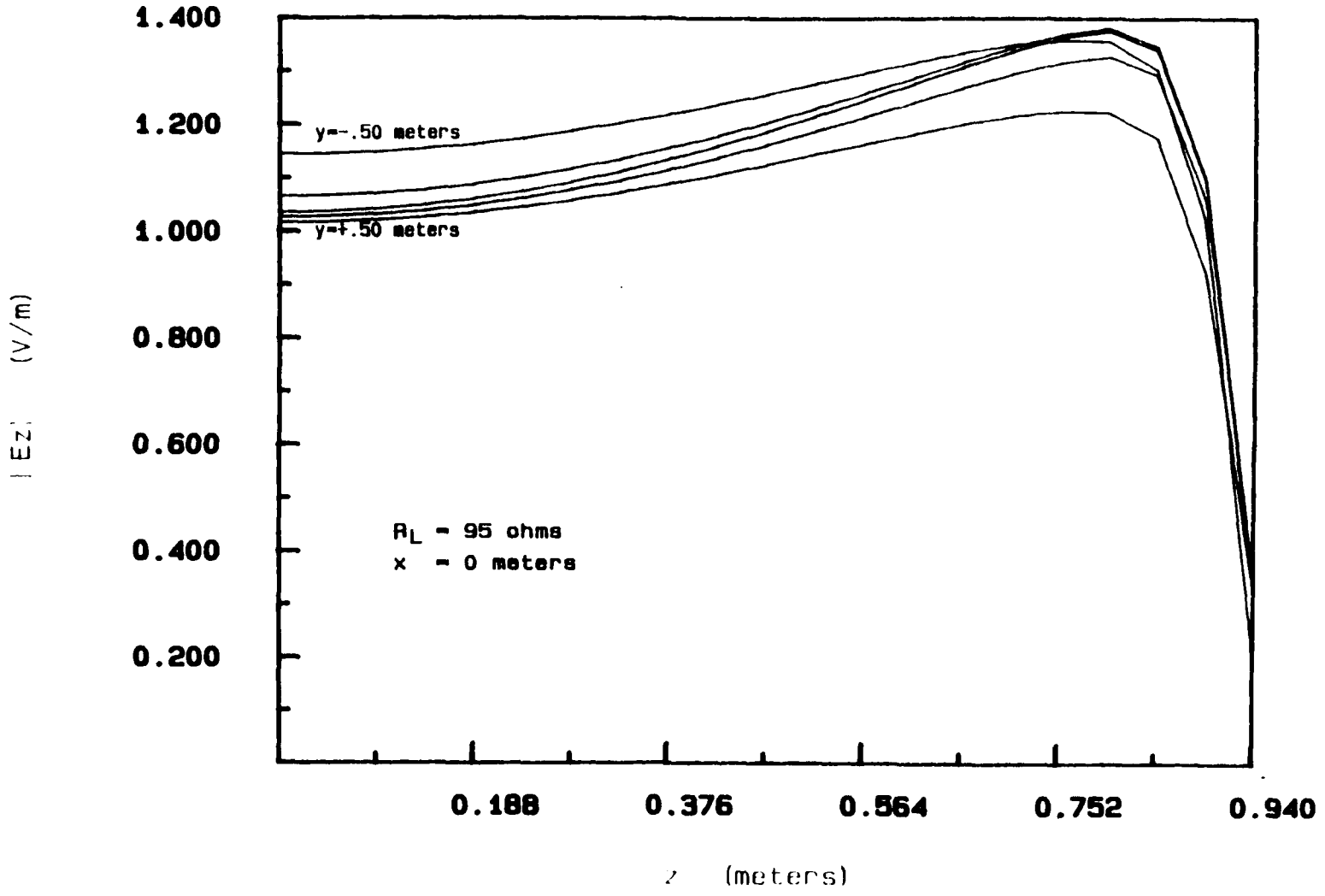

Figure 13. Magnitude of the vertical E-field computed along the vertical direction at various longitudinal positions due to a 125 MHz unit-amplitude excitation.

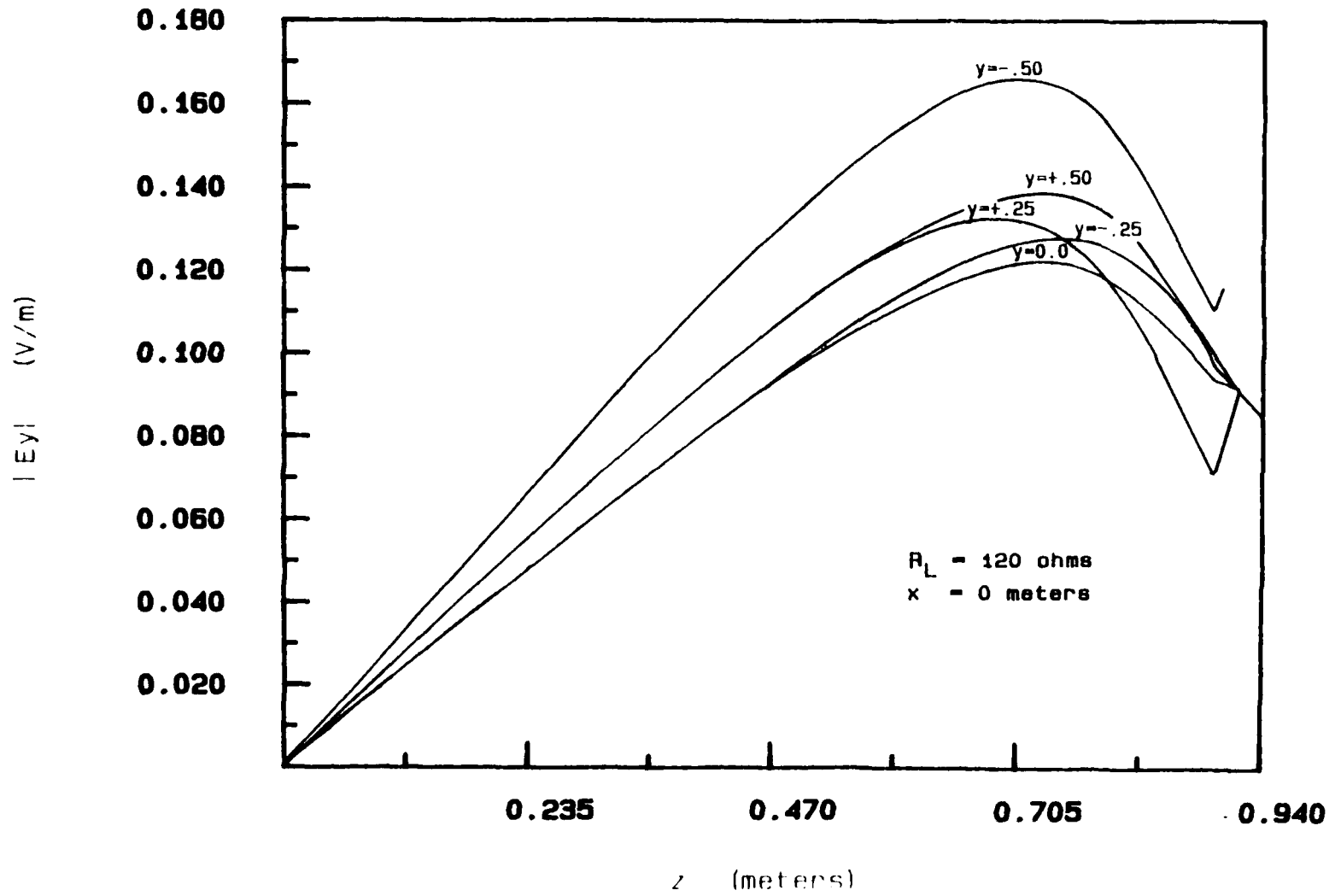

Figure 14. Magnitude of the longitudinal E-field computed along the vertical direction at various longitudinal positions due to a 75 MHz unit-amplitude excitation.

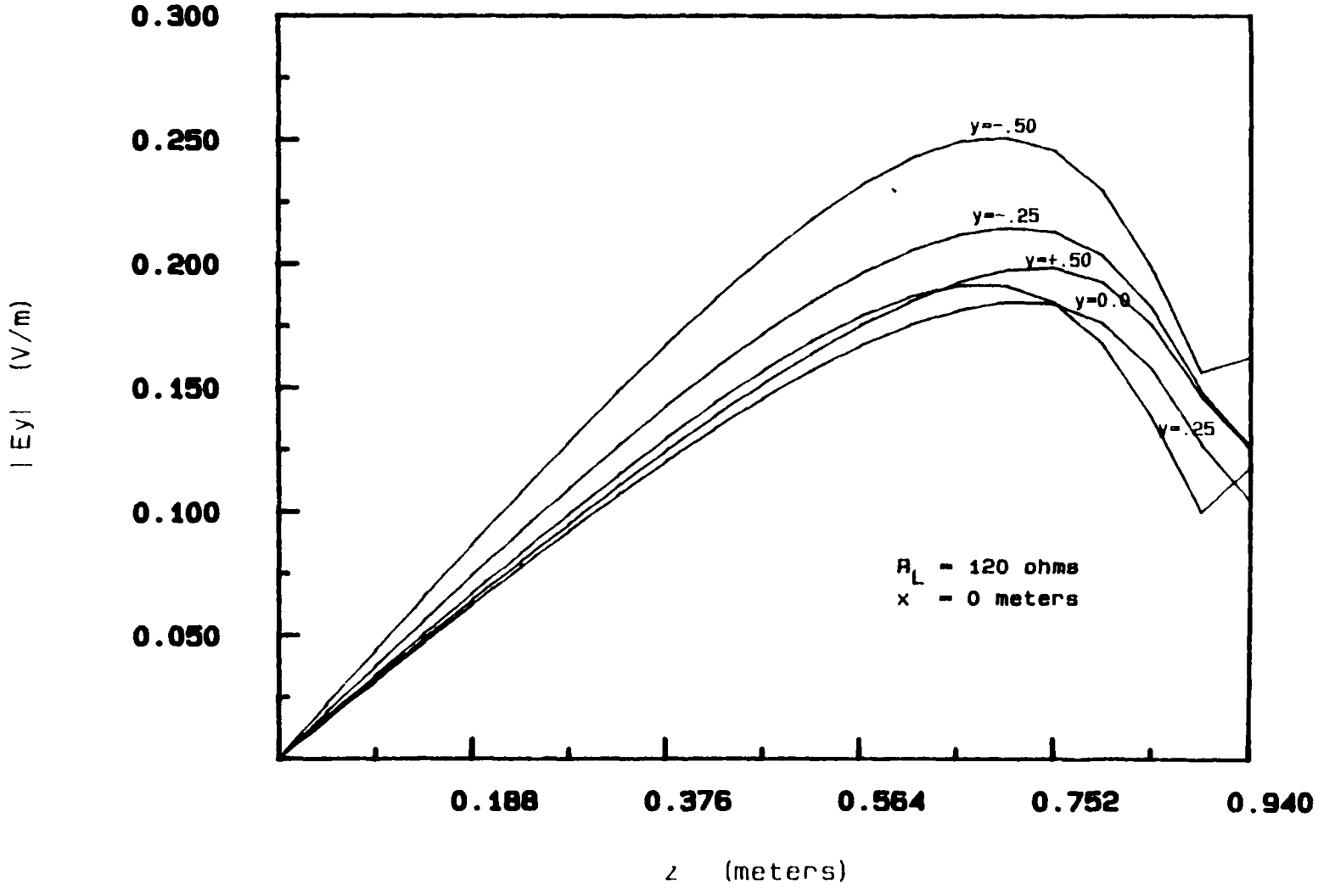

Figure 15. Magnitude of the longitudinal E-field computed along the vertical direction at various longitudinal positions due to a 100 MHz unit-amplitude excitation.

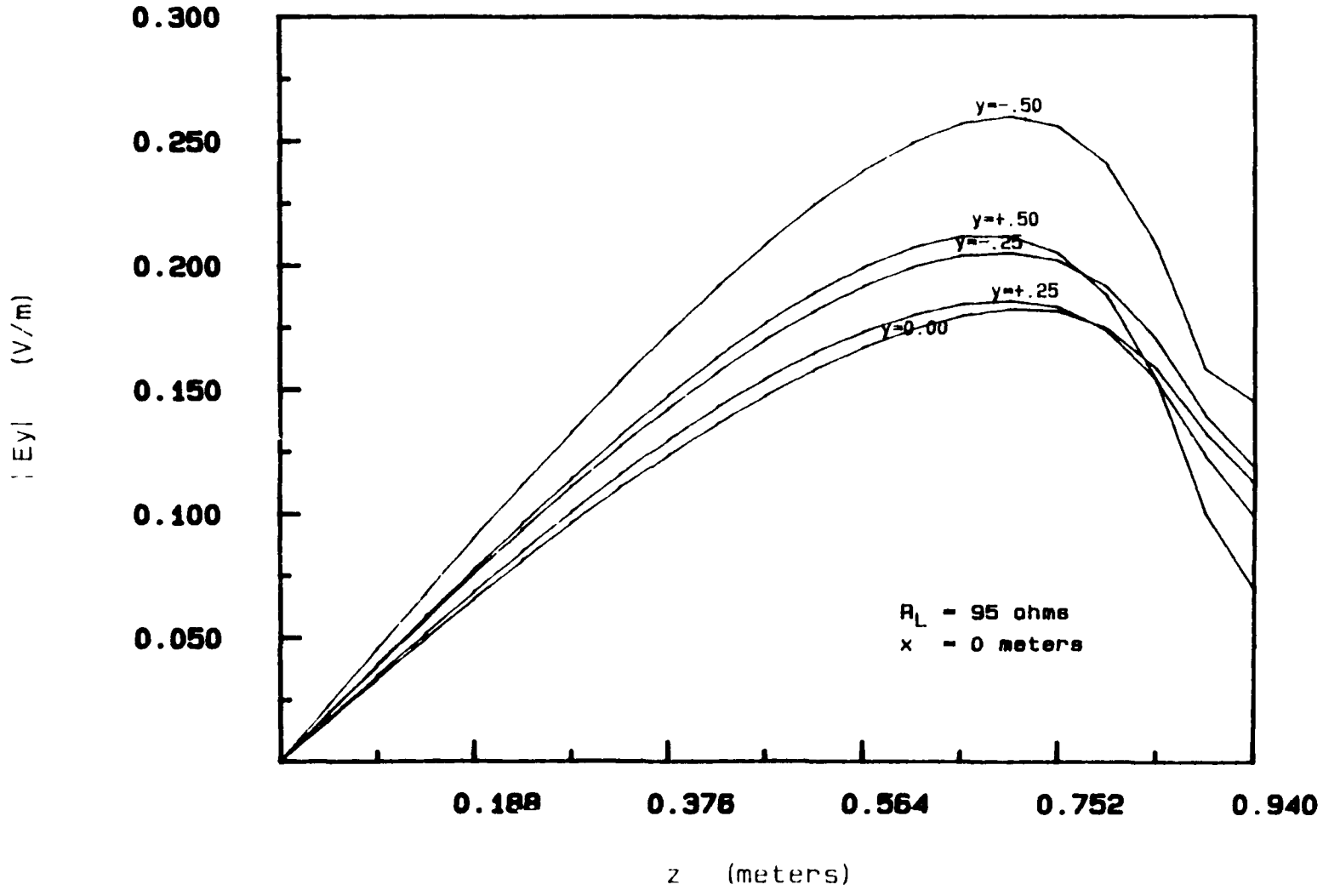

Figure 16. **Magnitude of the longitudinal E-field computed along the vertical direction at various longitudinal positions due to a 125 MHz unit-amplitude excitation.**

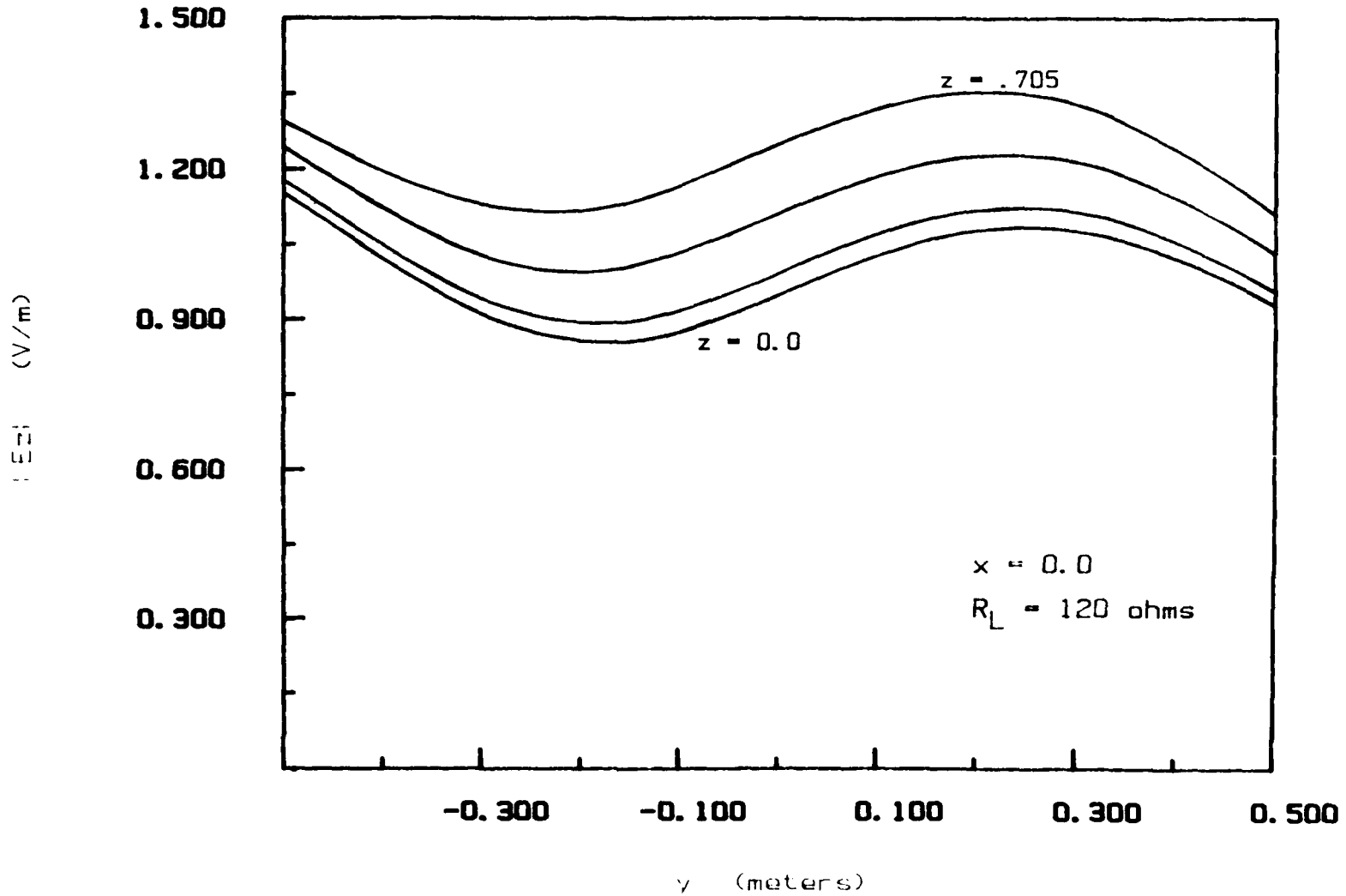

(a) Magnitude 0f E_z

Figure 17. **Vertical E-field computed along the longitudinal direction at various heights in the parallel-plate region of the 450 MHz bandwidth EMP simulator due to a 158.6 MHz unit-amplitude excitation.**

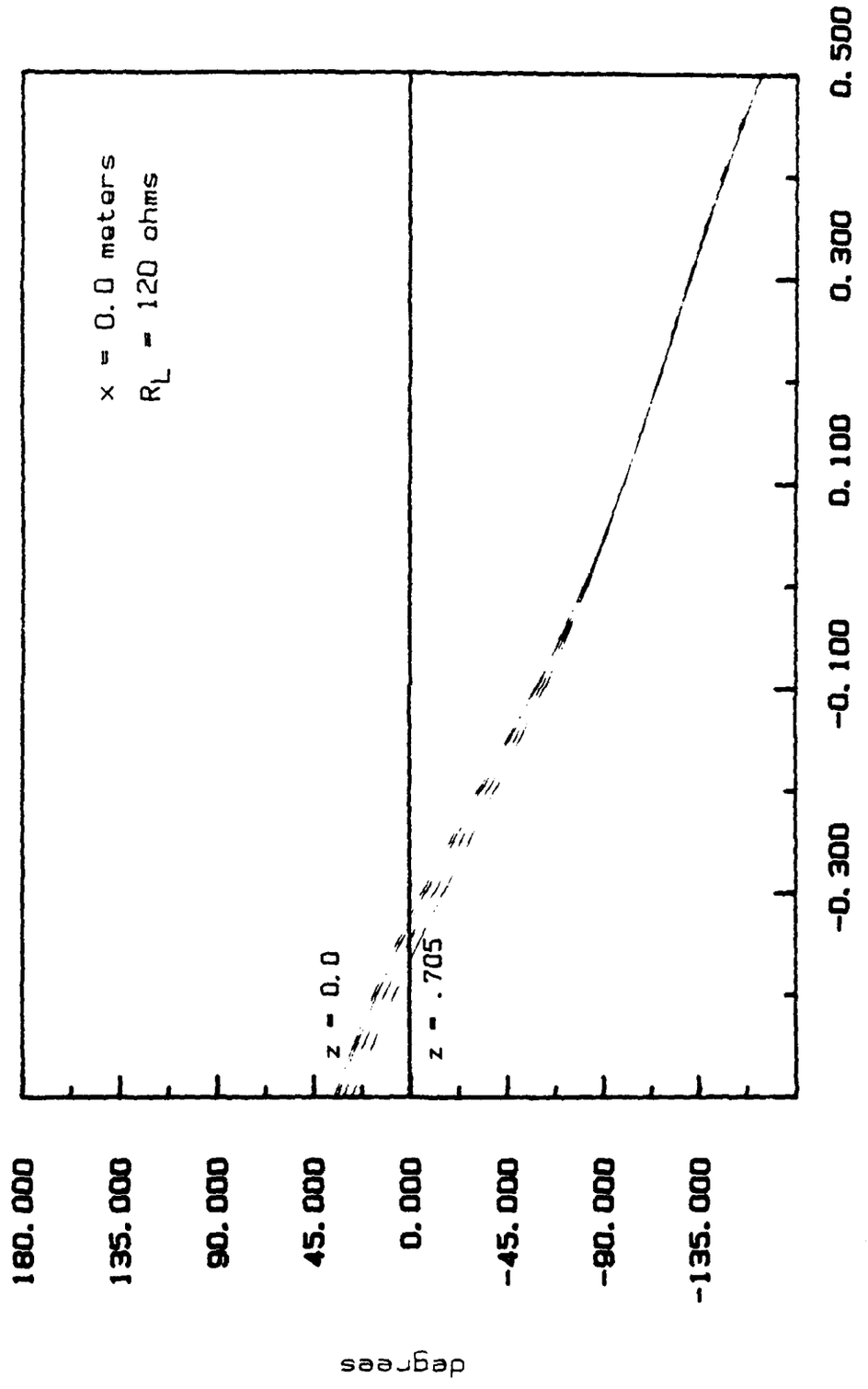

(b) Phase of E_z

Figure 17. (Cont'd).

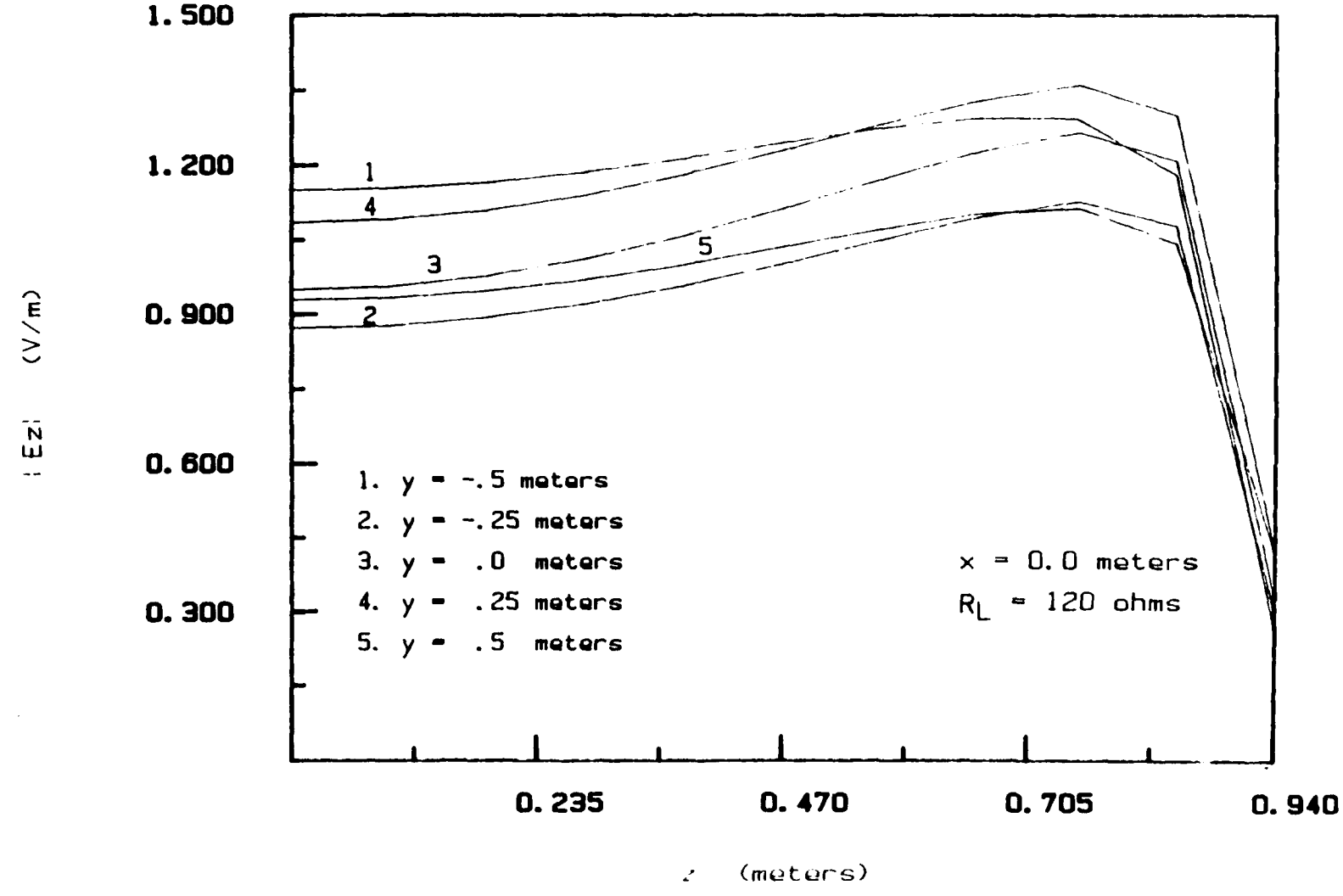

Figure 18. Magnitude of the vertical E-field computed along the vertical direction at various longitudinal positions in the parallel-plate region of the 450 MHz bandwidth EMP simulator due to a 158.6 MHz unit-amplitude excitation.

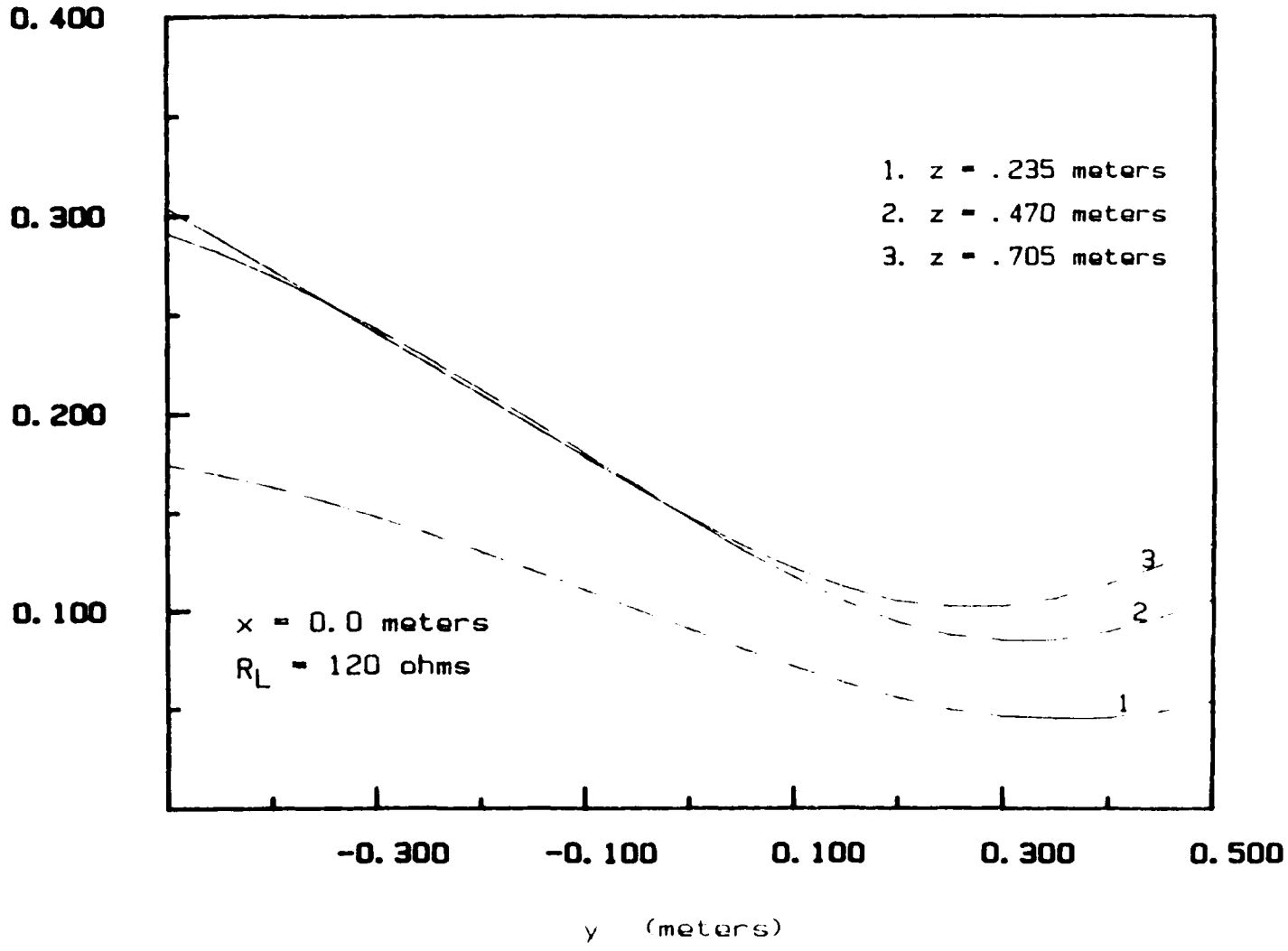

(a) Magnitude of E_z

Figure 19. Longitudinal E-field computed along the longitudinal direction at various heights in the parallel-plate region of the 450 MHz bandwidth EMP simulator due to a 158.6 MHz unit-amplitude excitation.

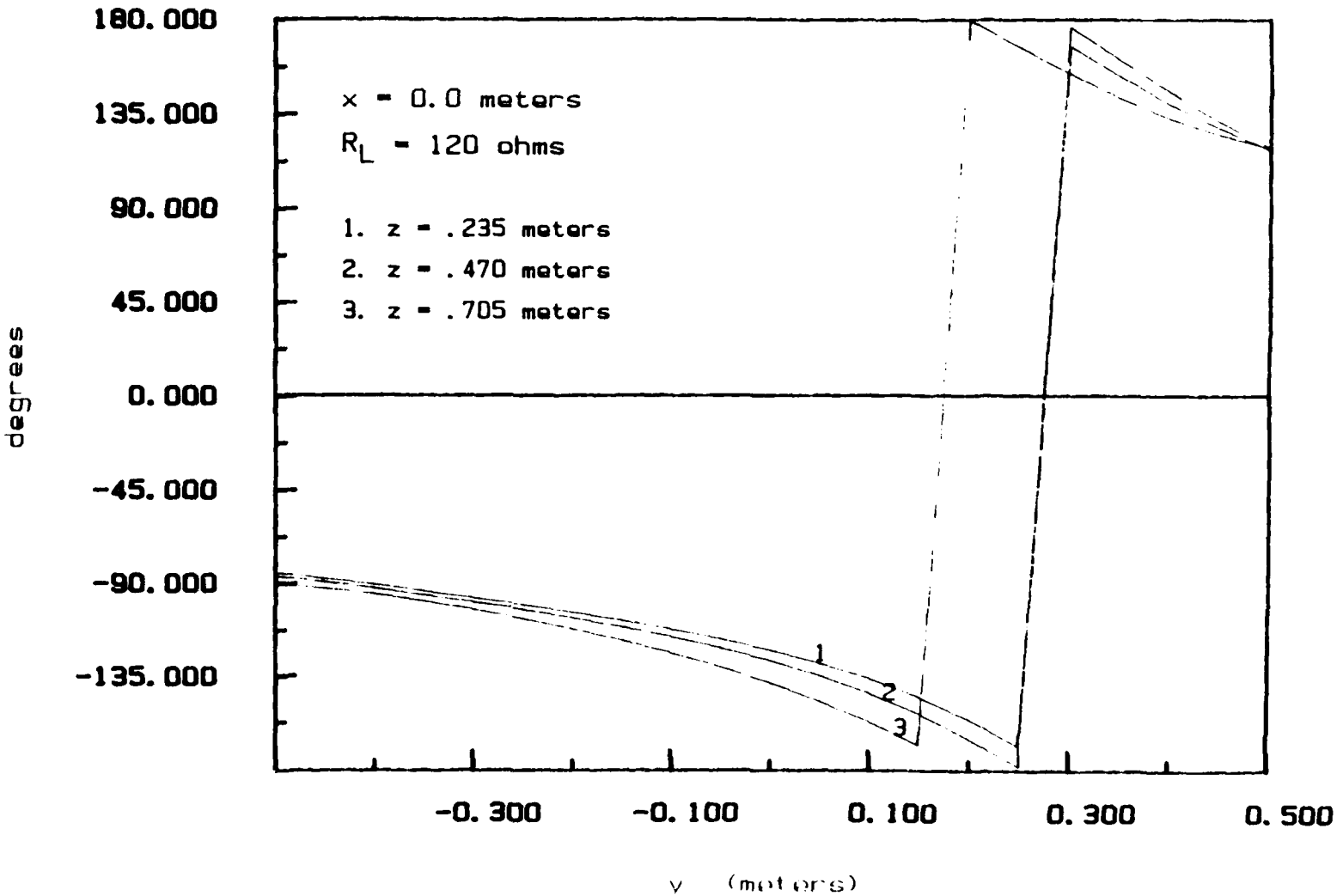

(b) Phase of E_y.

Figure 19. (Cont'd).

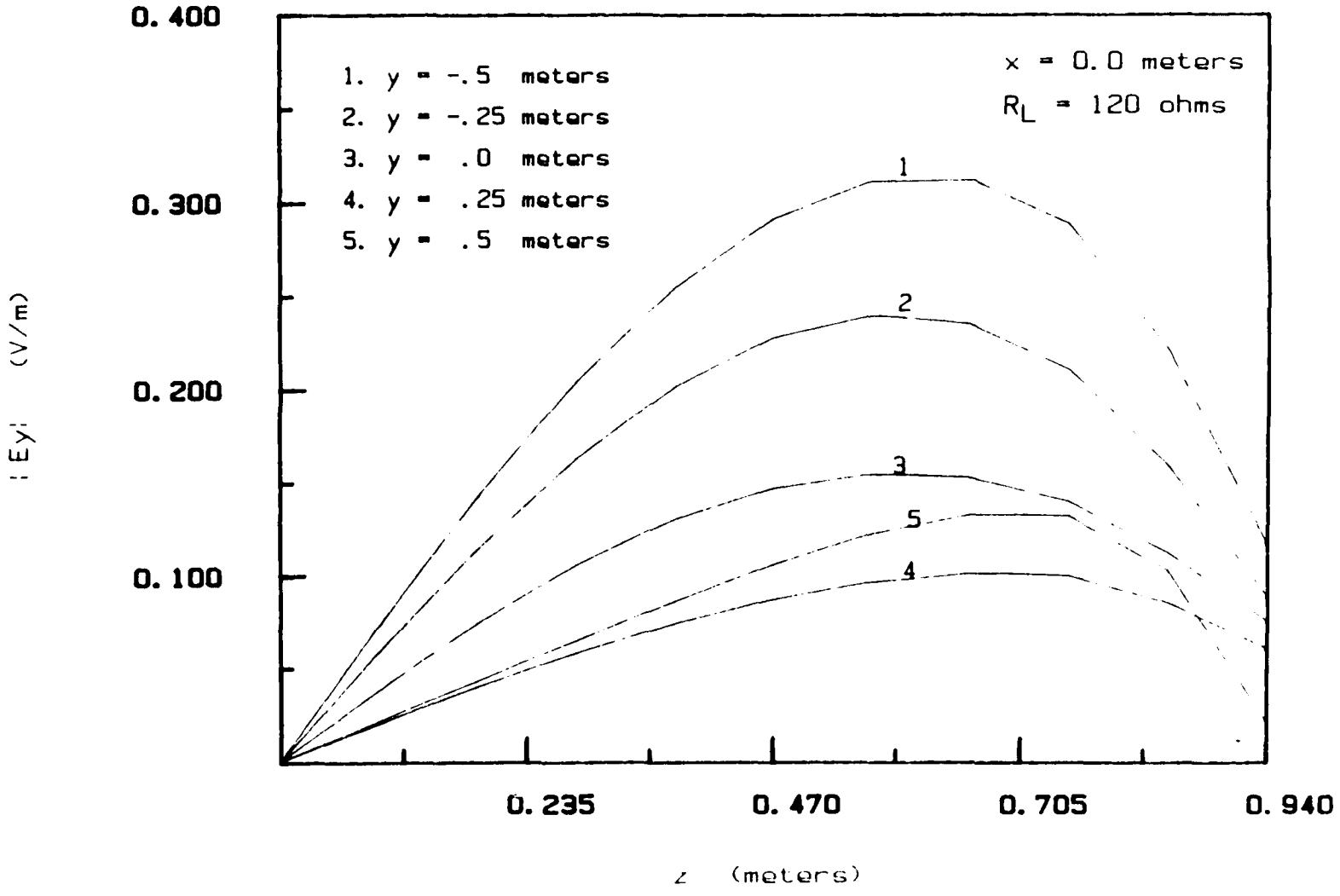

Figure 20. **Magnitude of the longitudinal E-field computed along the vertical direction at various longitudinal positions in the parallel-plate region of the 450 MHz bandwidth EMP simulator due to a 158.6 MHz unit-amplitude excitation.**

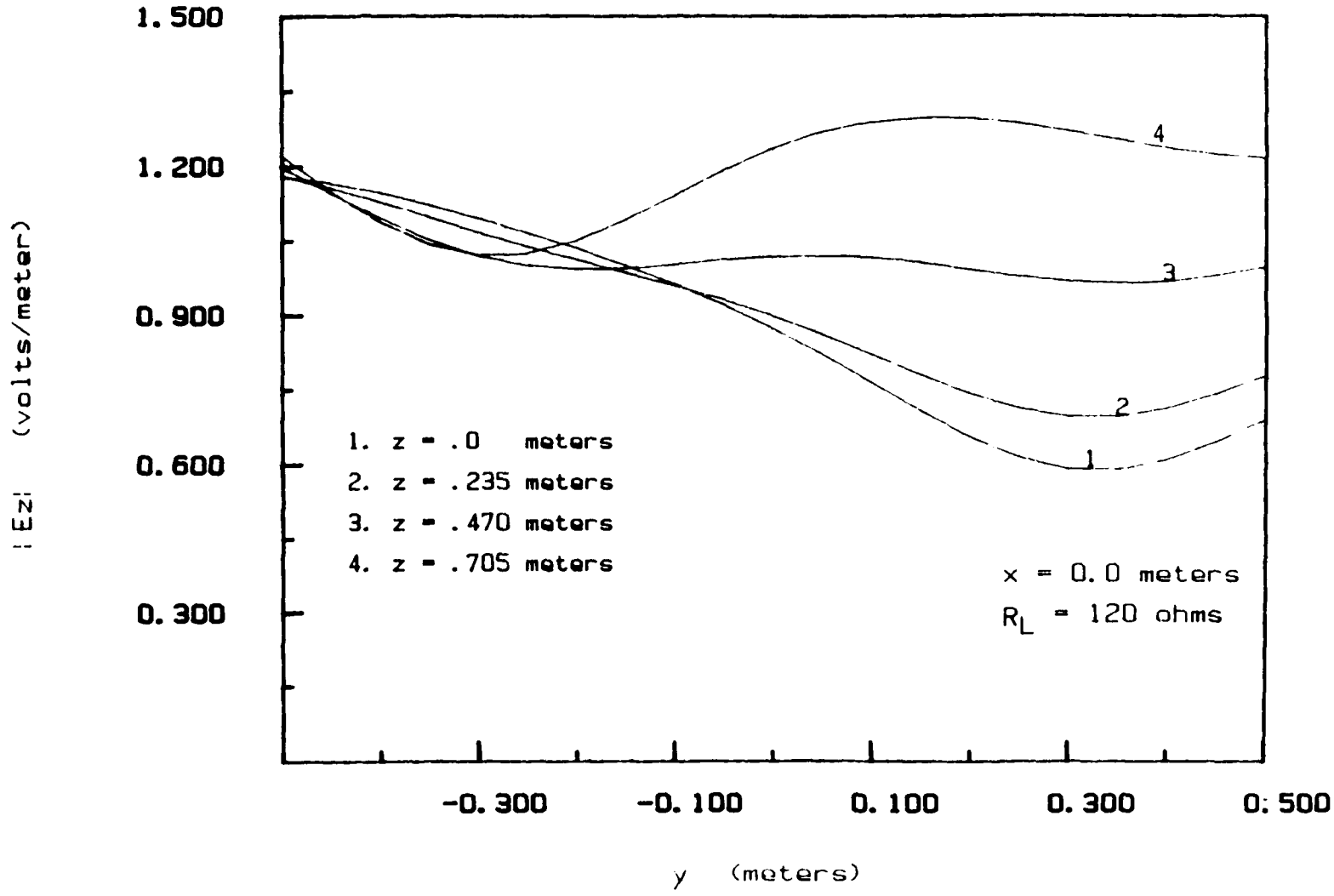

(a) Magnitude of E_z

Figure 21. Vertical E-field computed along the longitudinal direction at various heights in the parallel-plate region of the 450 MHz bandwidth EMP simulator due to a 203 MHz unit-amplitude excitation.

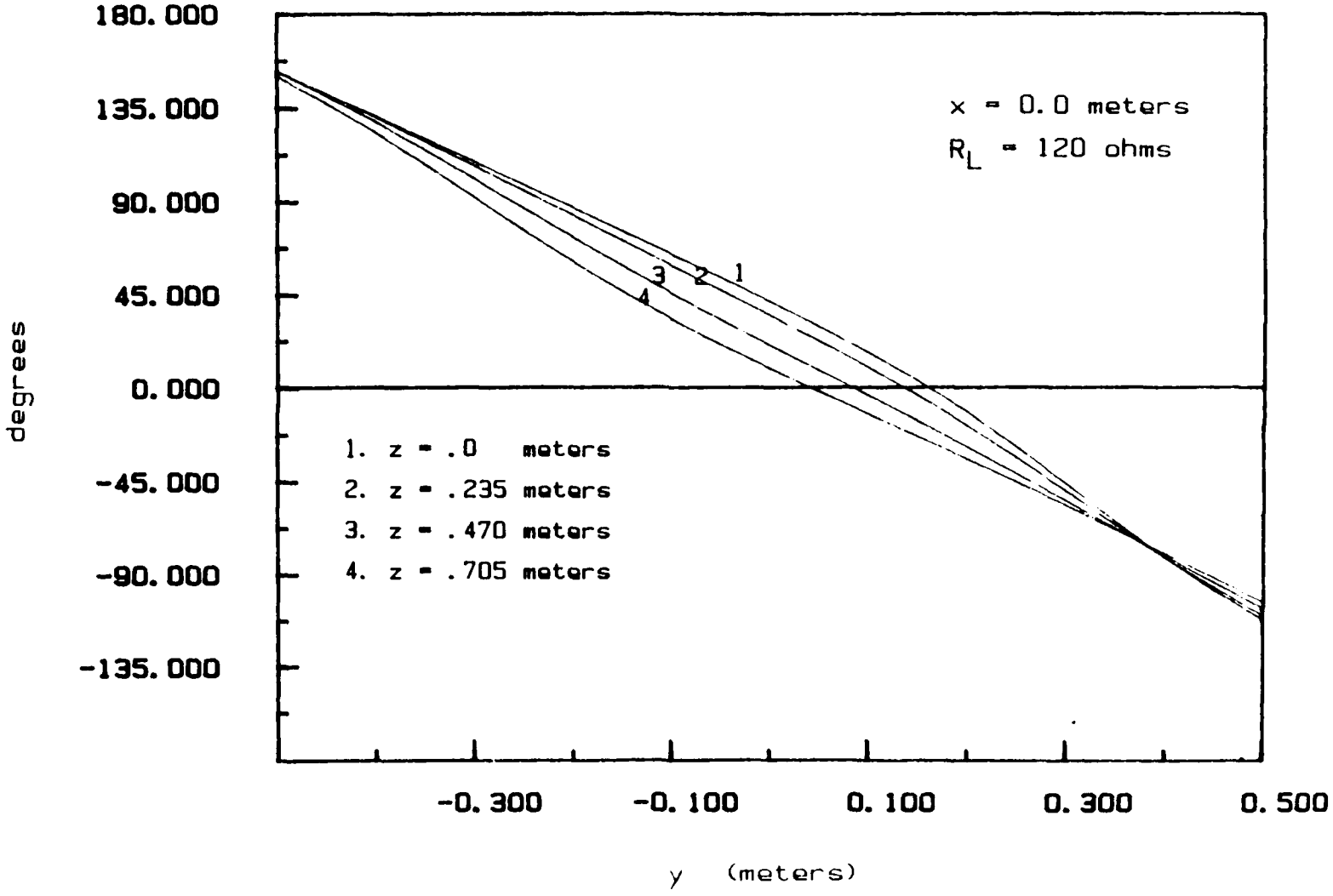

(b) Phase of E_z.

Figure 21. (Cont'd).

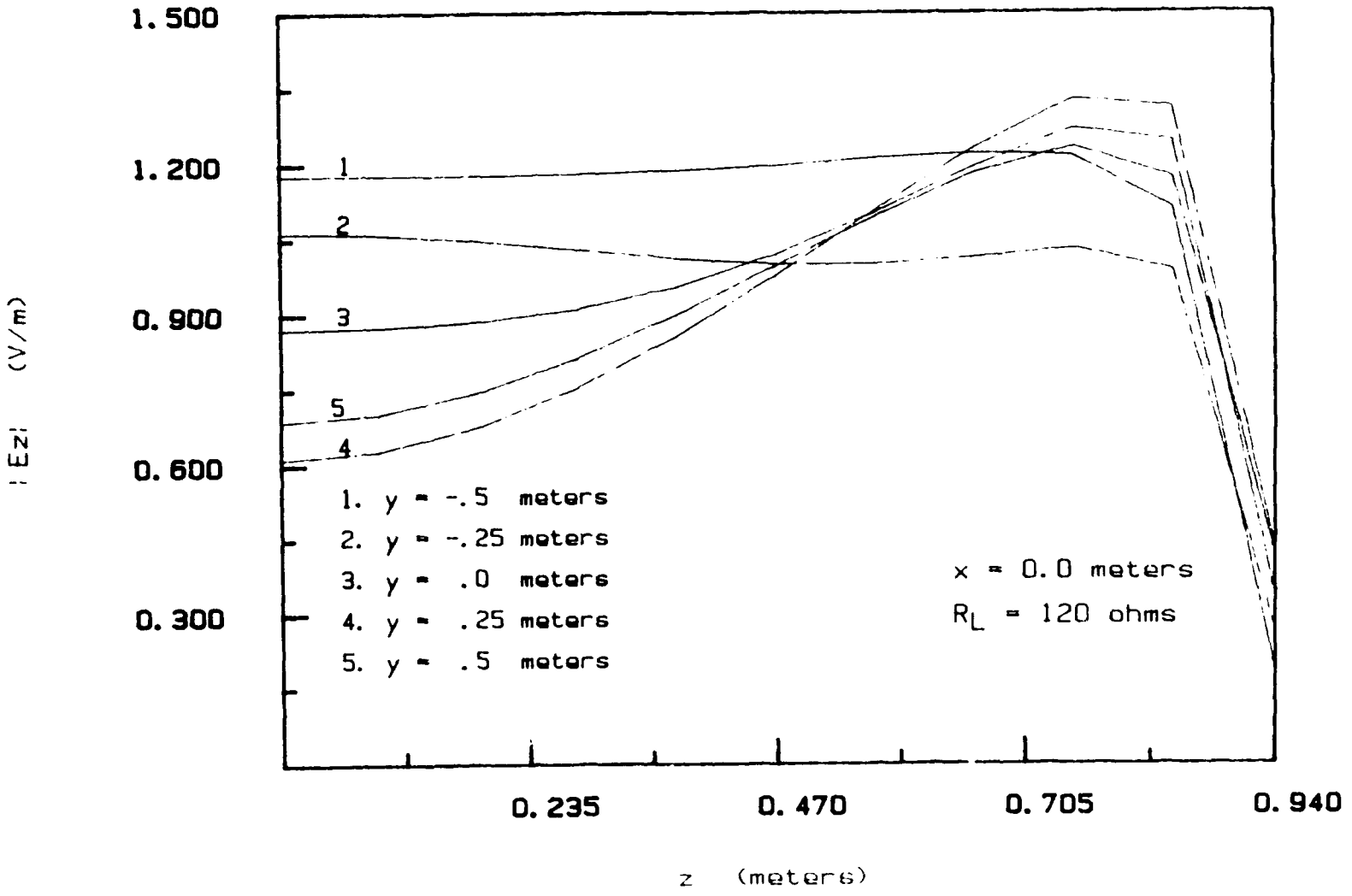

Figure 22. Magnitude of the vertical E-field computed along the vertical direction at various longitudinal positions in the parallel-plate region of the 450 MHz bandwidth EMP simulator due to a 203 MHz unit-amplitude excitation.

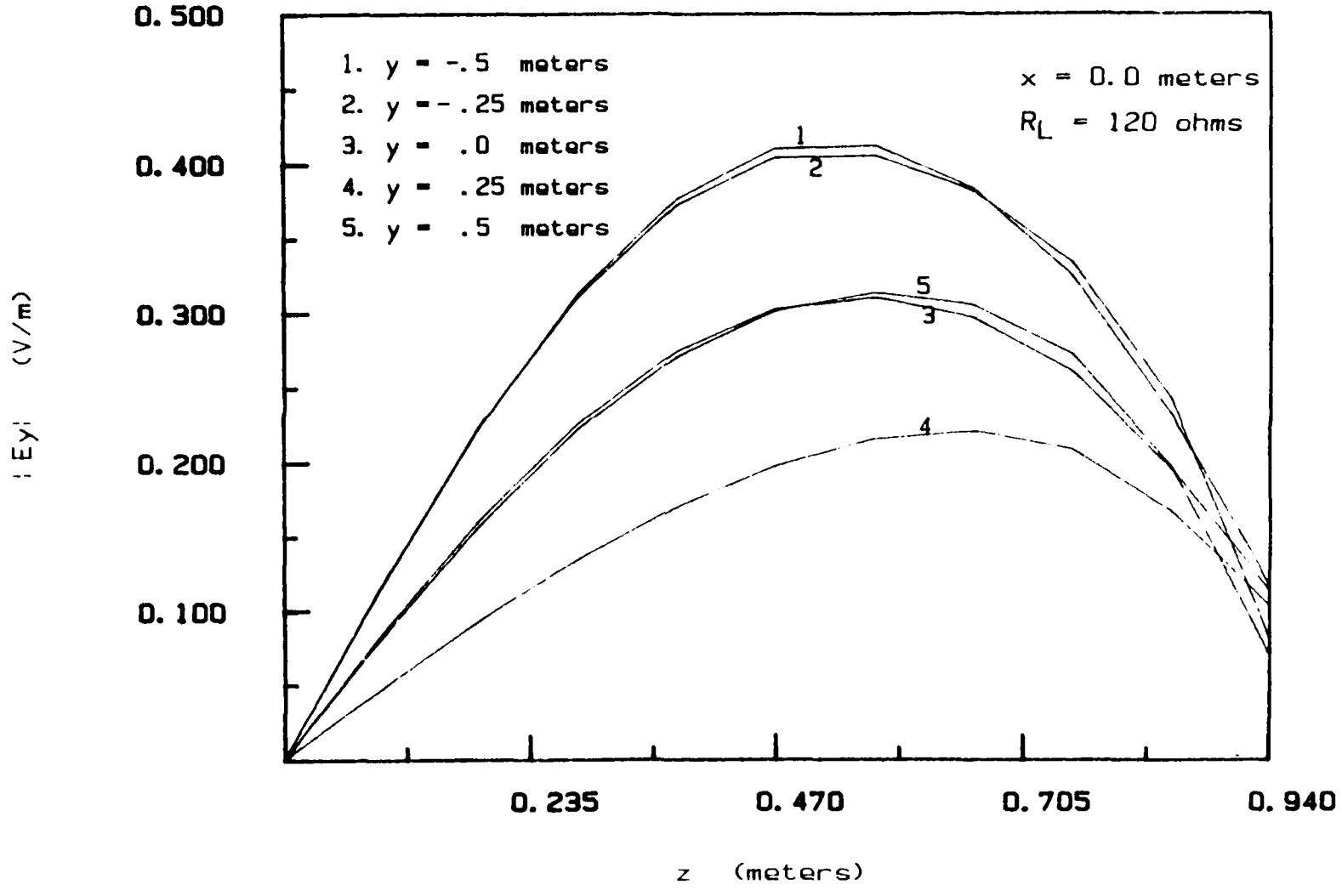

Figure 23. **Magnitude of the longitudinal E-field computed along the vertical direction at various longitudinal positions in the parallel-plate region of the 450 MHz bandwidth EMP simulator due to a 203 MHz unit-amplitude excitation.**

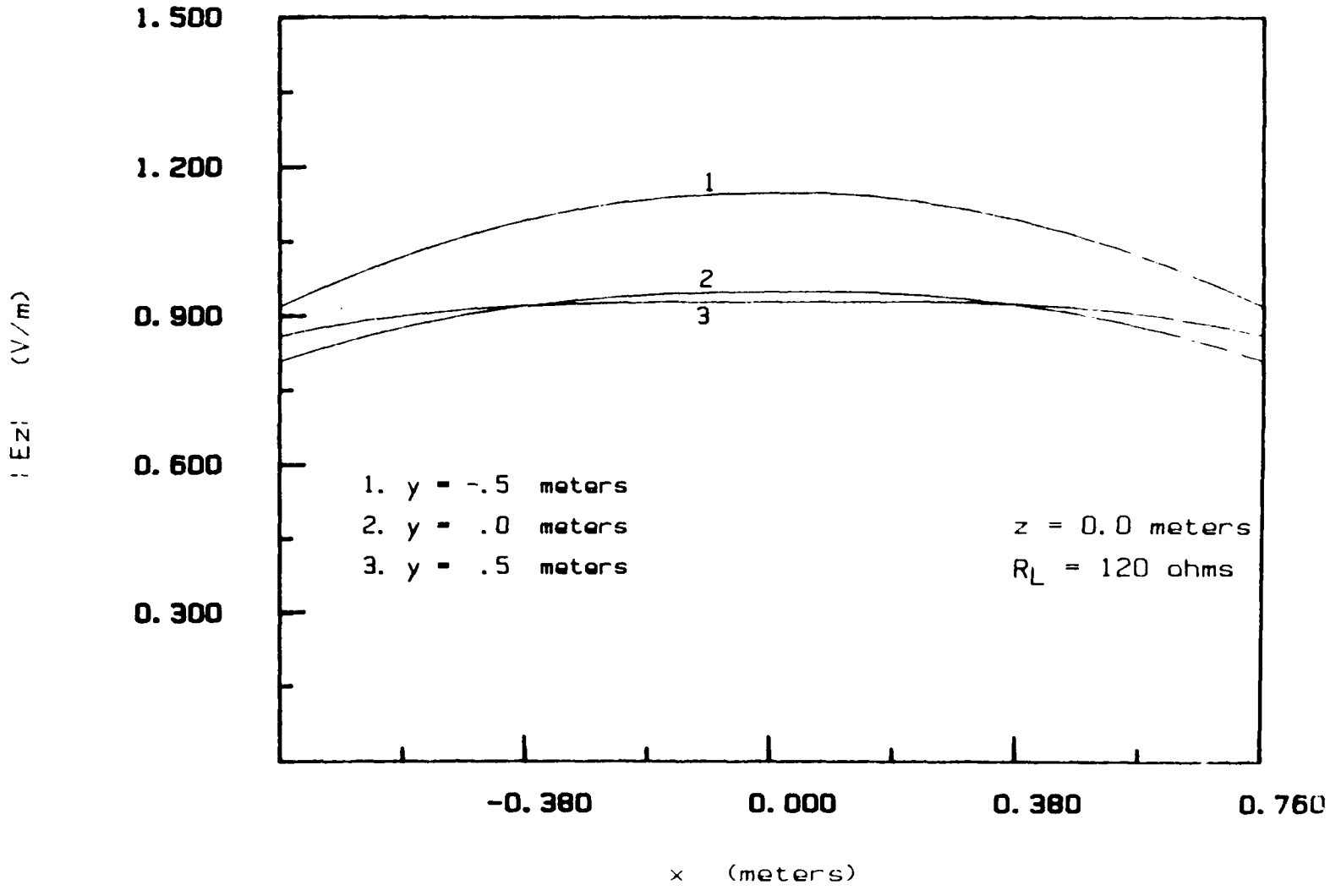

Figure 24. Magnitude of the vertical E-field computed along the ground plane along the transverse direction at various longitudinal positions due to a 158.6 MHz unit-amplitude excitation.

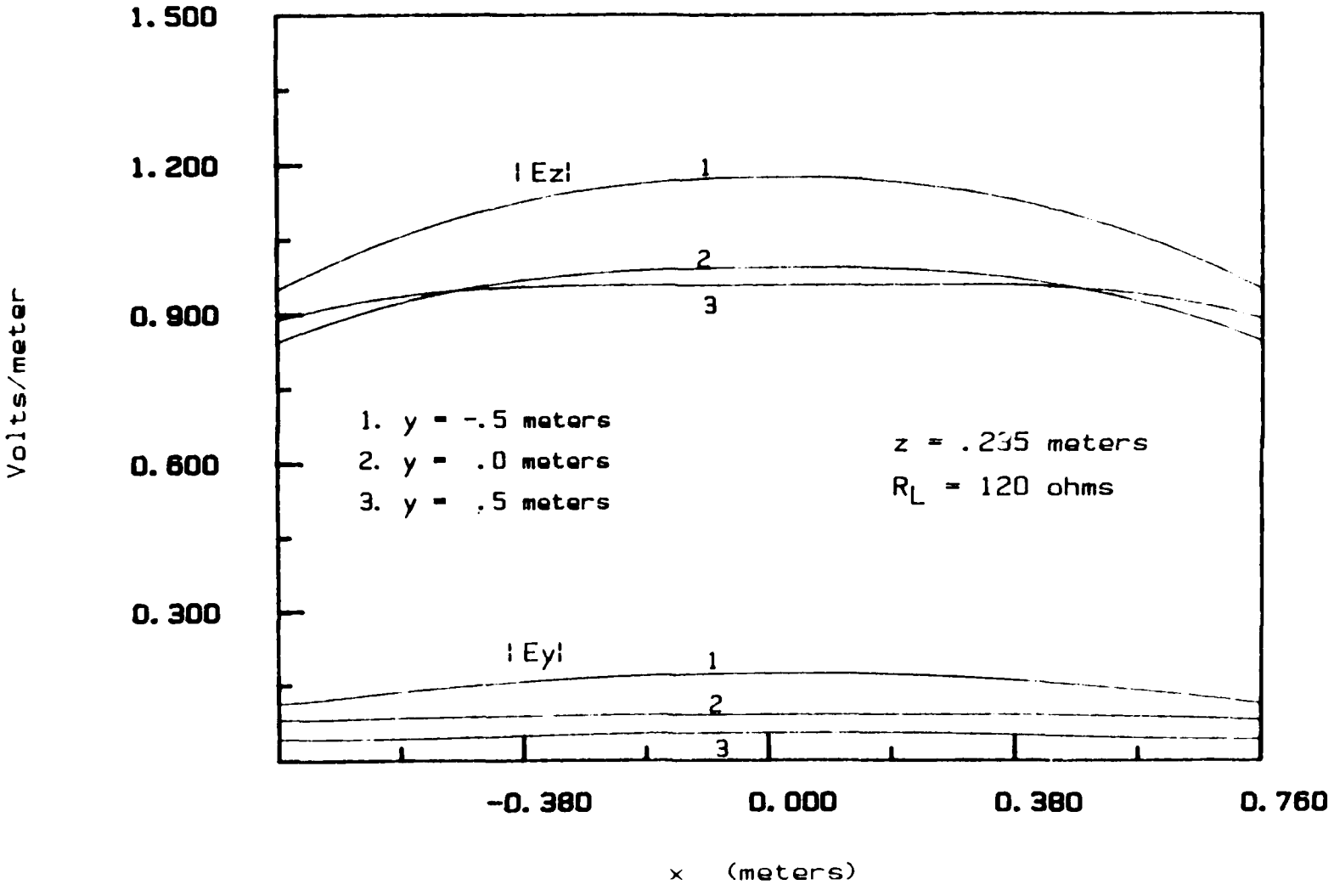

Figure 25. **Magnitude of the vertical and longitudinal E-field computed at z = 0.235 m along the transverse direction at various longitudinal positions due to a 158.6 MHz unit-amplitude excitation.**

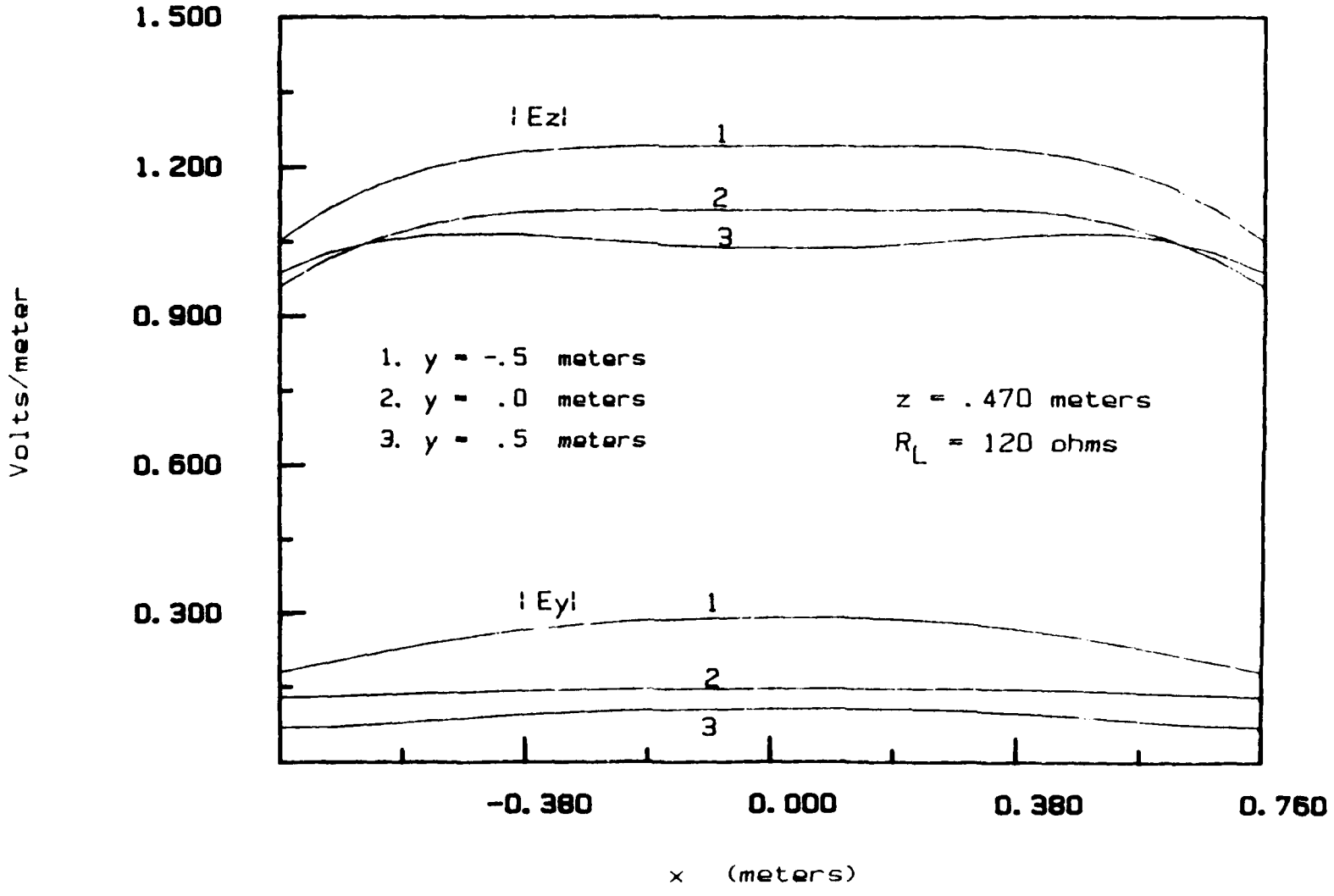

Figure 26. **Magnitude of the vertical and longitudinal E-field computed at z = 0.470 m along the transverse direction at various longitudinal positions due to a 158.6 MHz unit-amplitude excitation.**

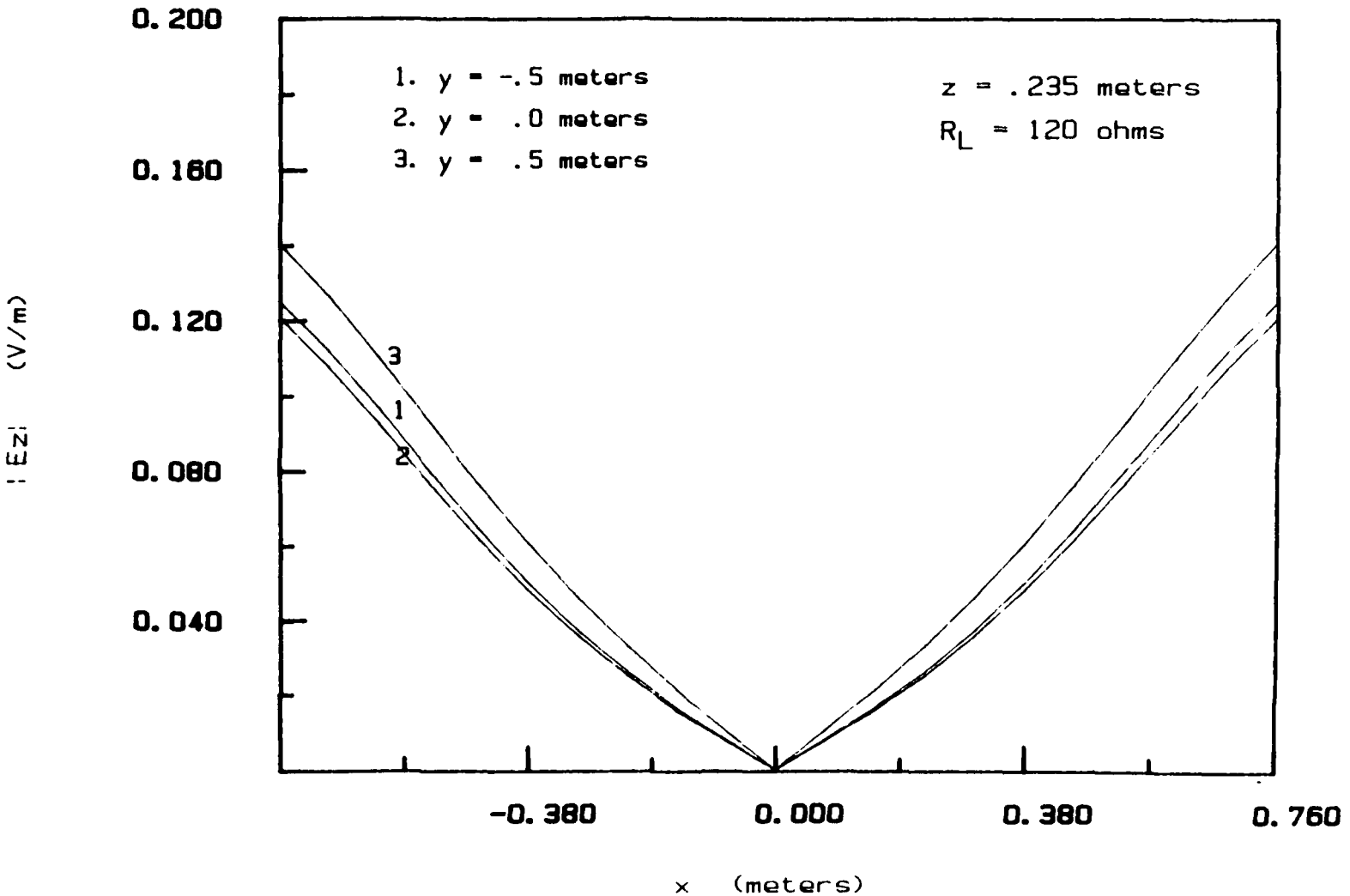

Figure 27. **Magnitude of the transverse E-field computed at z = 0.235 m along the transverse direction at various longitudinal positions due to a 158.6 MHz unit-amplitude excitation.**

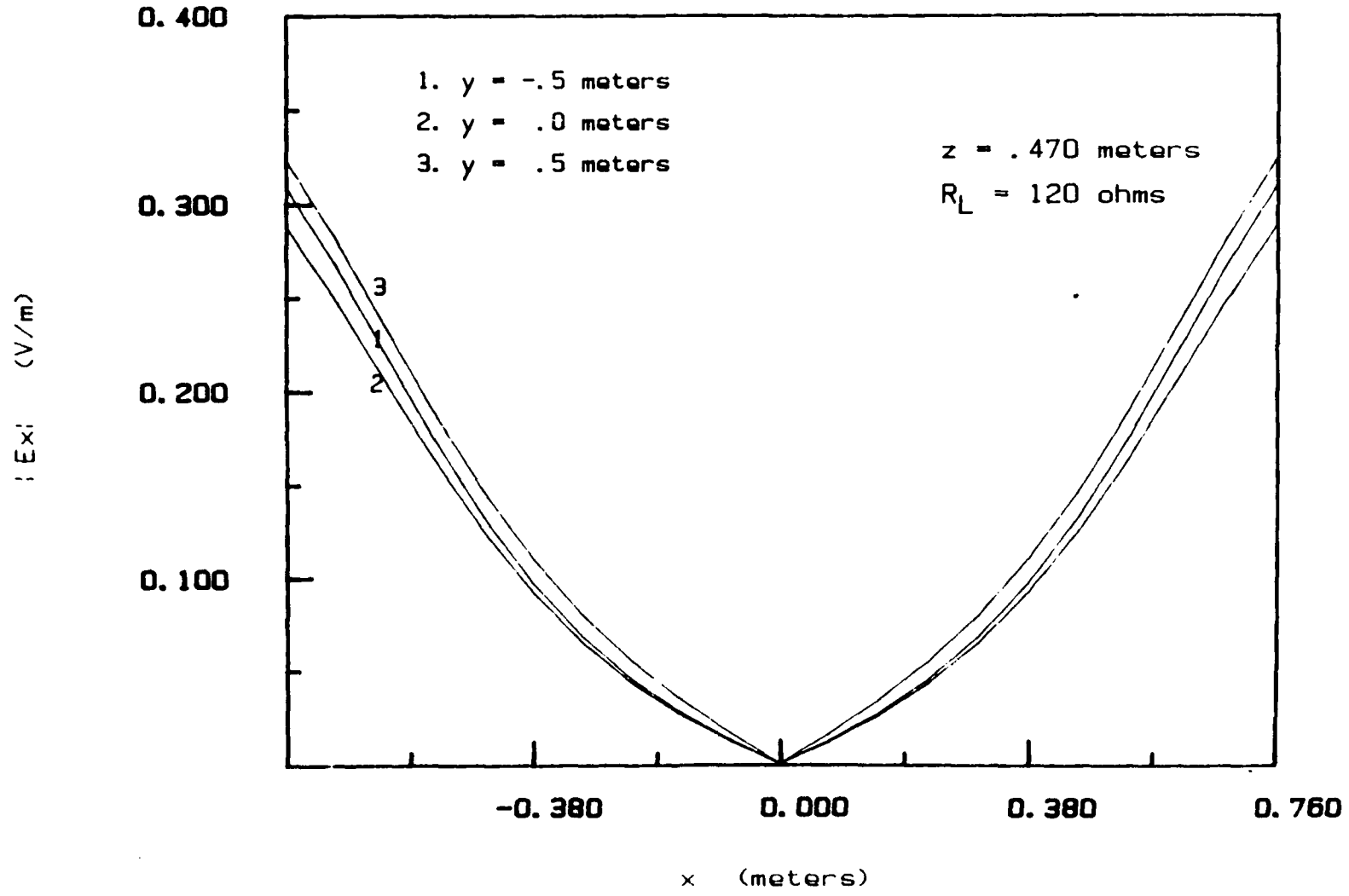

Figure 28. **Magnitude of the transverse E-field computed at z = 0.470 m along the transverse direction at various longitudinal positions due to a 158.6 MHz unit-amplitude excitation.**

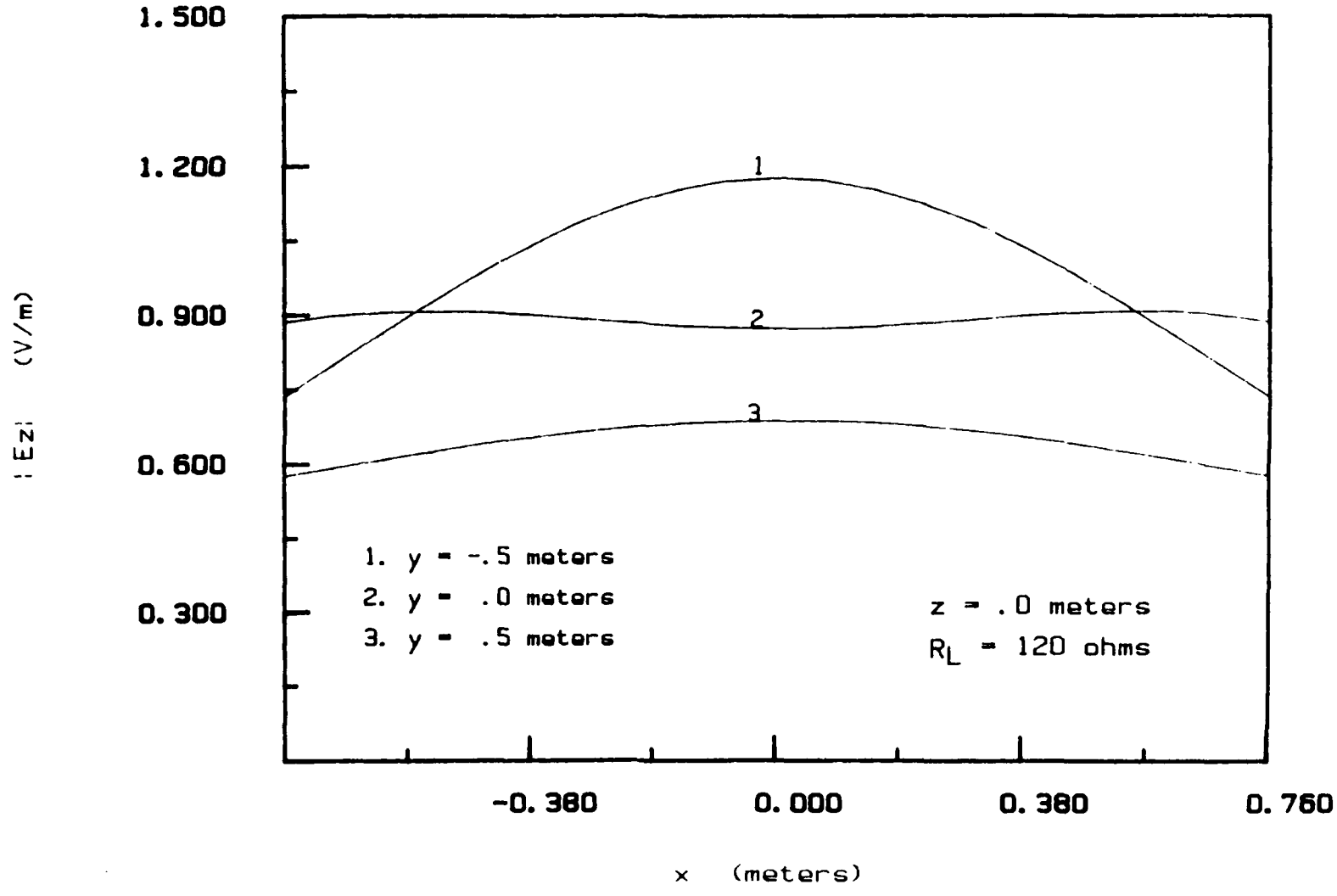

Figure 29. Magnitude of the vertical E-field computed on the ground plane along the transverse direction at various longitudinal positions due to a 203 MHz unit-amplitude excitation.

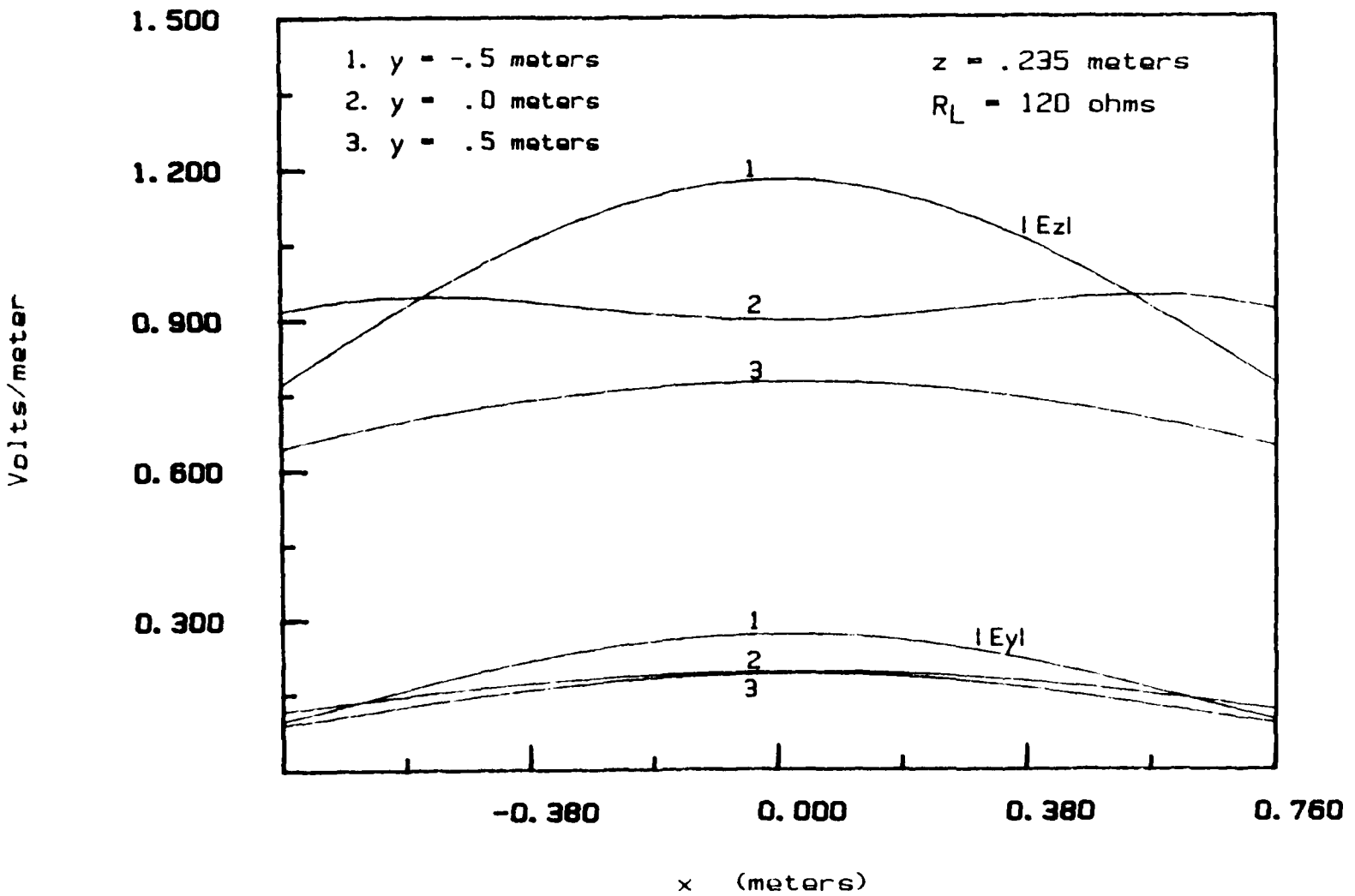

Figure 30. Magnitude of the vertical and longitudinal E-fields computed at z = 0.235 m along the transverse direction at various longitudinal positions due to a 203 MHz unit-amplitude excitation.

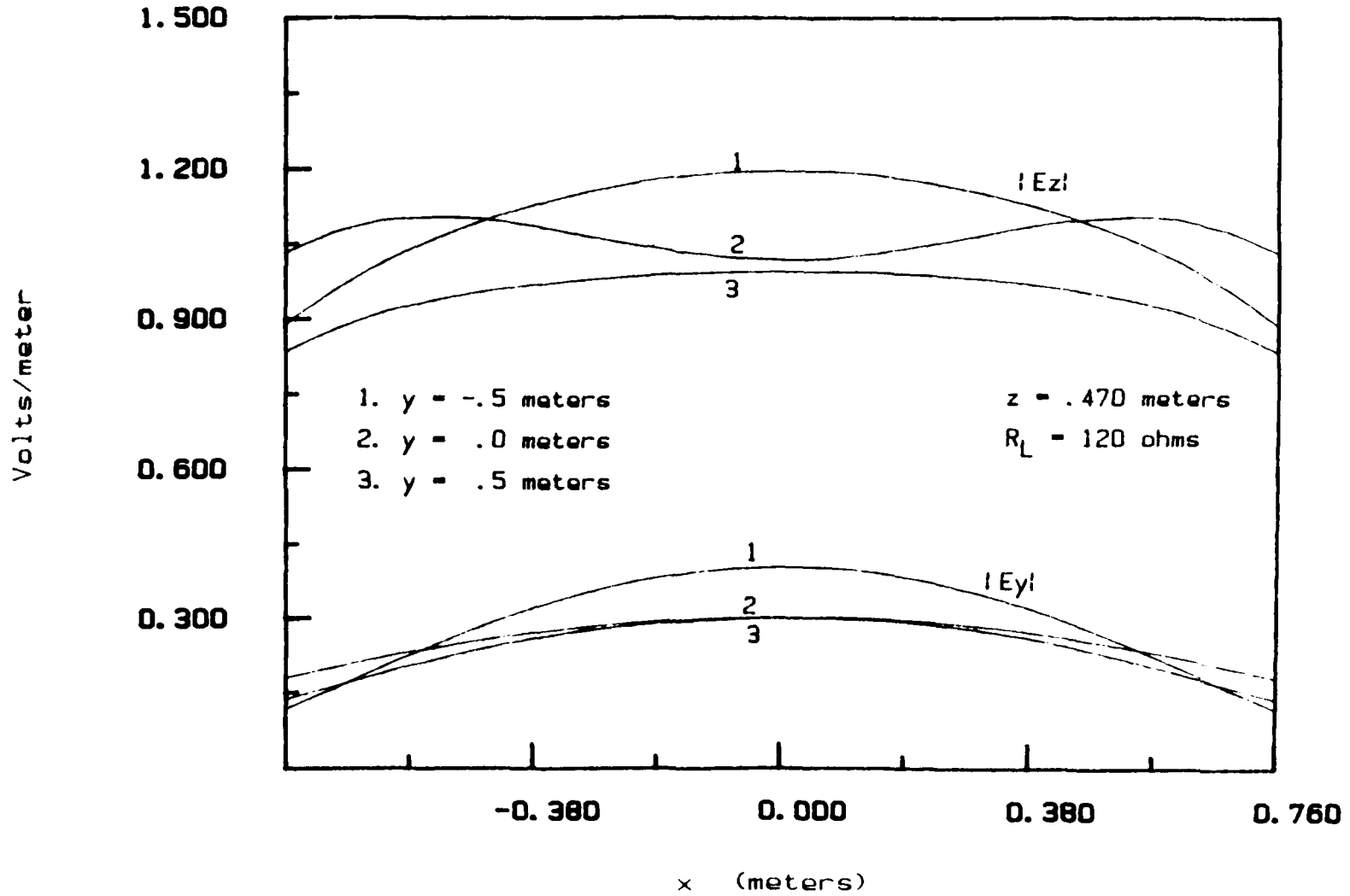

Figure 31. **Magnitude of the vertical and longitudinal E-fields computed at z = 0.470 m along the transverse direction at various longitudinal positions due to a 203 MHz unit-amplitude excitation.**

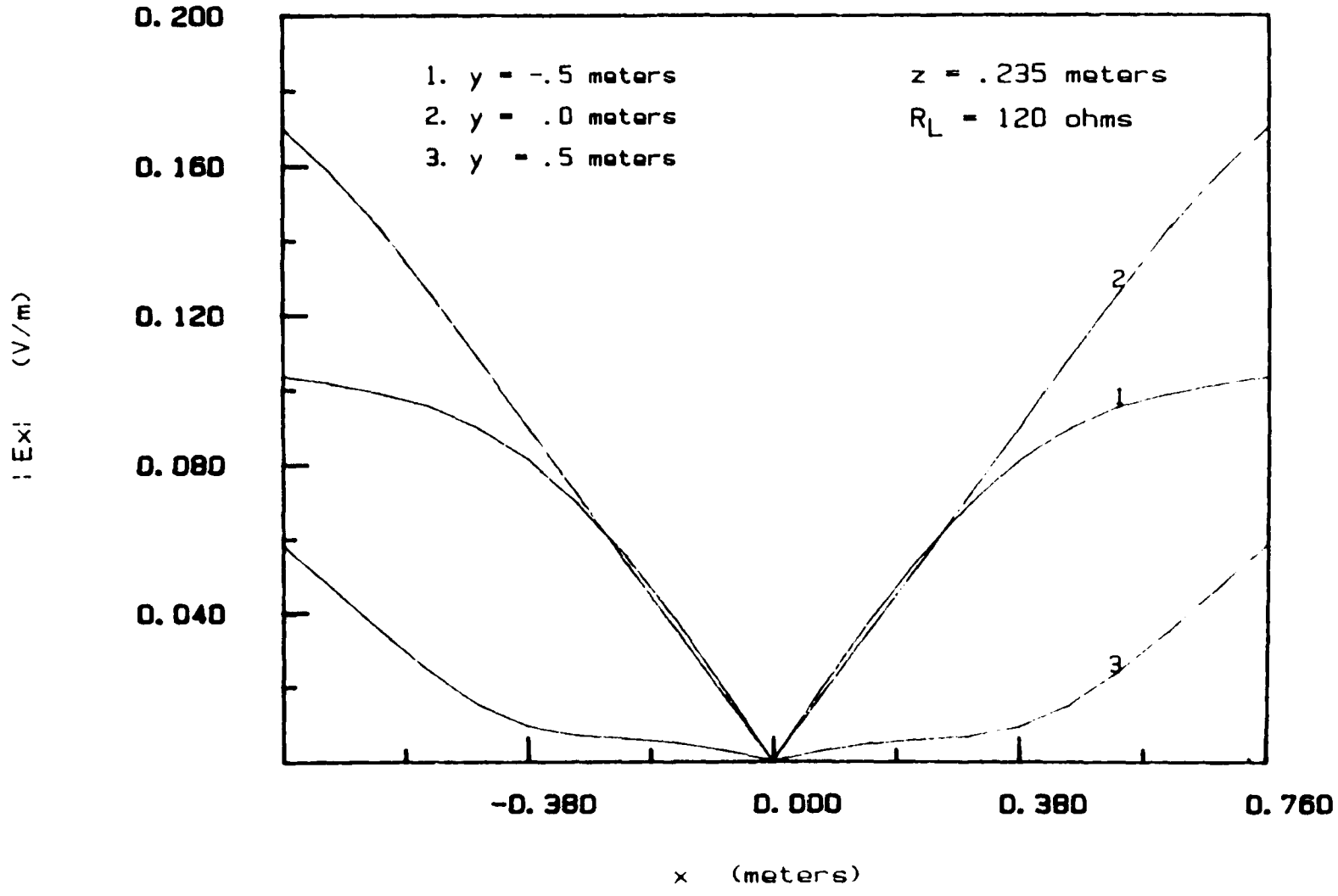

Figure 32. Magnitude of the transverse E-field computed at z = 0.235 m along the transverse direction at various longitudinal positions due to a 203 MHz unit-amplitude excitation.

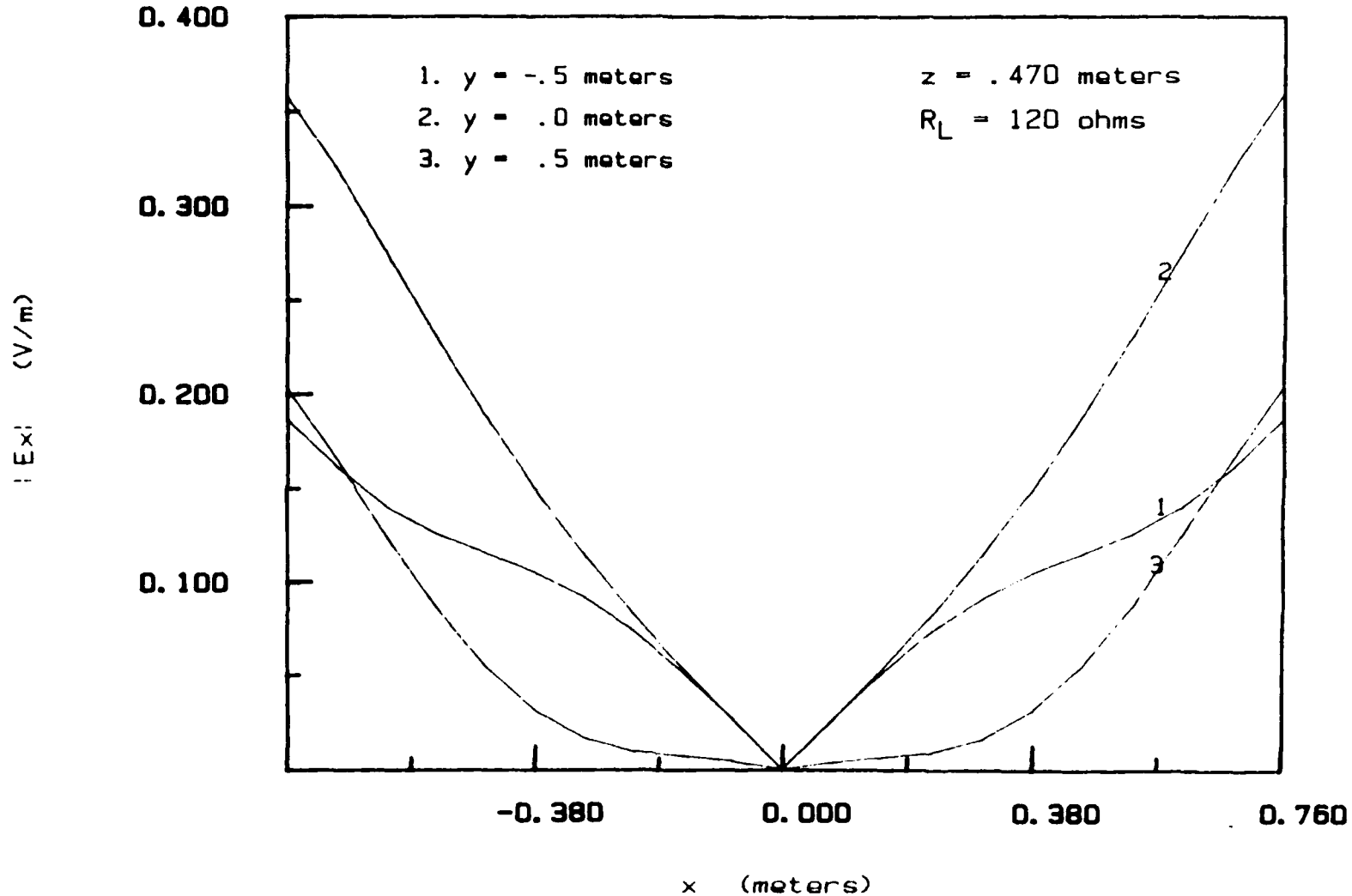

Figure 33. Magnitude of the transverse E-field computed at z = 0.470 m along the transverse direction at various longitudinal positions due to a 203 MHz unit-amplitude excitation.

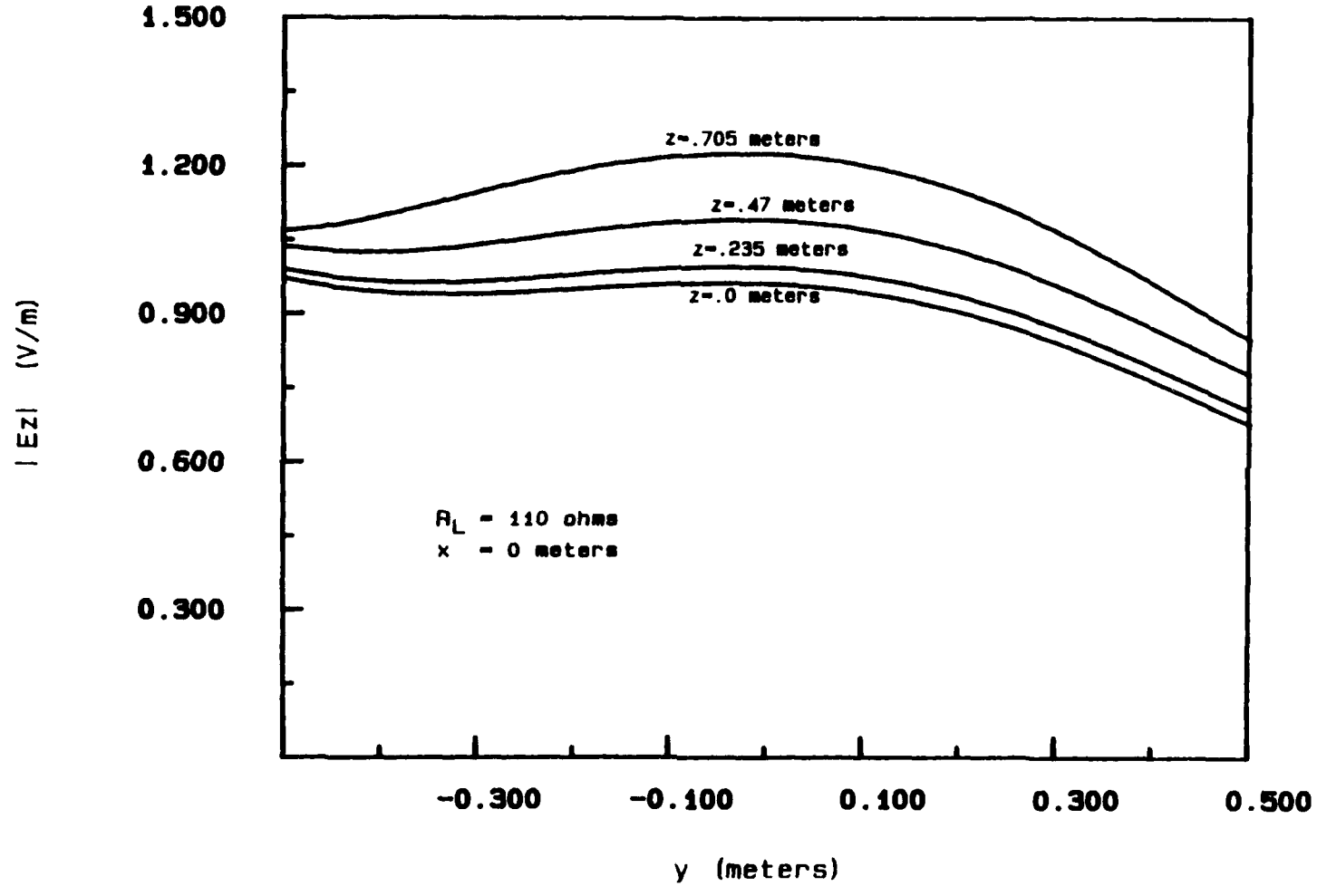

(a) Magnitude of E_z

Figure 34. Vertical E-field computed along the longitudinal direction at various heights in the parallel-plate region of the 200 MHz bandwidth ACHATES simulator due to a 100 MHz unit-amplitude excitation.

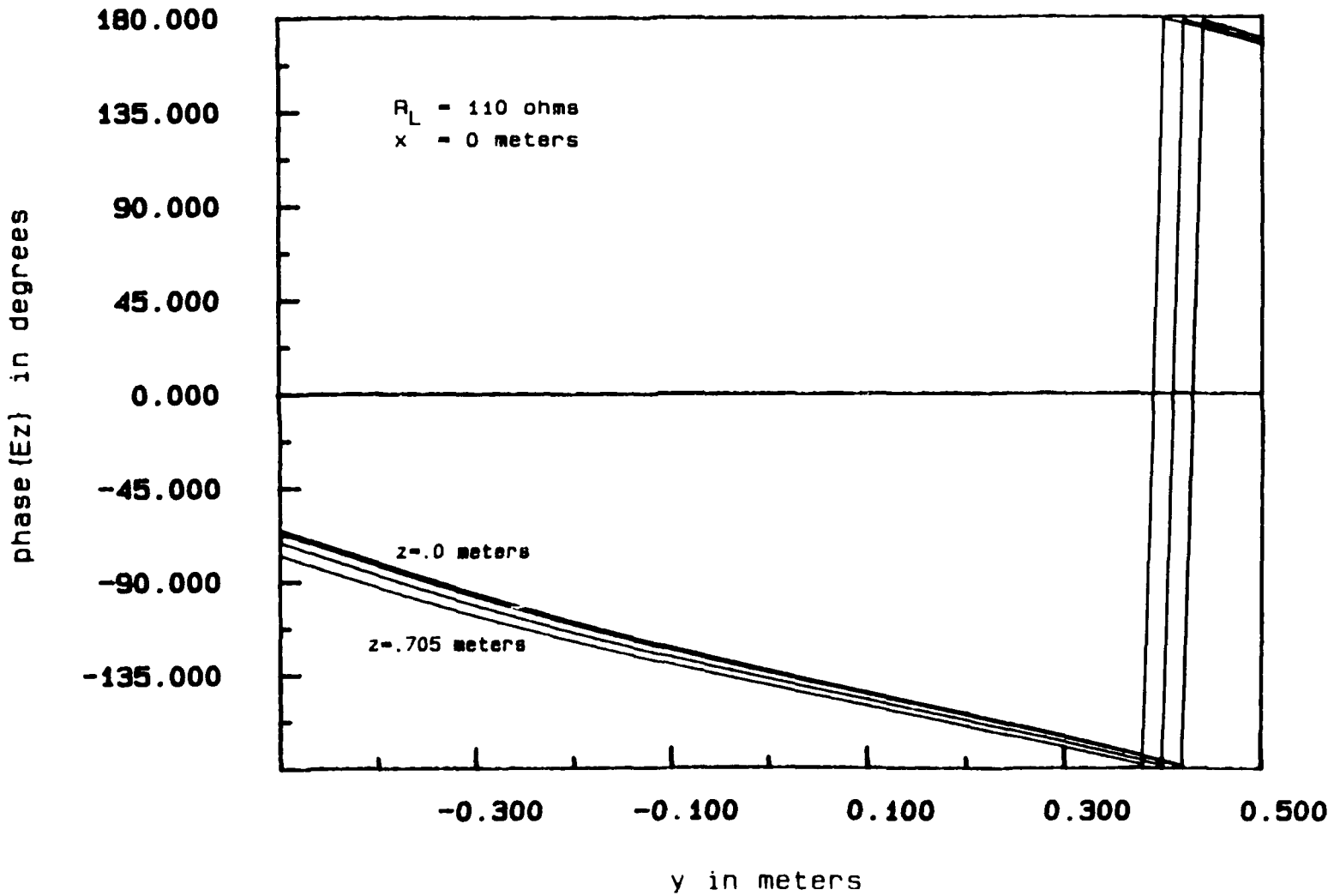

(b) Phase of E_z.

Figure 34. (Cont'd).

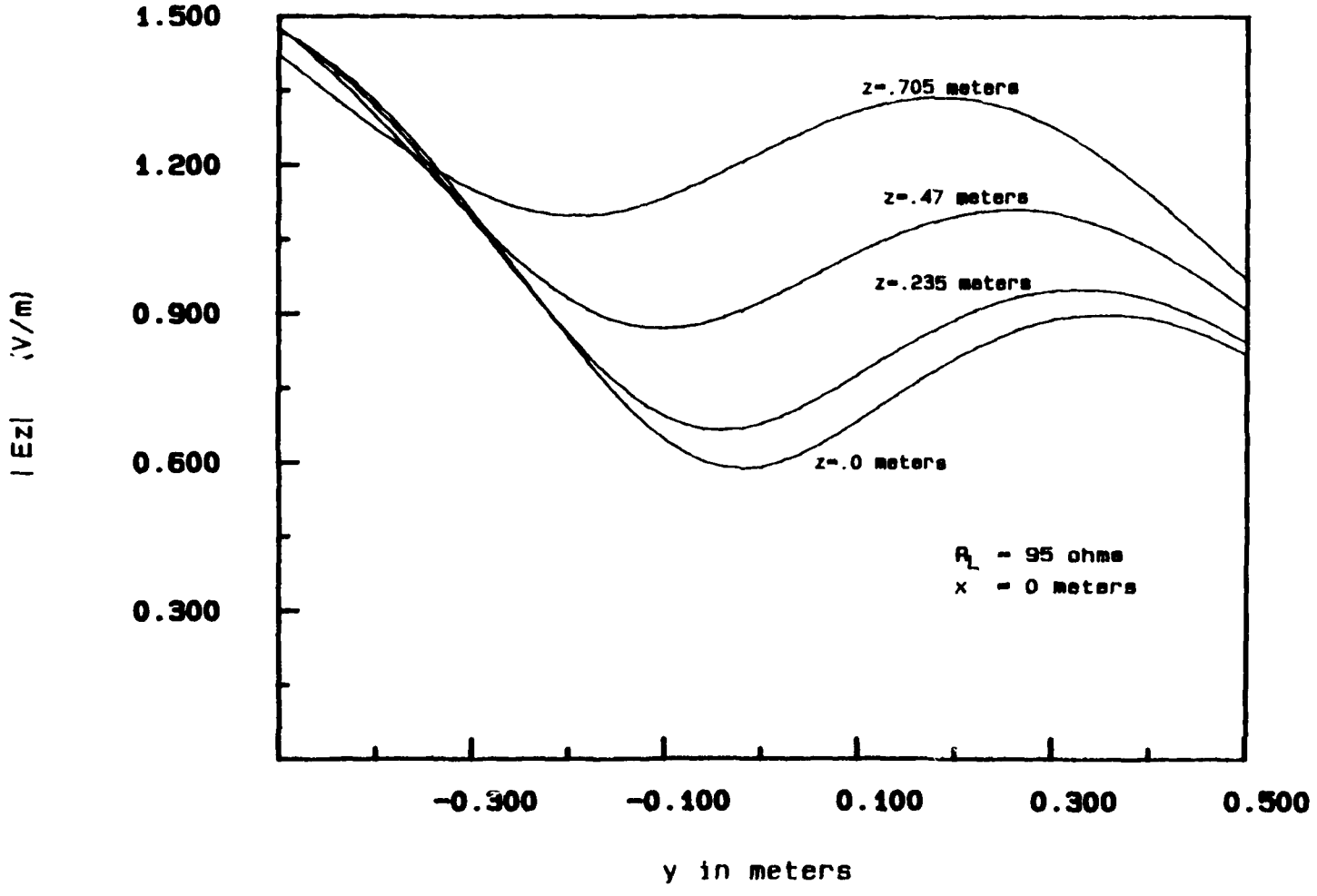

(a) Magnitude of E_z

Figure 35. Vertical E-field computed along the longitudinal direction at various heights in the parallel-plate region of the 200 MHz bandwidth ACHATES simulator due to a 175 MHz unit-amplitude excitation.

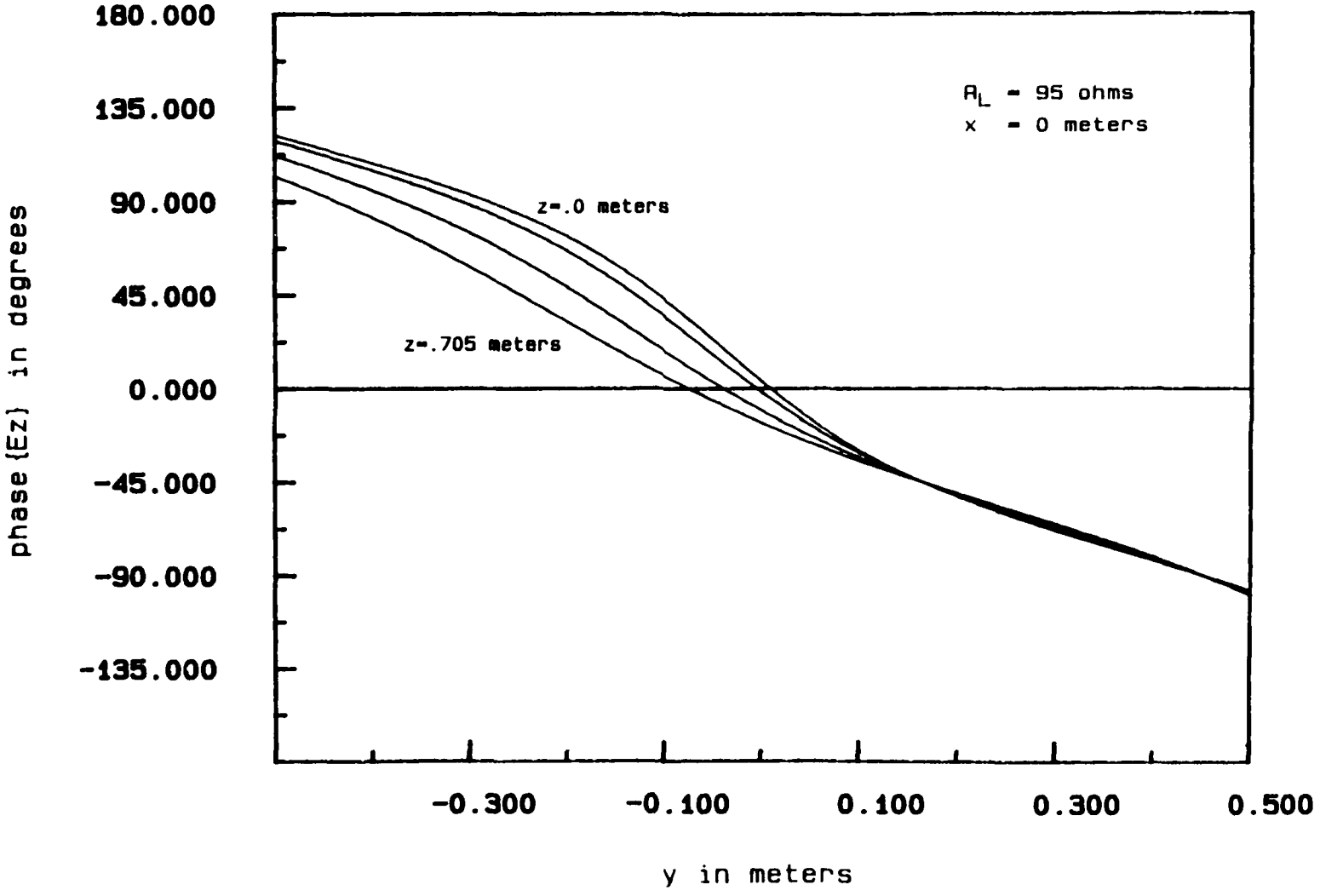

(b) Phase of E_z.

Figure 35. (Cont'd).

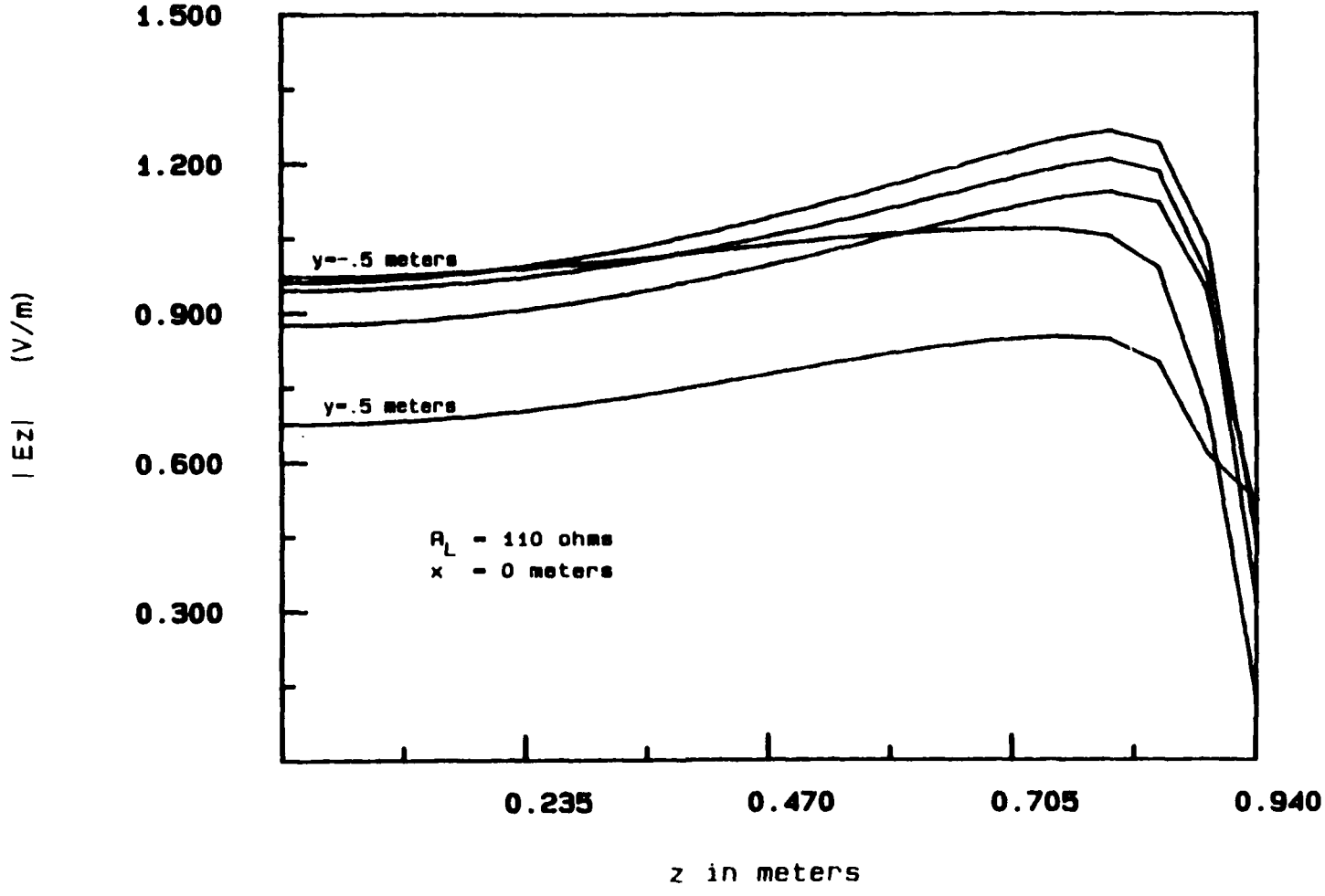

(a) Magnitude of E_z

Figure 36. Vertical E-field computed along the vertical direction at various longitudinal positions in the parallel-plate region of the 200 MHz bandwidth ACHATES simulator due to a 100 MHz unit-amplitude excitation.

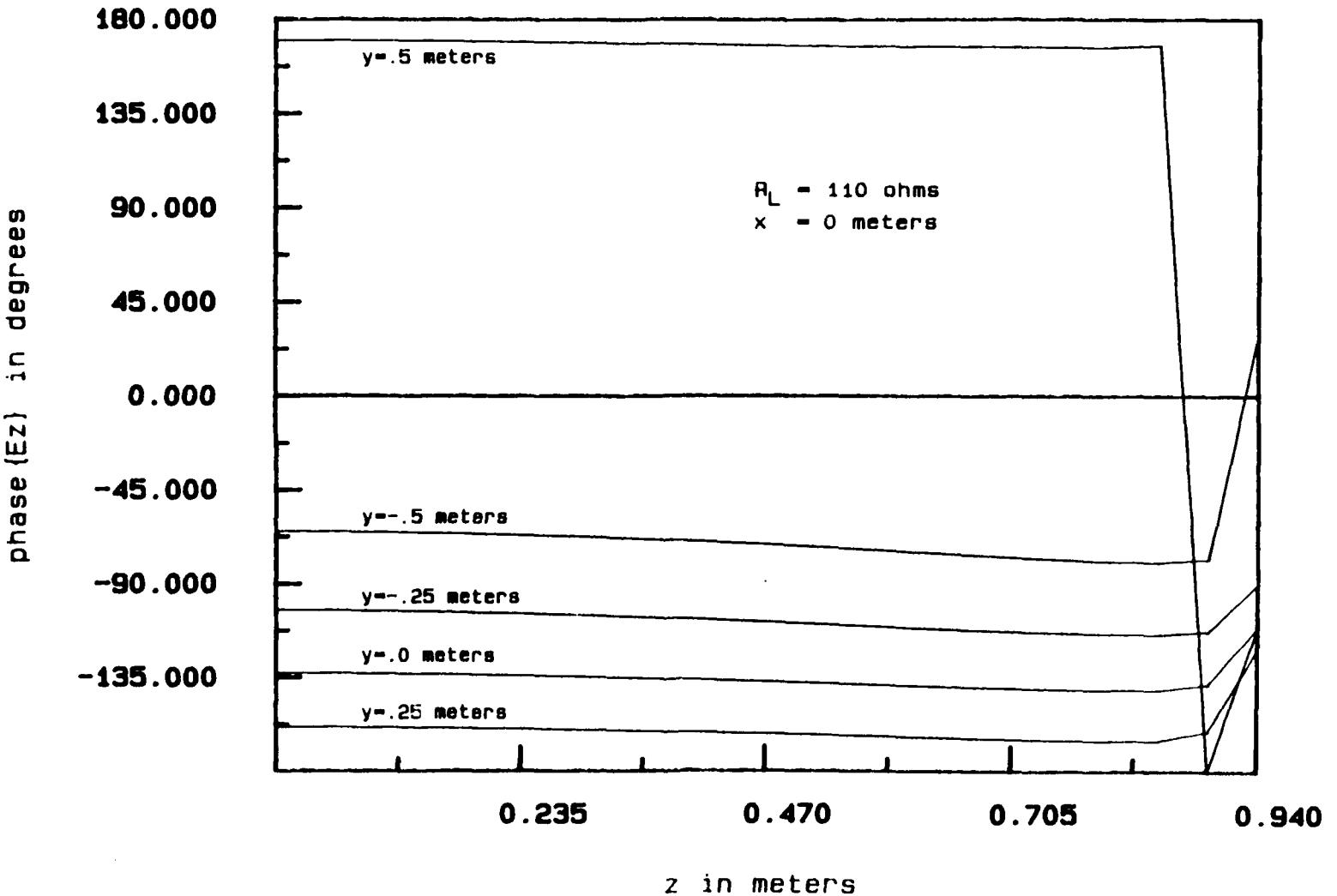

(b) Phase of E_z.

Figure 36. (Cont'd).

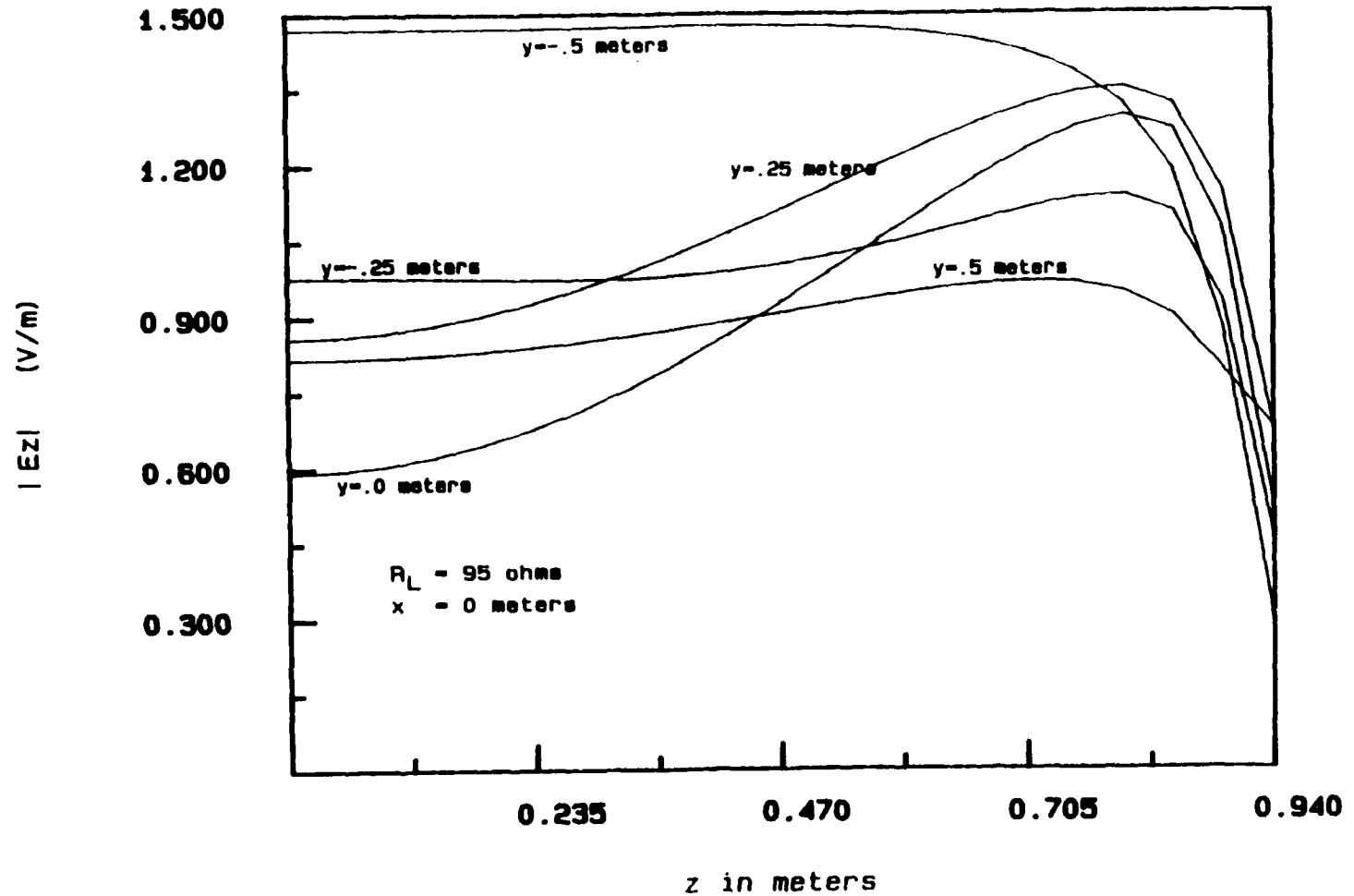

(a) Magnitude of E_z

Figure 37. Vertical E-field computed along the vertical direction at various longitudinal positions in the parallel-plate region of the 200 MHz bandwidth ACHATES simulator due to a 175 MHz unit-amplitude excitation.

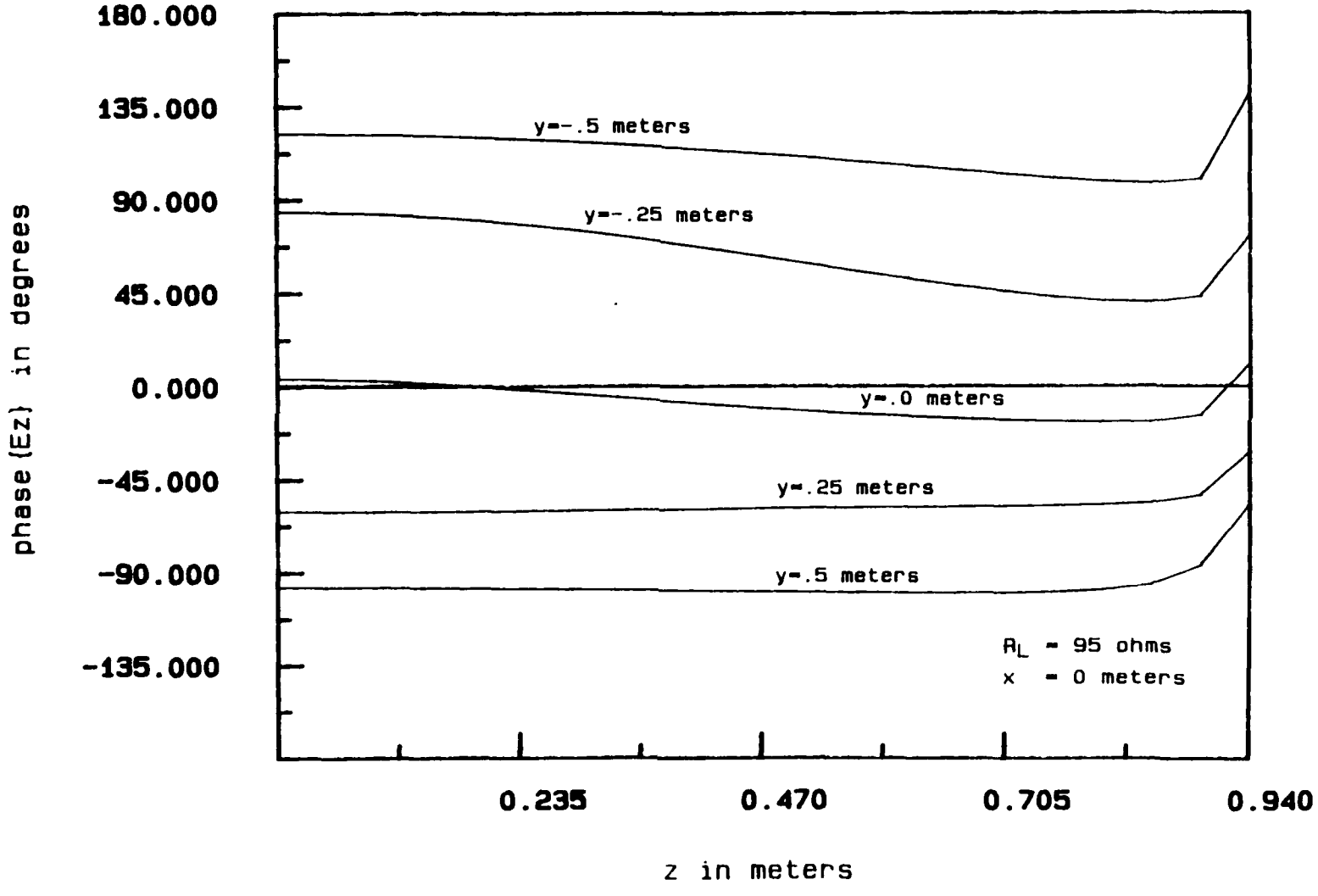

(b) Phase of E_z.

Figure 37. (Cont'd).

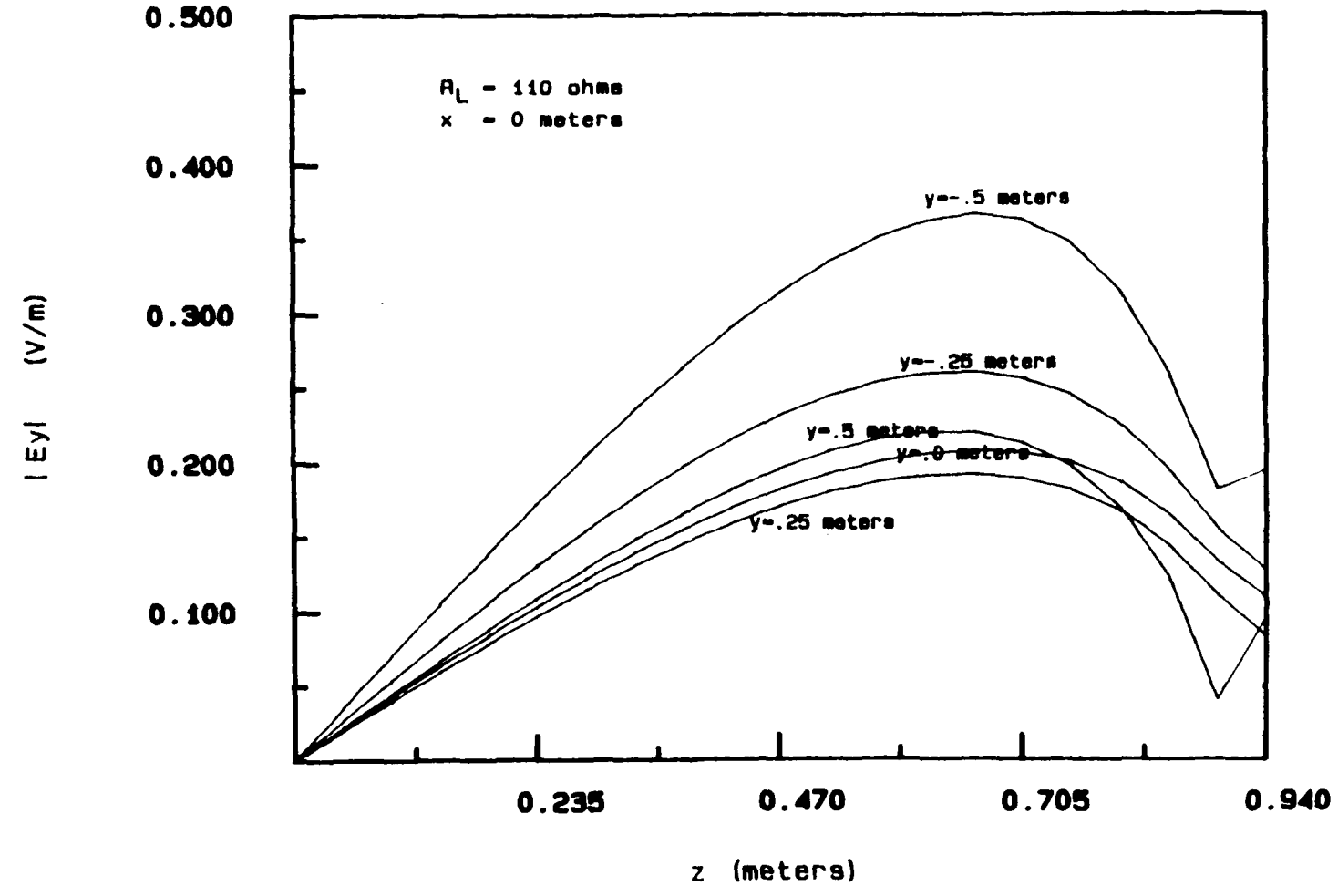

(a) Magnitude of E_t

Figure 38. Longitudinal E-field computed along the vertical direction at various longitudinal positions in the parallel-plate region of the 200 MHz bandwidth ACHATES simulator due to a 100 MHz unit-amplitude excitation.

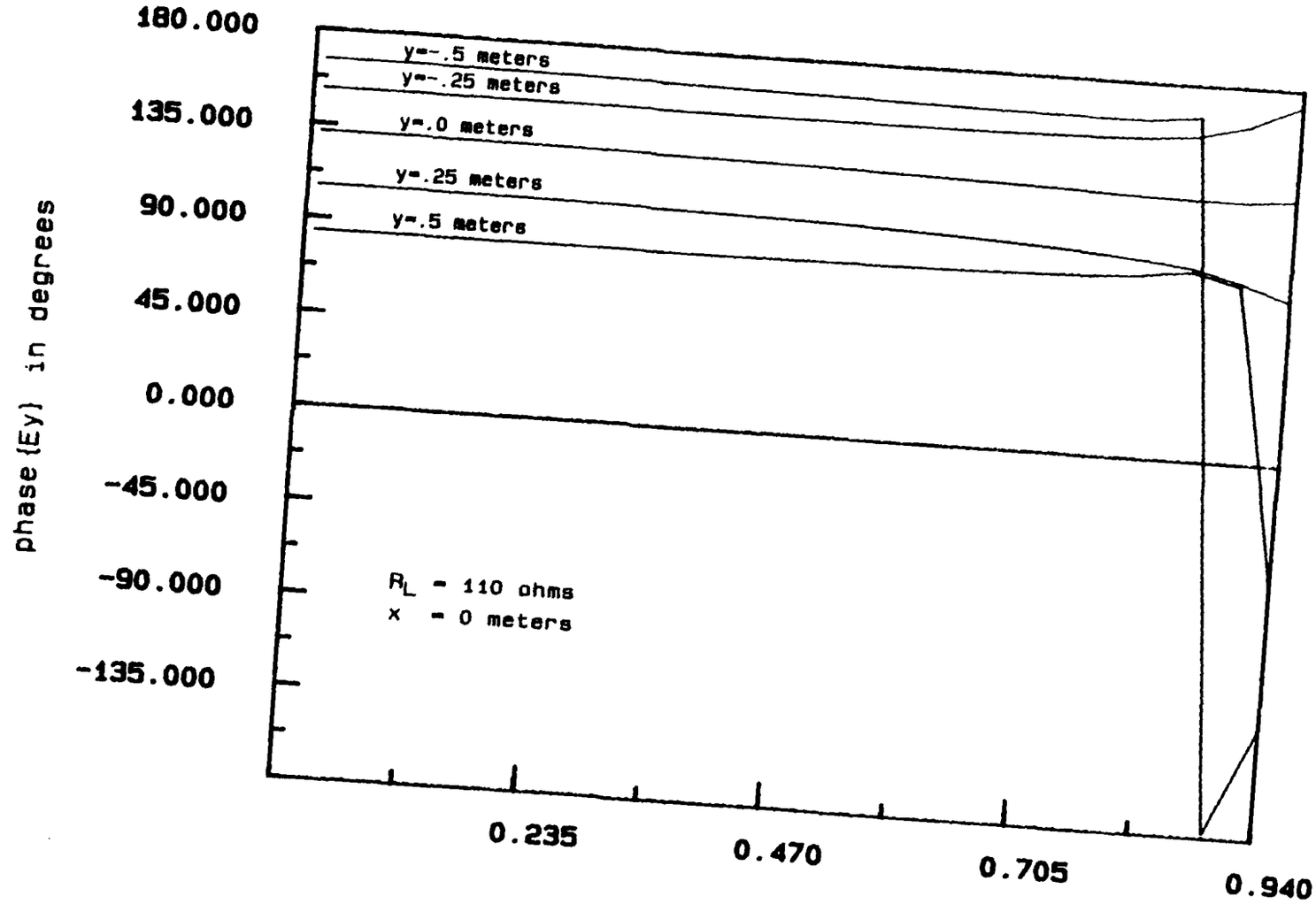

(b) Phase of E_y.

Figure 38. (Cont'd).

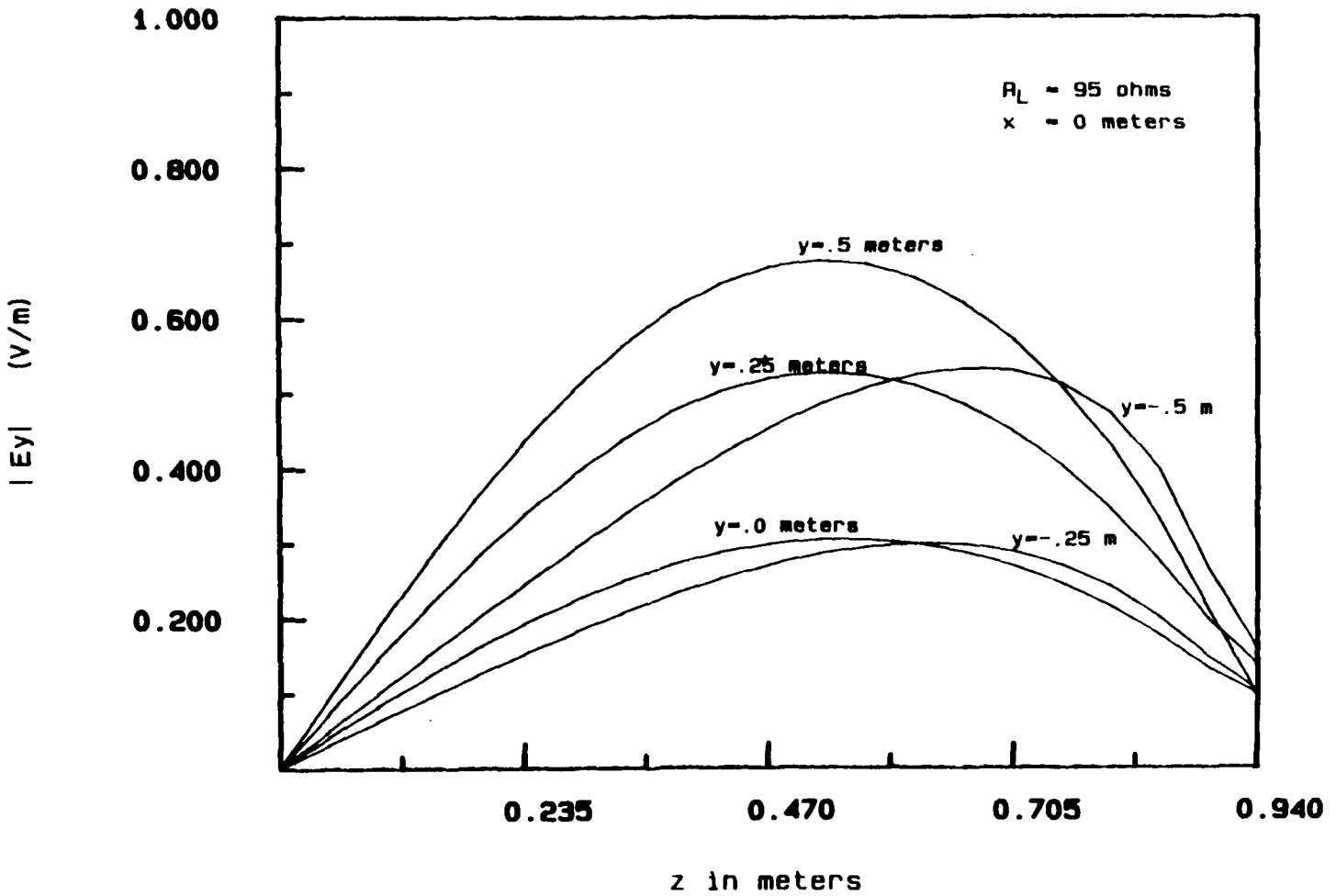

(a) Magnitude of E_z

Figure 39. Longitudinal E-field computed along the vertical direction at various longitudinal positions in the parallel-plate region of the 200 MHz bandwidth ACHATES simulator due to a 175 MHz unit-amplitude excitation.

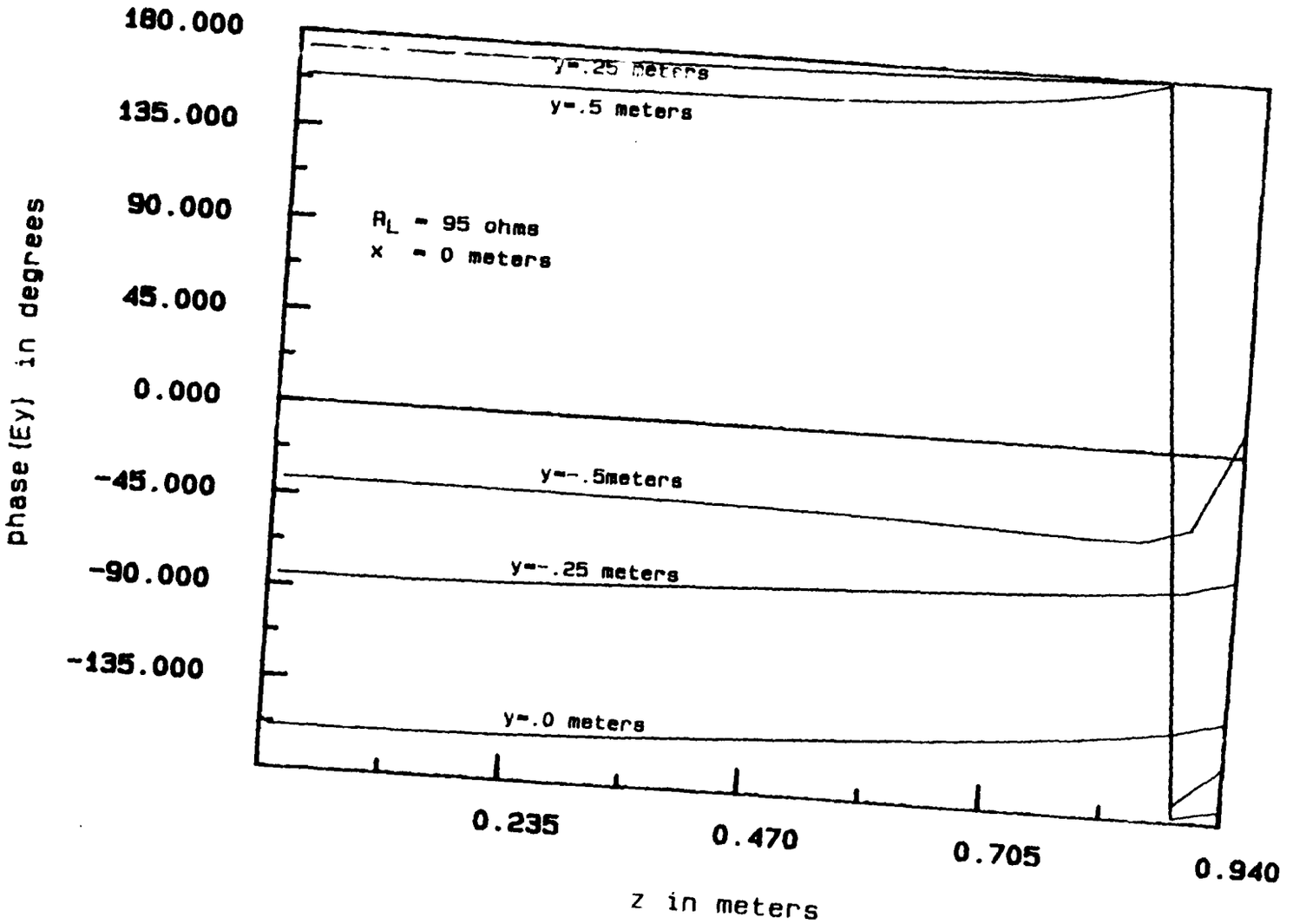

(b) Phase of E_y.

Figure 39. (Cont'd).

4 SIMULATOR-OBSTACLE INTERACTION

The purpose of an EMP simulator is to approximate the electromagnetic pulse environment produced by a high altitude nuclear burst. To determine its vulnerability, an object is placed within the simulator and subjected to the EMP environment. The currents induced on the object, and the fields coupled within it, are measured to determine its vulnerability. It was shown in the previous section that the parallel-plate simulator with an empty working volume closely approximates the plane-wave pulse environment desired. However, once the test object is placed within the simulator, the desired environment may deviate due to interaction between the simulator and the test object. As a result, the fields and currents measured experimentally may differ substantially from those induced by an EMP. Thus an understanding of the interaction between the simulator and the test object is quite important.[22] This chapter compiles these results to explain the simulator-obstacle interaction and the various phenomena that contribute to it.

Simulator-Obstacle Interaction

The asymmetric parallel-plate EMP simulator consists of an asymmetric parallel-plate waveguide that is excited and terminated by conical tapered end-sections. Once a test object is placed inside of the parallel-plate region, there is a certain amount of interaction between the test object and the simulator. If the interaction is significant, then measured values such as coupled currents in an electronic system could deviate greatly from those produced by an actual EMP exposure. The characteristics inherent can be to the parallel-plate simulator that contribute to this simulator-obstacle interaction attributed to three phenomena: (1) mutual coupling between the obstacle, the ground plane, and the top plate, (2) fringing effects due to the finite width of the parallel plates, and (3) multiple reflections between the obstacle and the tapered end-sections of the simulator.

The largest contribution of interaction between the object and the simulator is caused by mutual coupling. The coupling will introduce undesirable currents on both the object and the conducting surfaces of the simulator. One can initially approximate these induced currents by analyzing the ideal case of the mutual coupling between the object and an infinite parallel-plate waveguide. This ideal case eliminates the effects of field fringing and multiple reflections. One of the earliest investigations[23] of this problem considered the special case of a thin dipole placed within a parallel-plate waveguide and oriented perpendicular to the plates. Figure 40 illustrates the geometry of the problem studied. This case illustrated that, if the ratio of the distance between an end of the dipole and the plate, d, and the dipole length, h, exceeded 60 percent, the currents induced on the dipole due to mutual coupling will be negligible over a broad frequency range. In the high frequency region, where the separation distance becomes much longer than the wavelength, the mutual coupling effects are negligible. An important result of Taylor's work was that the largest coupling between the dipole and the parallel-plates occurs near the dipole's lowest resonant frequency. Near resonance, the magnitude of the current induced on the dipole differs greatly from the free space condition. Additionally, as d/h becomes very small, the location of the lowest resonance may change. This work concentrated on a thin dipole placed symmetrically between two infinite parallel plates. The case of a cylindrical post placed perpendicularly but asymetrically between

---

[22] Reference sources specifically dealing with simulator-test object interaction are marked with a †.

[23] J.P. Taylor, "Thin-Wire Receiving Antenna in a Parallel-Plate Waveguide," *IEEE Transactions on Antennas and Propagation*, vol. AP-15 (July 1967), pp. 572-574; C.D. Taylor and G.A. Steigerwald, *On the Pulse Excitation of a Cylinder in a Parallel Plate Waveguide*, Sensor and Simulation Note 99 (Air Force Weapons Laboratory, March 1970)

two plates[24] is illustrated in Figure 41. This case also presumes infinite plates. It was found that, as the object is placed closer to one of the plates the effects of mutual coupling becomes significant, even for cylinders much shorter in length than the plate separation. As should be expected, this mutual coupling is most prevalent when the obstacle is located near one of the plates and the closest image is in the near field of the obstacle. In this region, there is very little coupling with the other plate. This is illustrated by comparing the currents induced on the object near the ground plane in an infinite parallel-plate waveguide to those induced when the top plate is removed. It was also shown that this mutual coupling mainly affects the first resonance of the cylinder. It should be realized that the late time behavior of the current induced on the post is determined by the lowest resonant frequency, since the late response decay time is proportional to the magnitude of the lowest resonance, and is inversely proportional to its location. It was also shown that the late time response of the post can be greatly affected when the location of the first resonance is shifted, or its magnitude is varied.[25] Thus far, only cylinders placed perpendicularly to the parallel plates have been considered. Later studies presented an analysis of a thin cylindrical post placed arbitrarily within a parallel-plate waveguide, and the same problem with the top plate removed.[26] These studies showed that the largest interaction due to coupling occurs when the wire is oriented in parallel to the conducting plates. Also, as the wire axis approaches a direction parallel to the plates, higher order resonances become greatly affected. The same tendency was found in the case of a perfectly conducting sphere where dominant currents induced on the sphere lie in a direction parallel to the plates.[27] This contrasts to the case where the cylinder is perpendicular to the plates and only the first resonance is perturbed by mutual coupling. The perturbation of the higher order resonances leads to errors in the early time response of the test object.

The case of a thick cylinder placed asymmetrically and perpendicularly within a parallel-plate waveguide is illustrated in Figure 41. At the cylinder's end, the azimuthal current will be very large due to the edge discontinuity, and for the same reason, the vertical current will be quite small. As a result, there will be a large amount of coupling due to the azimuthal current on the cylinder edge closest to the parallel plates. For very thick cylinders, this would introduce a large deviation in the currents.

The previous analogies have been restricted to that of an infinite parallel-plate waveguide. These solutions are easily obtained since an integrodifferential operator can be derived for the boundary value problem and illustrate the contribution of mutual coupling between the test object and the parallel plates of the simulator. However, the simulator is an open structure with a finite width and a finite length. Due to the finite width there will be field fringing effects. The field fringing of the TEM mode can be approximated in the quasi-static sense by the fringe lines of a two-dimensional finite-width parallel-plate capacitor. If the plate width is much larger than the separation, the TEM field will be mostly uniform in

---

[24] K.S.H. Lee, *A Vertical Post Inside a Two-Parallel-Plate Simulator*, Sensor and Simulation Note 139 (Air Force Weapons Laboratory, October 1971)

[25] Lennert Marin, *A Cylindrical Post Above a Perfectly Conducting Plate, II (Dynamic Case)*, Sensor and Simulation Note 136 (Air Force Weapons Laboratory, August 1971); F.M. Tesche, *On the Behavior of Thin-Wire Scatterers and Antennas Arbitrarily Located Within a Parallel-Plate Region I (The Formulation)*, Sensor and Simulation Note 135 (Air Force Weapons Laboratory, August 1971).

[26] F.M. Tesche, *On the Behavior of Thin-Wire Scatterers and Antennas Arbitrarily Located Within a Parallel-Plate Region I (The Formulation)*, Sensor and Simulation Note 135 (Air Force Weapons Laboratory, August 1971); F.M. Tesche, "On the Behavior of Thin-Wire Antennas and Scatterers Arbitrarily Located Within a Parallel-Plate Region," *IEEE Transactions on Antennas and Propagation*, vol. AP-20 (July 1972), pp. 482-486.

[27] A.R. Neureuther, G.J. Burke, E.K. Miller, and G.M. Pjerrou, "Resonance Region Scatterer Studies by a Rail Line Range," *IEEE Transactions on Antennas and Propagation*, vol. AP-19 (November 1971), pp. 789-792; A.D. Varvatsis and M.I. Sancer, *Electromagnetic Interaction Between a Perfectly Conducting Sphere and a Two-Parallel-Plate Simulator, I (Top Plate Removed)*, Sensor and Simulation Note 140 (Air Force Weapons Laboratory, October 1971).

the central region and there will be very little fringing effect. However, if the width of the test object is comparable to the width of the simulator, this could have a substantial effect. In the mid-frequency and high-frequency range, higher-order modes will propagate and the quasi-static approximation alone may not be valid. In this region, fringing fields may have a larger contribution.

The parallel-plate simulator is of finite length, and conical tapered end-sections are often used to excite and terminate the parallel-plate region. Multiple reflections will occur between the test object and the conical tapered end-sections. The obstacle presents a perturbation to the field and will couple energy into higher order modes. This energy will be reflected by the tapered end-sections back into the parallel-plate region due to impedance mismatches. In the early time response of the pulse excitation, the distortion due to multiple reflections will be negligible since the distances travelled are many wavelengths. In the late time response, the distortion will be more prevalent, yet its significance may be reduced since the higher order modes will be attenuated along the waveguide.

It was shown in Chapter 3 that the field within the parallel-plate simulator is nearly uniform and is predominantly a TEM plane wave with a linearly progressive phase shift. The conical tapered end-section launches a quasi-spherical wave into the parallel-plate region and as a result, TM and TE modes also exist. For a gradually tapered end-section, and for sufficiently low frequencies, these modes are negligible. However, in the mid-frequency range where the plate separation is on the order of a wavelength, these higher order modes can carry a significant amount of energy. As a result, unwanted currents are induced on the object and consequently couple to the top plate and the ground plane. Furthermore, the discontinuity at the interface with the end-section can be thought of as an impedance mismatch[28] and multiple reflections will occur. The following section presents a numerical analysis of an obstacle placed within a finite-width bounded-wave parallel-plate EMP simulator. The analysis is performed with the use of a wire mesh approximation and the Numerical Electromagnetics Code, as presented in Chapter 3. From this study, a comprehension of the mechanisms contributing to the simulator-obstacle interaction is obtained.

Numerical Solution

The problem to be considered here is the response of a cylindrical tube placed within the working volume of a parallel-plate EMP simulator when excited by a unit excitation at a single frequency. The currents on the cylinder are computed and then compared to those induced on a similar cylinder situated in free space, when illuminated by a TEM plane wave with a vertically polarized E-field.

In this case, the cylindrical tube is placed on a ground plane in free space and the conducting surface of the cylinder is approximated by a thin-wire mesh. The wire mesh consists of horizontal and vertical wires placed such that the area of the mesh openings is less than 0.01 λ^2. If a polygon is drawn in which the center of the vertical wires coincides with the polygon vertices, the radial distance of the vertices from the origin is chosen such that the area of the polygon equals that of the area of the horizontal cross section of the original cylinder. This is illustrated in Figure 42. Furthermore, the radius of the wires are chosen such that the circumference of the wire is equal to that of an edge of the polygon.

The wire model is placed on a perfectly conducting ground plane and is illuminated by a TEM plane wave that has a vertically polarized E-field. The response of a cylinder with dimensions a/h = 0.1 ('a'

[28] Lam.

is the cylinder radius, 'h' is its height) is illustrated in Figure 43. The verified location[29] of the first resonance is illustrated in Figure 43. Figure 44 illustrates the response of a cylinder with the dimension a/h = 0.5. Figure 44, J_1 represents the current computed on the surface of the cylinder in the lit region at a height of h/6. J_2 is computed at h/2, and J_3 at 5h/6. It is noted that the cylinder with a/h = 0.1 was approximated by a tenth order polygon, and the cylinder with a/h = 0.5 was approximated by a twentieth order polygon.

The EMP parallel-plate simulator approximates the environment of an EMP propagating through free space. In Chapter 3, it was illustrated that the field distribution within a 450 MHz bandwidth asymmetric EMP simulator with an empty working volume was predominately uniform TEM in the low- and mid-frequency regions. However, over a broad band of frequencies, extending into the high-frequency region, the fields deviate from that of a propagating plane wave in free space since the field distribution is nonuniform and higher order modes carry significant energy. The response of the cylinder in the simulator is affected by the nonuniformities of the simulator fields. However, it should be realized that the response will also be affected due to the mechanisms discussed in the previous section. It may be possible to use a method of moment solution to analyze the response of the cylindical tube placed inside of the EMP simulator and to compare that response to one created by a plane wave excitation in free space.

The conducting surfaces of the EMP simulator and the cylinder are modeled by a thin-wire mesh and the method of moment solution is obtained as described in Chapter 3. The dimensions of the simulator were chosen such that a 1-V excitation across the source gap produces a vertical E-field of 1 V/m on the ground plane on the center axis of the parallel-plate region. Thus the incident field is assumed to be of unit amplitude for the computed response. Near the interface of the conical tapered end-section and the parallel-plate region, the fields were nearly uniform and planar in nature if the frequency excitation was well within the simulator bandwidth. It is desirable to place the test object near this interface (Figure 45). The response of the cylinder excited within the parallel-plate region of the simulator is compared to its response to a plane wave excitation in free space for a/h = 0.1 and 0.5 (Figures 46 and 47). In both examples, the ratio of h/s (where s is the plate separation) was 0.4. At the location of the first resonance (kh = 1.25), illustrated in Figure 46, there is a large deviation in the magnitude of the induced current on the cylinder. In this example, kh corresponds to a frequency excitation of 158.6 MHz (h = 0.376 meters). In Chapter 2, it was shown that the lowest order resonance of the parallel-plate waveguide is located at 159 MHz. Therefore, at 158.6 MHz, both the parallel-plate waveguide and the cylinder are in a resonant condition, resulting in a large interaction between the cylinder and the parallel-plate waveguide. Figure 47 illustrates that the location of the first resonance is slightly shifted (from 1.00 to 1.05). Furthermore, there is a shift in magnitude near the resonance. The response of the cylinder within the parallel-plate simulator, when compared to the response under free space conditions, is distorted due to the simulator-obstacle interaction. One of the largest contributions to this interaction is the mutual coupling between the object and the top plate of the simulator. However, it is apparent that there are other contributing factors. These can be variation of the uniformity of the fields over the broad frequency range, multiple reflections between the test object and the tapered end-sections, and field fringing.

The interaction between the obstacle and the simulator not only affects the response of the object, but also the operating characteristics of the simulator as well. Due to mutual coupling and multiple reflections, currents will be induced onto the conducting plates, changing operating characteristics of the simulator (Figures 48 through 53). These figures illustrate the currents coupled onto the top parallel-plate

[29]Marian (August 1971).

when the test object is placed in the simulator. It is interesting to note that the largest coupling occurs near the resonant frequency of the parallel-plate waveguide. Table 2 shows the measured input impedance versus kh (where k is the free space wavenumber) over the band of interest.

These results illustrate the computed response near the first resonance of the cylinder. This will produce deviations in the late time response of the cylinder when excited by the simulated EMP. At higher frequencies, where the wavelength becomes small with respect to the plate separation, mutual coupling will be minimal.[30] The differences in the response, when compared to the free space case, will then be due to field fringing and nonuniformities in the field. In the mid-frequency region where the wavelength becomes comparable to the plate separation, higher order modes will propagate in the simulator and multiple reflections have a larger contribution to the field distortion. Finally, as illustrated in Chapter 3, the nonuniformities in the fields may be quite large if the highest frequency component is near or surpasses the cutoff frequency of the simulator's bandwidth.

Table 2

Perturbation of the Input Impedance of the EMP Simulator When a Test Object is Placed in the Working Volume (h = 0.376 m)

kh	Z_{in} *(empty W.V.)*	Z_{in} *(a/h = 0.1)*	Z_{in} *(a/h = 0.5)*
	(Ω)	(Ω)	(Ω)
0.50	77.74 - j 5.11	78.52 - j 7.50	75.35 - j 14.08
0.90	97.11 + j 7.20	97.98 + j 14.92	122.3 + j 13.12
1.00	65.74 + j 20.02	74.12 + j 15.23	62.04 + j 6.66
1.10	44.26 + j 23.17	38.40 + j 25.96	44.51 + j 35.23
1.20	85.90 + j 17.03	98.24 + j 21.72	88.78 + j 5.35
1.25	85.05 + j 36.70	96.09 + j 21.85	78.82 + j 27.01
1.30	93.96 + j 18.49	77.36 + j 11.13	83.07 + j 24.19
1.40	103.1 + j 13.45	113.0 + j 31.06	110.9 + j 19.43
1.50	1002. + j 17.17	90.16 + j 1.42	89.15 + j 5.47

[30]Taylor.

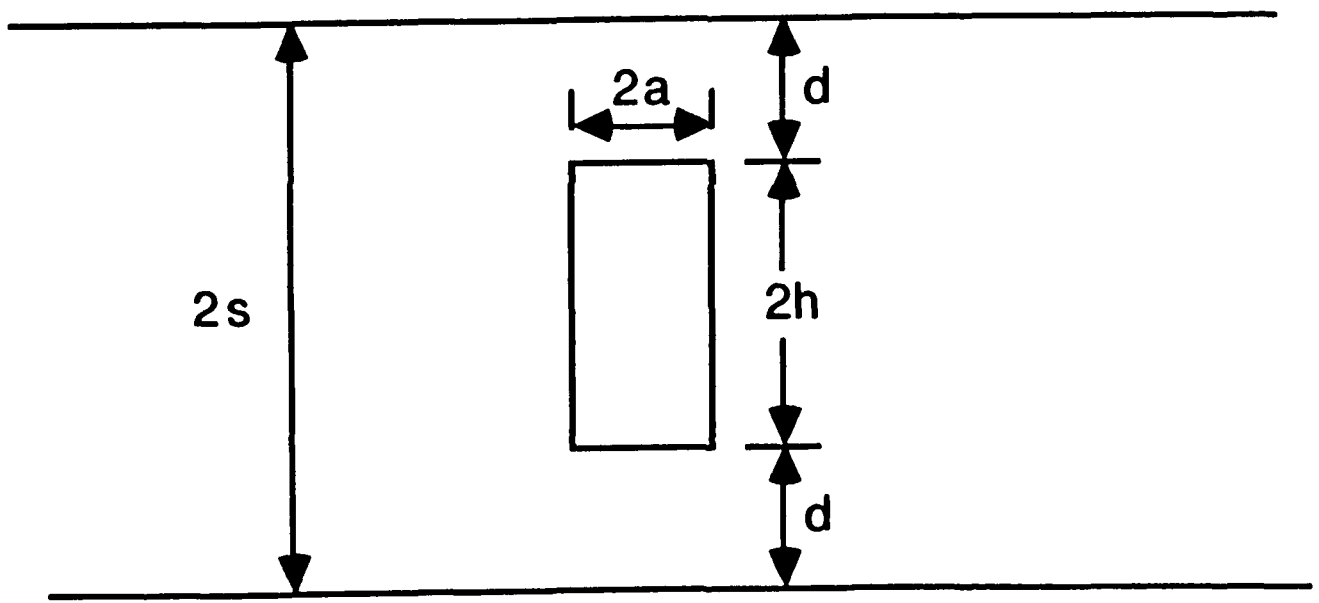

Figure 40. Thin-wire dipole placed perpendicularly but symertrically between the two plates of an infinite parallel-plate waveguide.

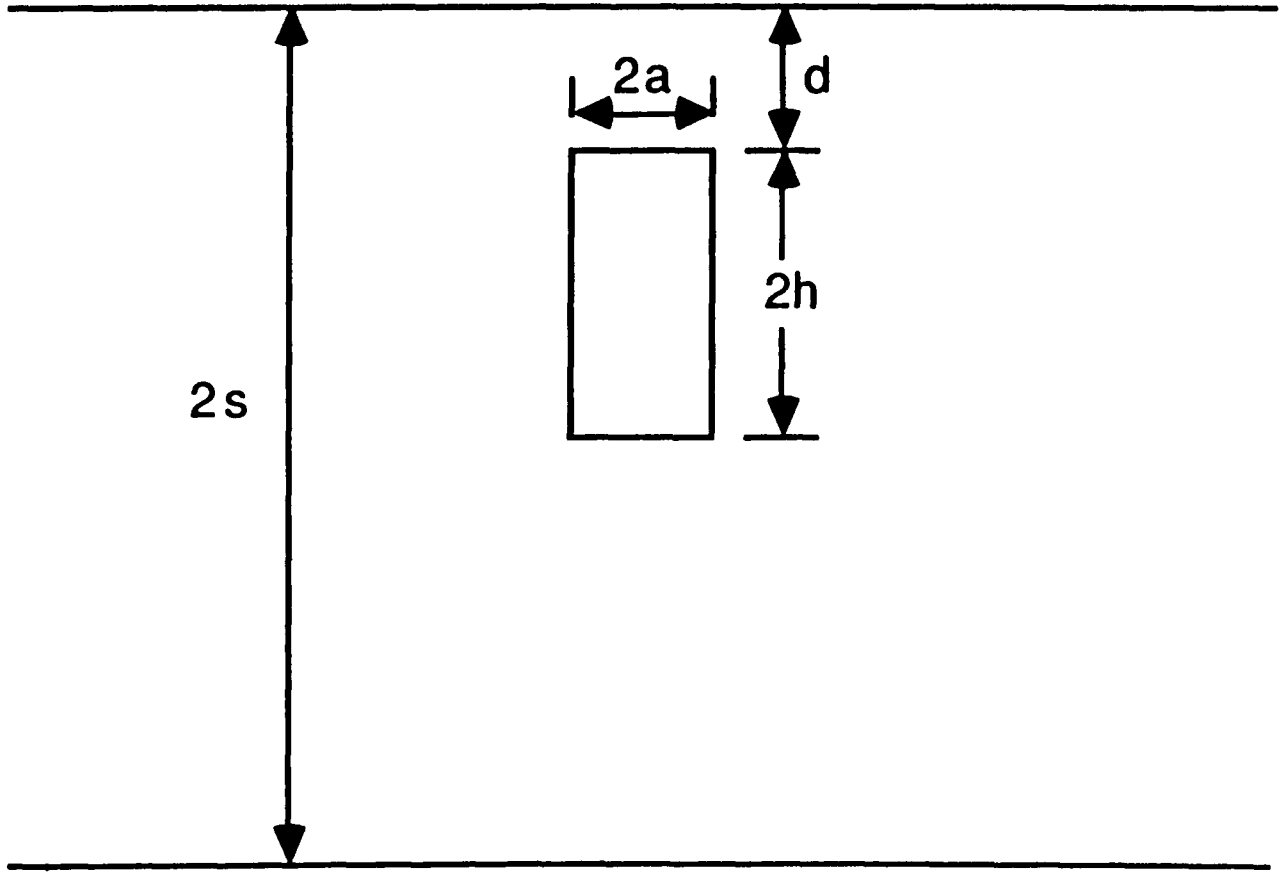

Figure 41. A cylindrical post placed perpendicularly but asymmetrically between the two plates of an infinite parallel-plate waveguide.

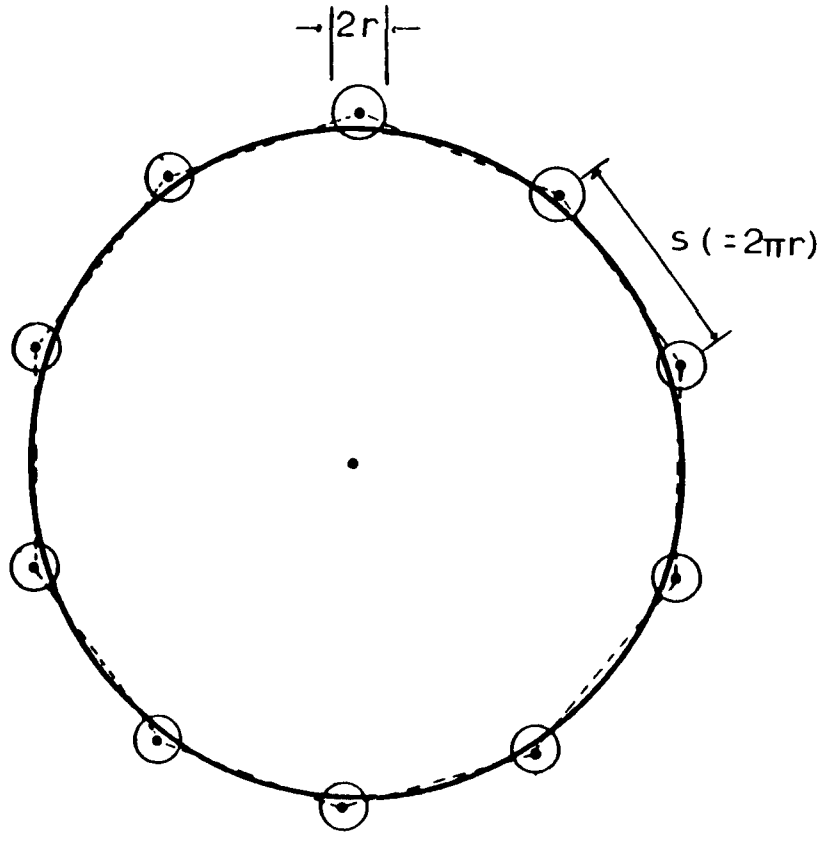

Figure 42. Horizontal cross section of a thin-wire approximation of a conducting cylinder.

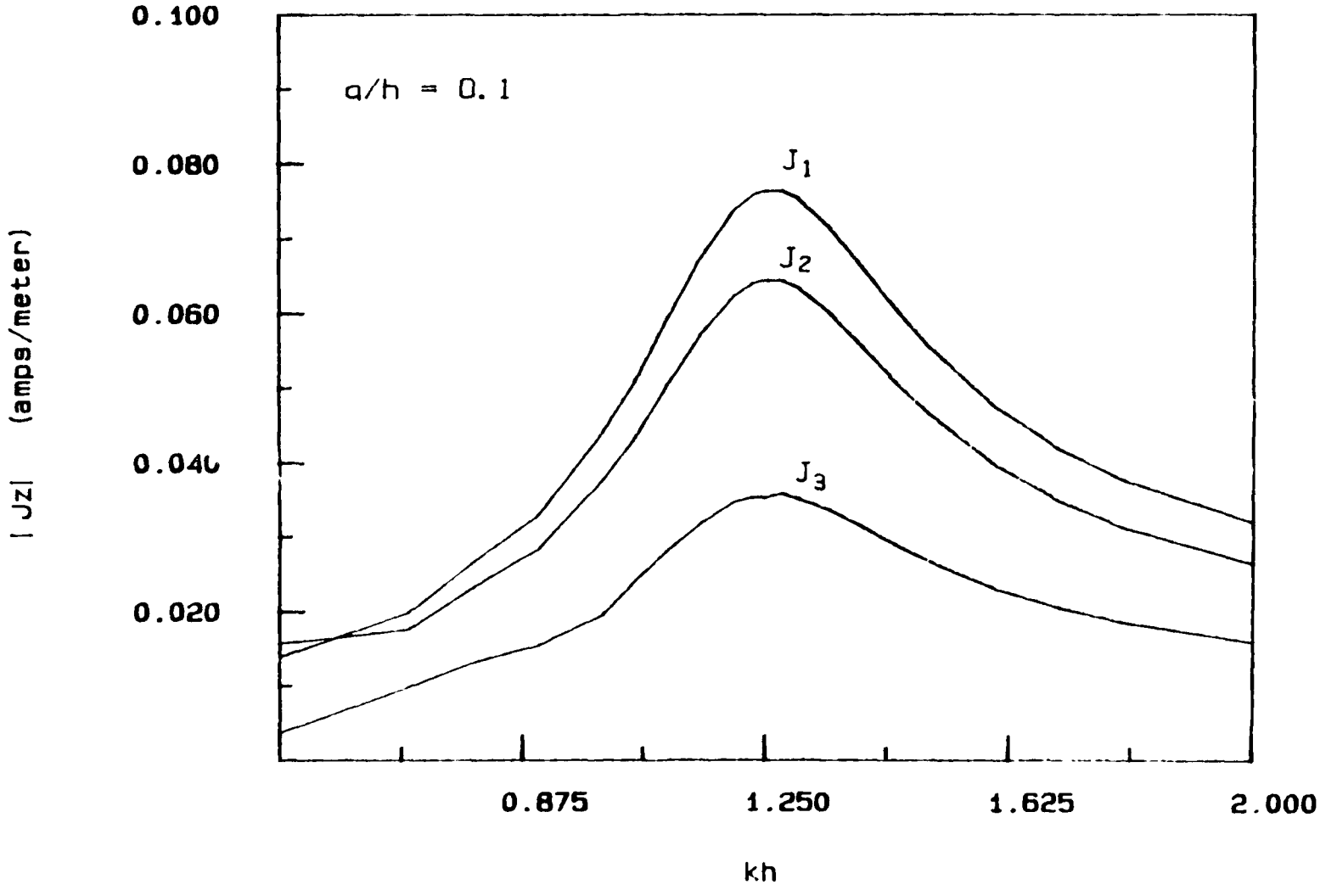

Figure 43. Currents induced on a cylindrical tube on a ground plane (a/h = 0.1) illuminated by a vertically polarized TEM plane wave (J_1 computed at h/6, J_2 computed at h/2, J_3 computed at 5h/6).

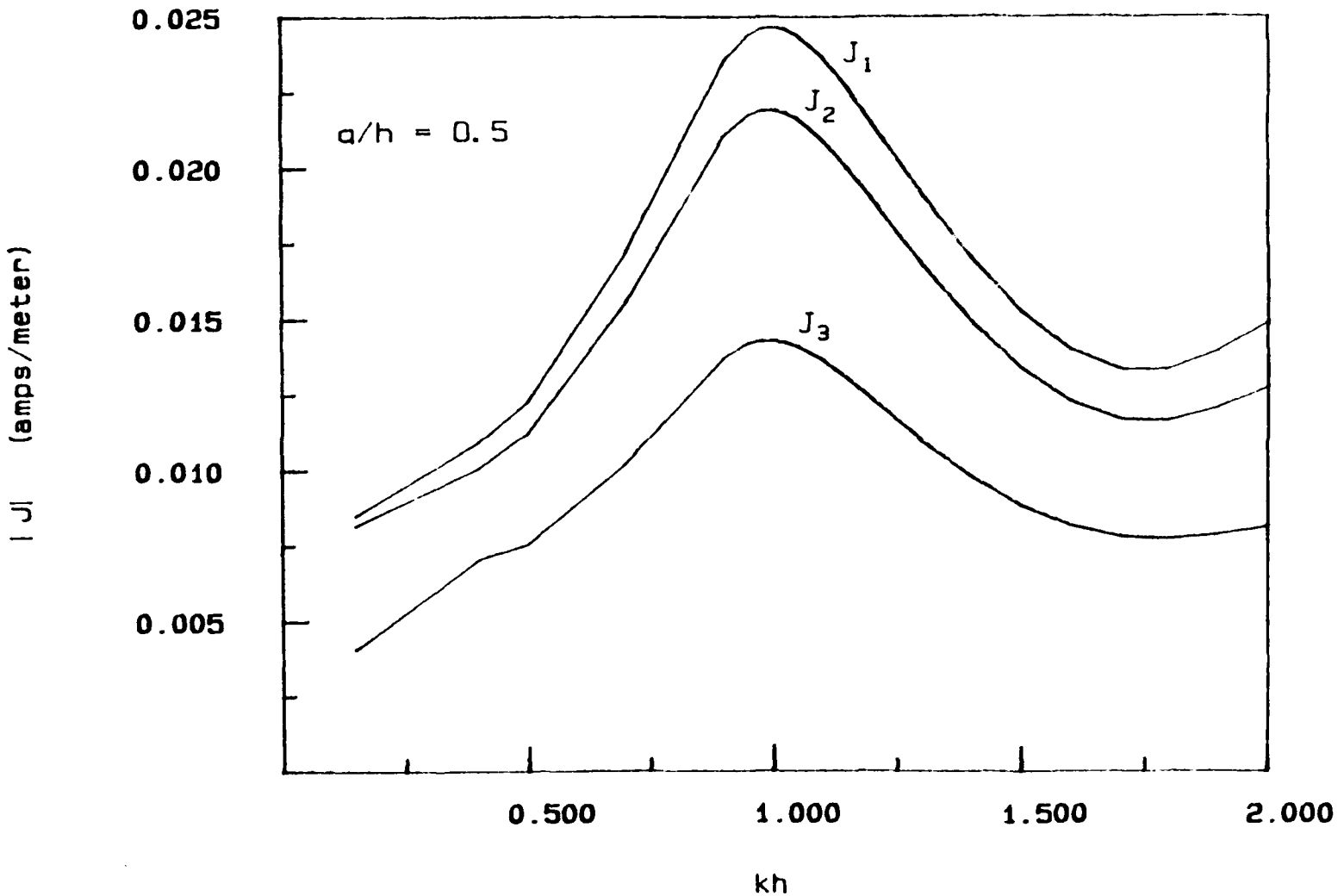

Figure 44. Currents induced on a cylindrical tube on a ground plane (a/h = 0.5) illuminated by a vertically polarized TEM plane wave J_2 computed at h/6, *J3* computed at 5h/6).

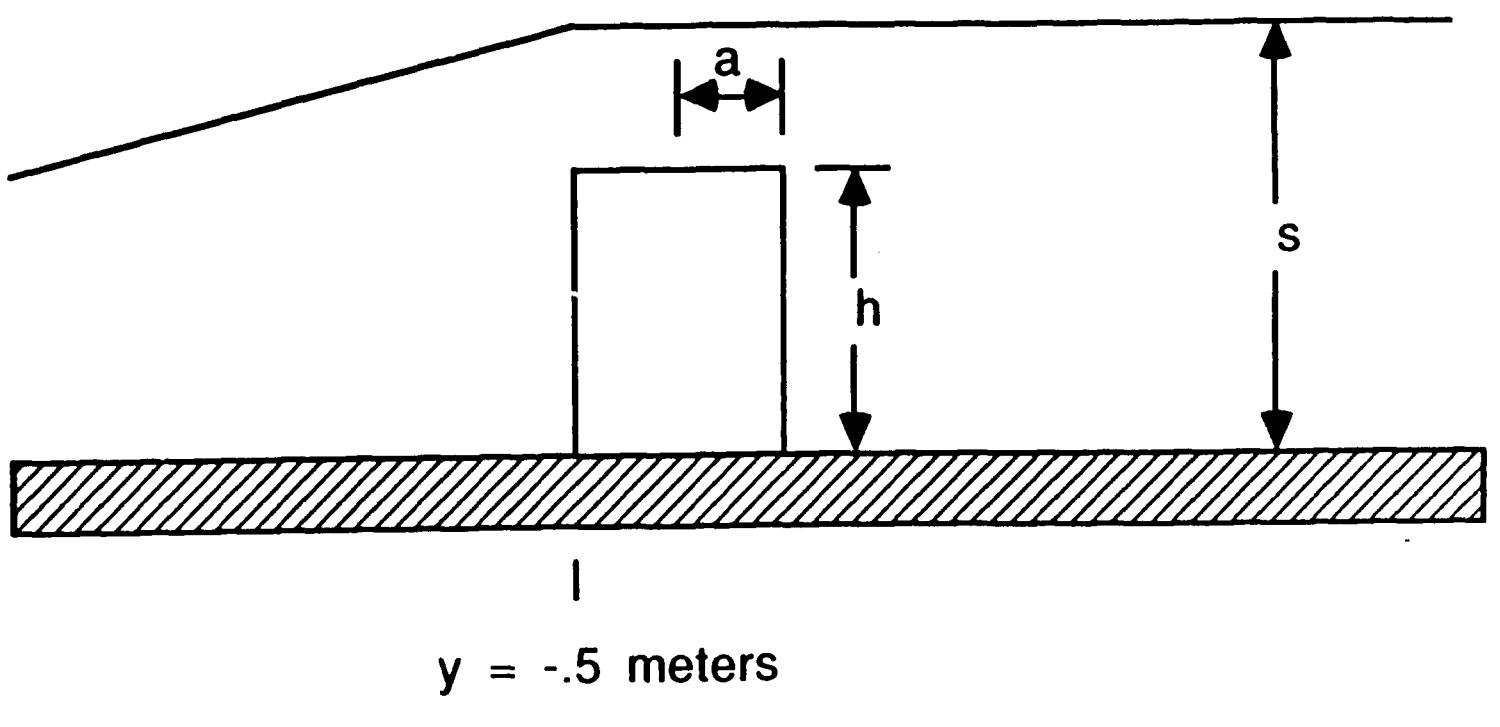

Figure 45. Location of the cylindrical tube placed within the parallel-plate EMP simulator.

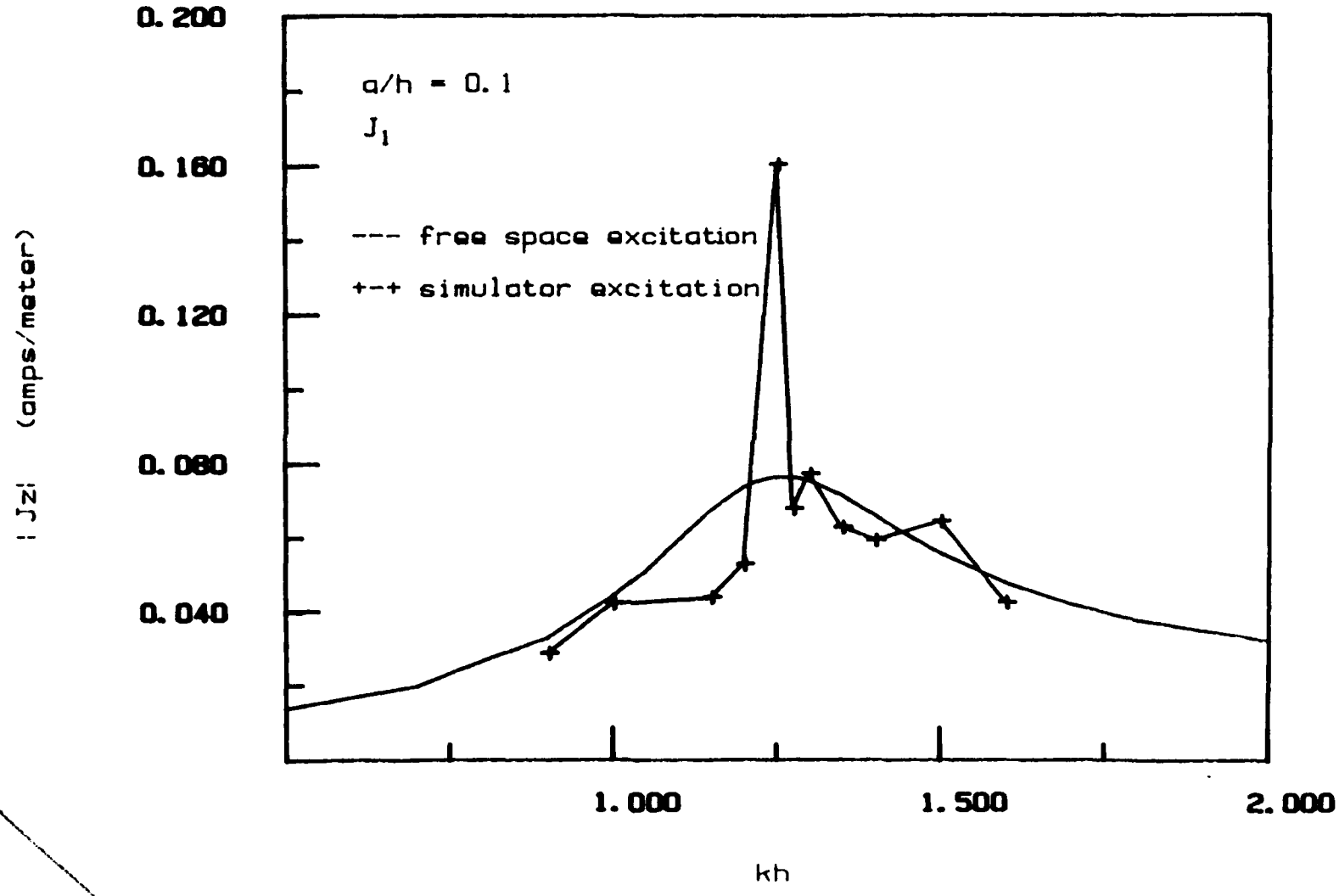

(a) Computed at h/6.

Figure 46. Currents induced on the surface of a cylindrical tube excited within the parallel-plate EMP simulator (a/h = 0.1).

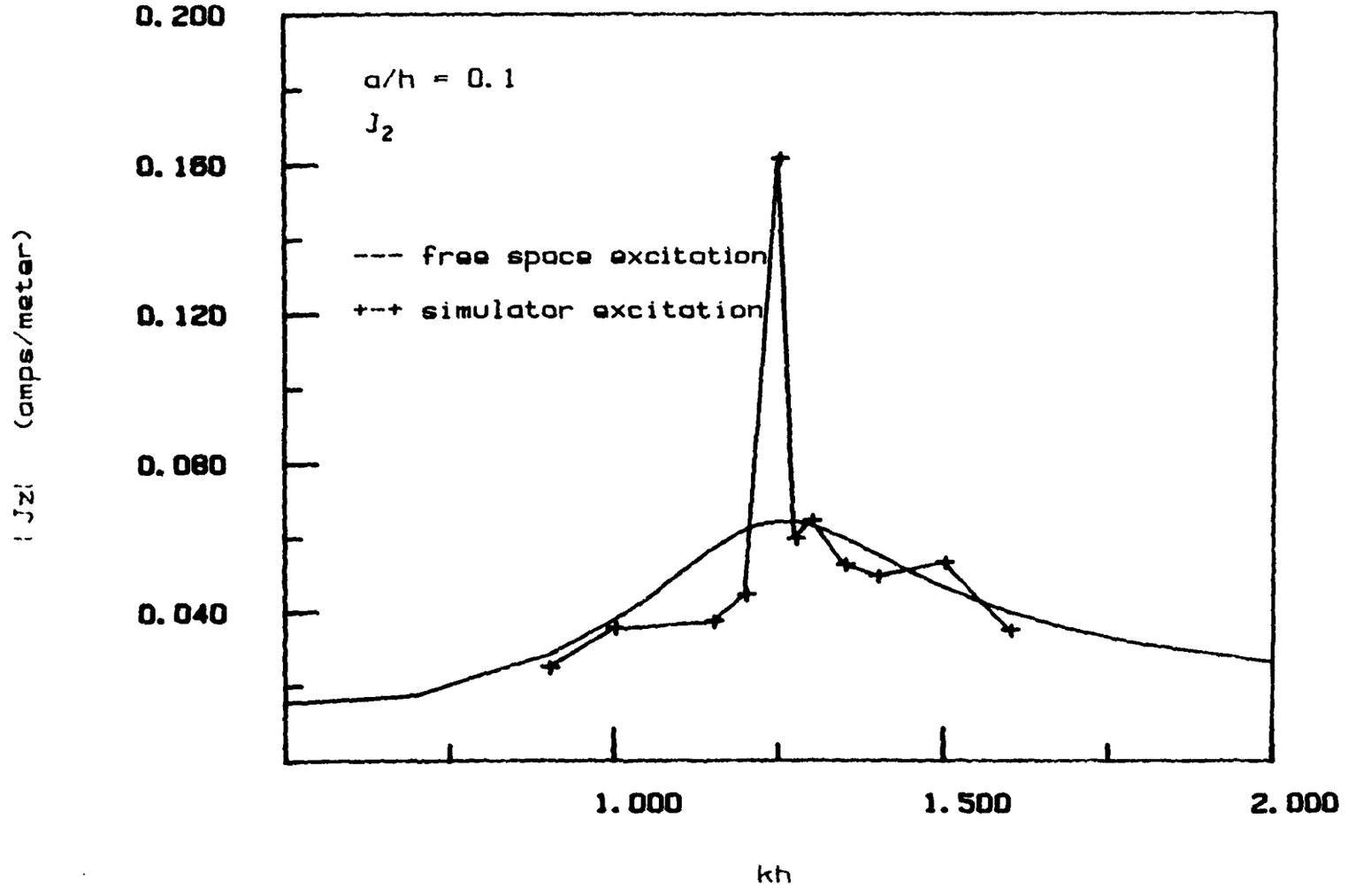

(b) Computed at h/2; a/h = 0.1.

Figure 46. (Cont'd).

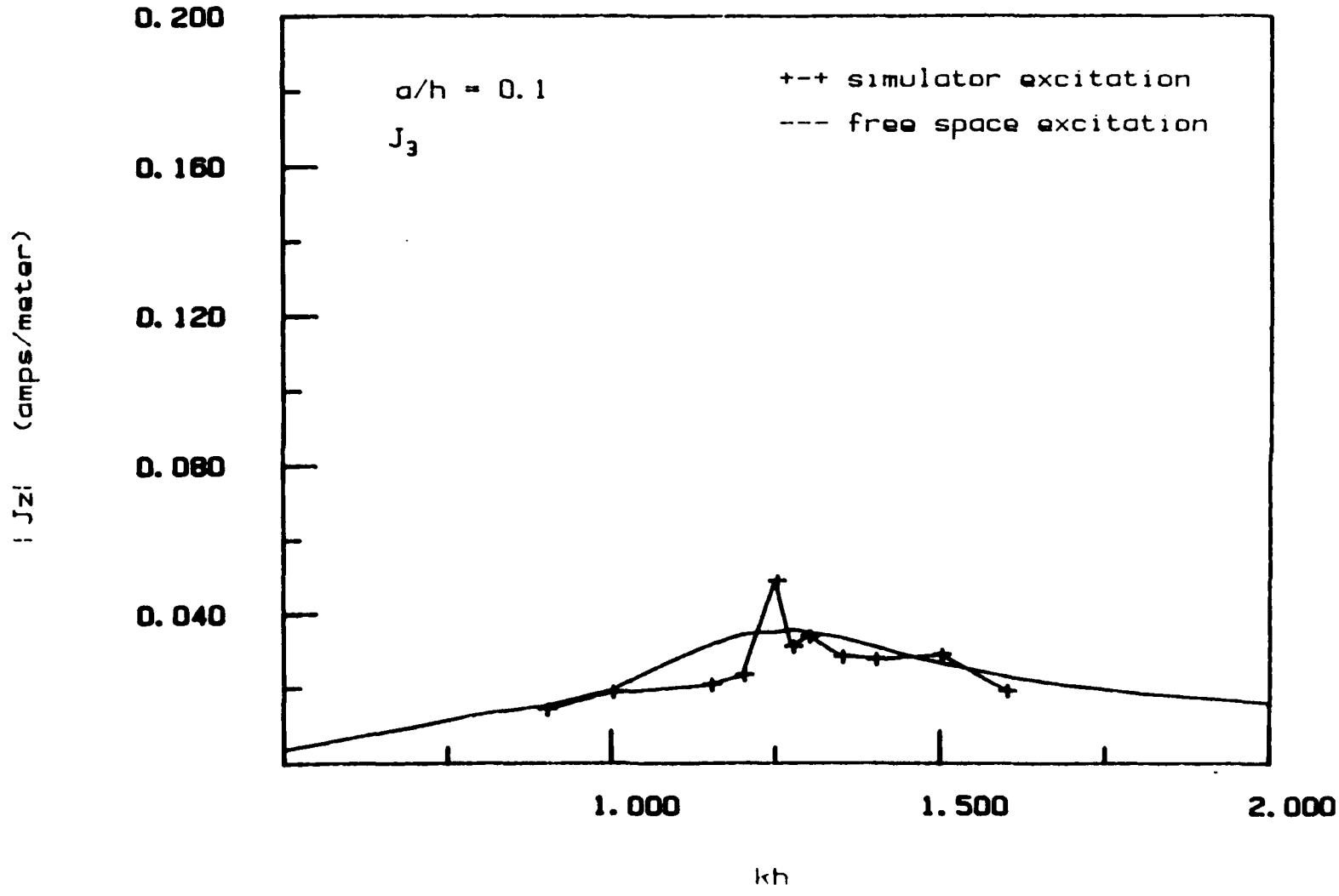

(c) Computed at 5h/6; a/h = 0.1.

Figure 46. (Cont'd).

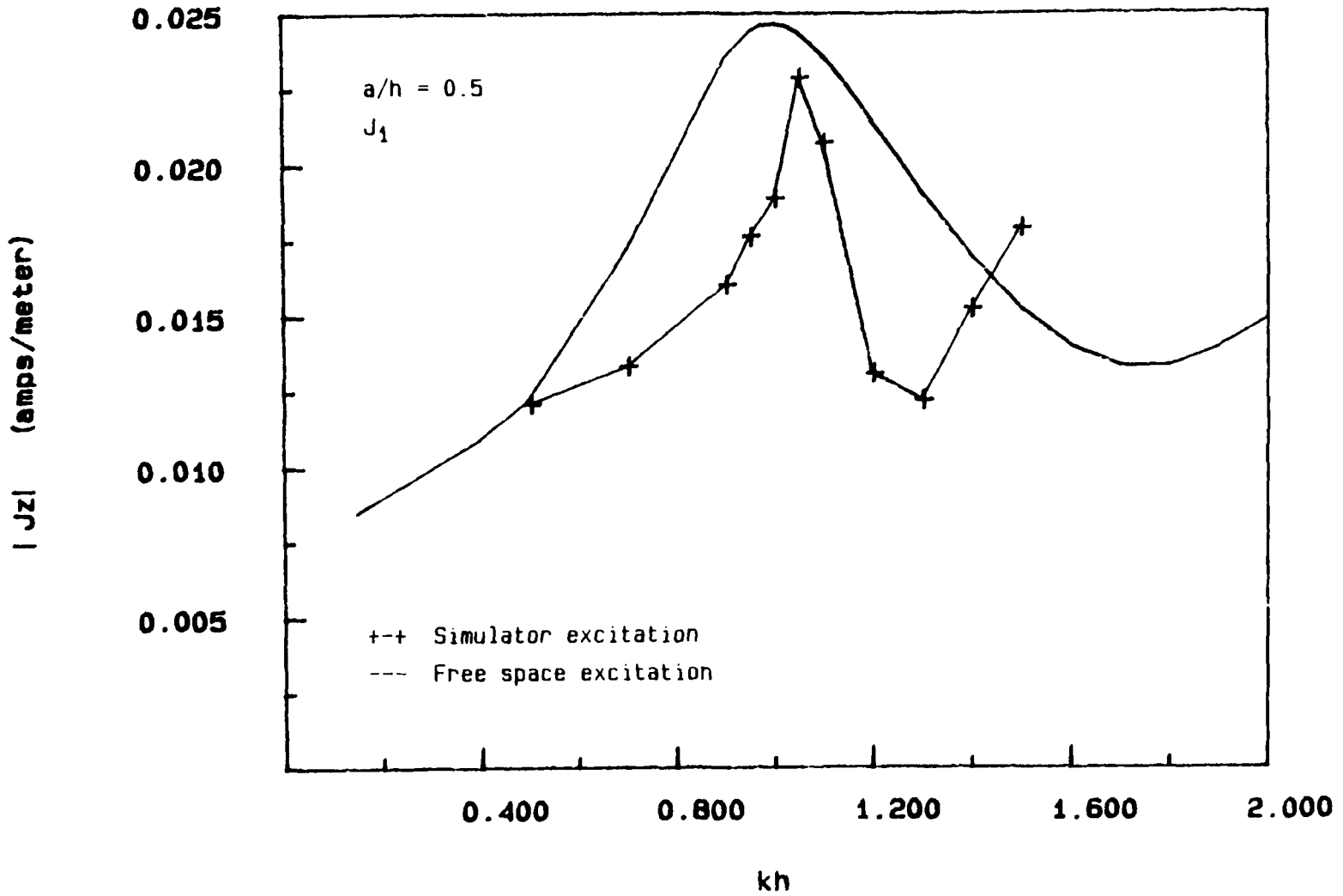

(a) Computed at h/6.

Figure 47. Currents induced on the surface of a cylindrical tube excited within the parallel-plate EMP simulator (a/h = 0.5).

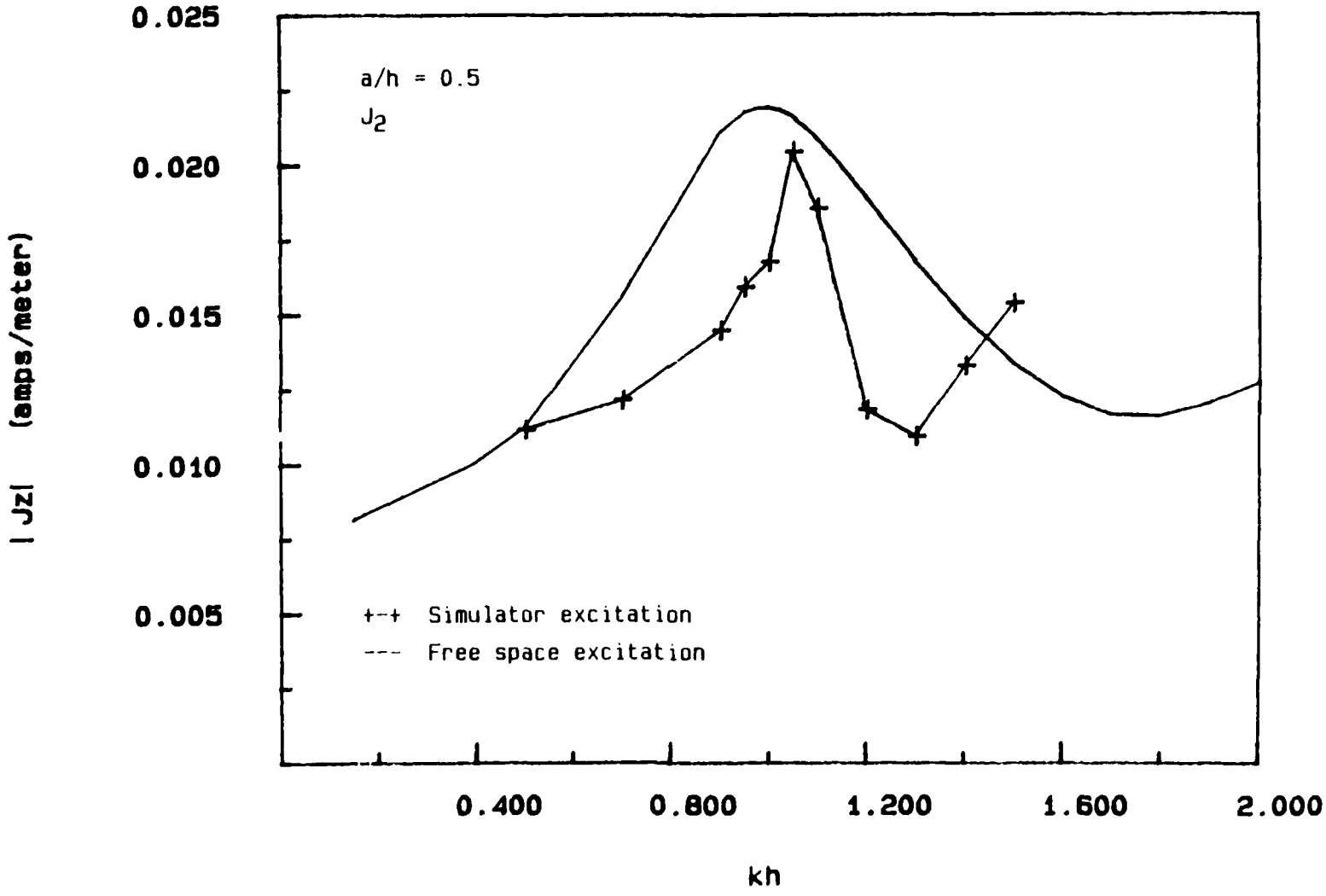

(b) Computed at h/2; a/h = 0.5.

Figure 47. (Cont'd).

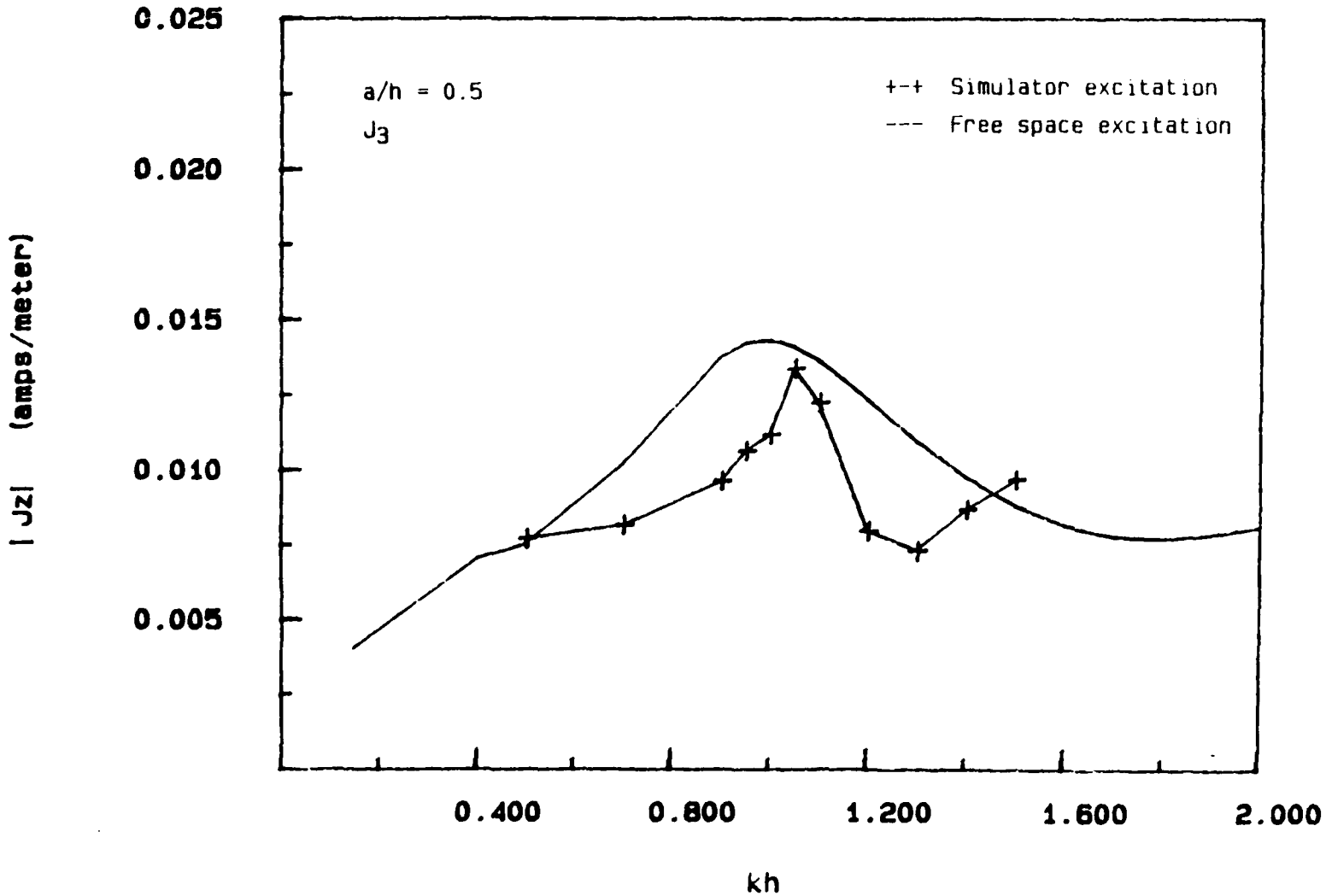

(c) Computed at 5h/6; a/h = 0.5.

Figure 47. (Cont'd).

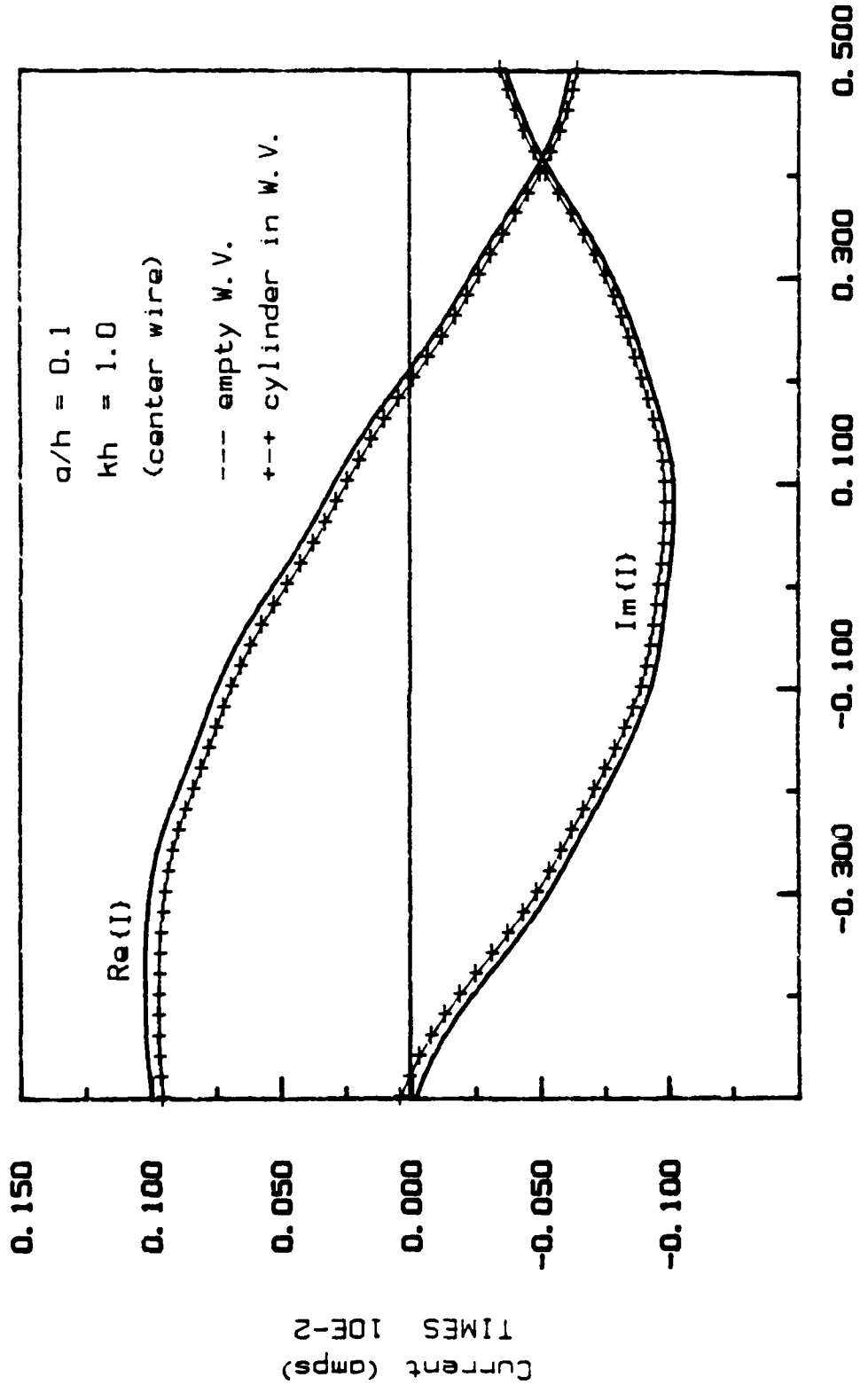

(a) Computed along the center wire (x = 0.076 m).

Figure 48. Currents computed on the surface of the conducting plates of the EMP simulator in the parallel-plate region: For an empty working volume, and with the cylinder in the working volume (a/h = 0.1, kh = 1.0).

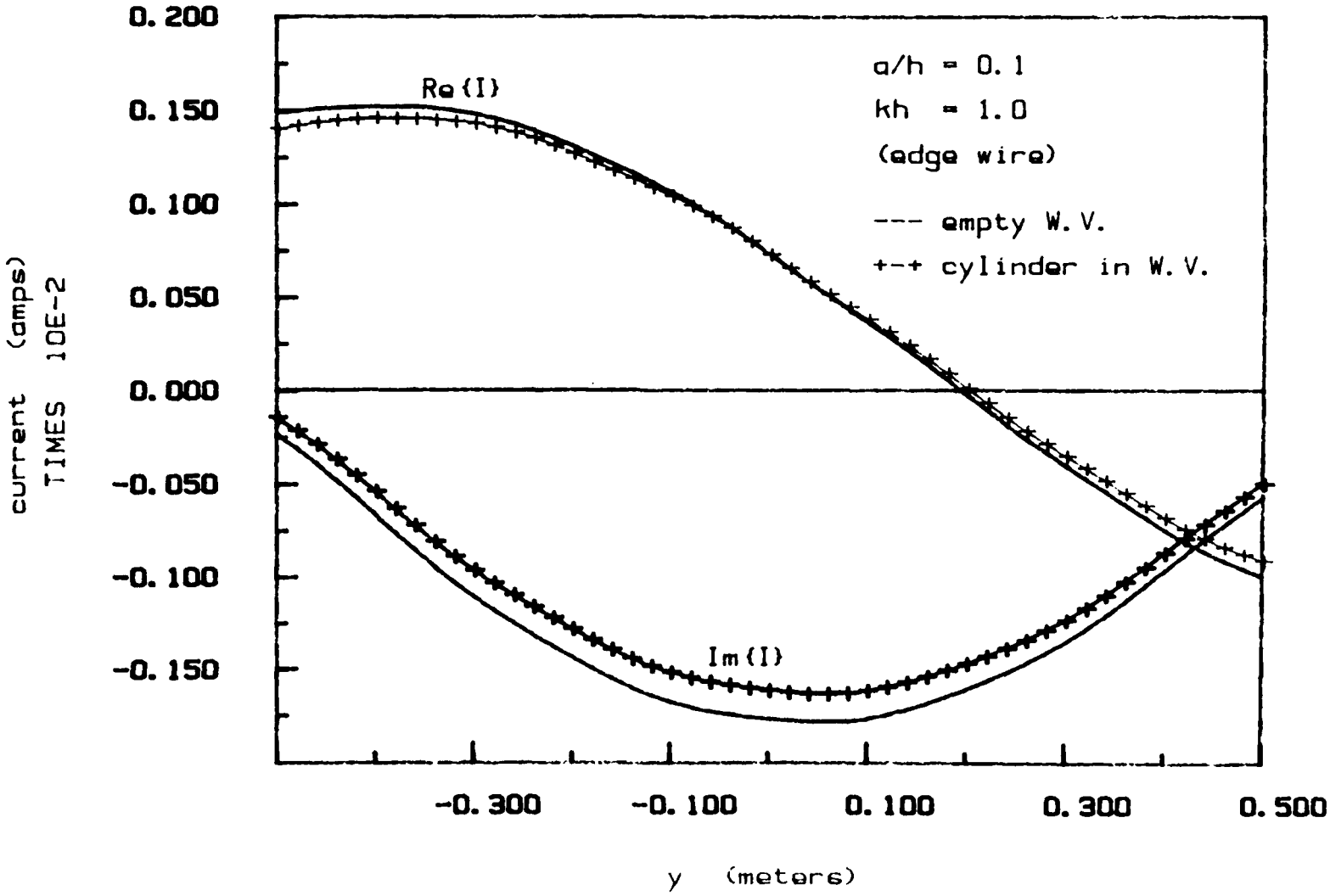

(b) Computed along the edge wire (x = 0.076 meters).

Figure 48. (Cont'd).

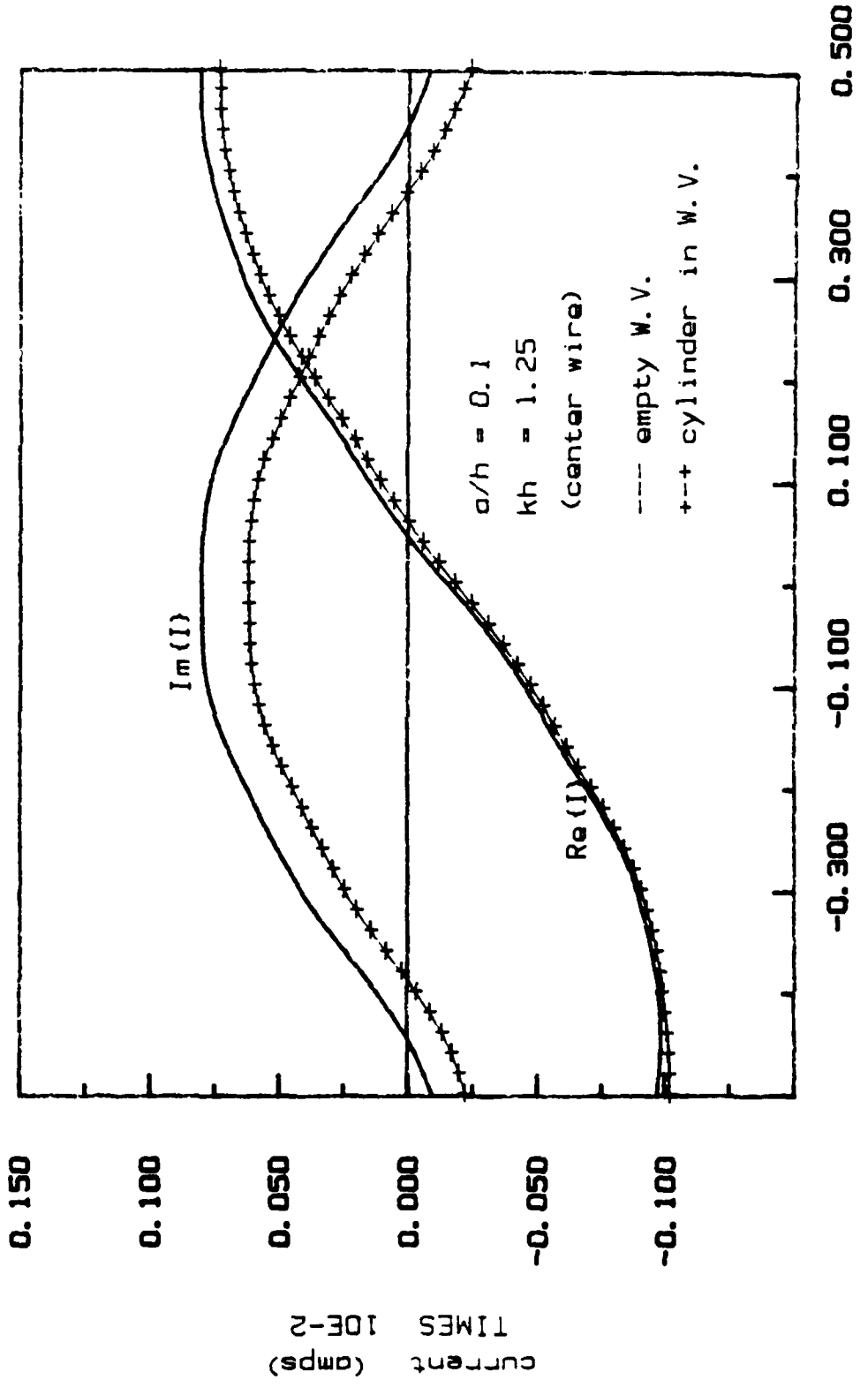

(a) Computed along the center wire (x = 0.076 m).

Figure 49. Currents computed on the surface of the conducting plates of the EMP simulator in the parallel-plate region: for an empty working volume, and with the cylinder in the working volume (a/h = 0.1, kh = 1.25).

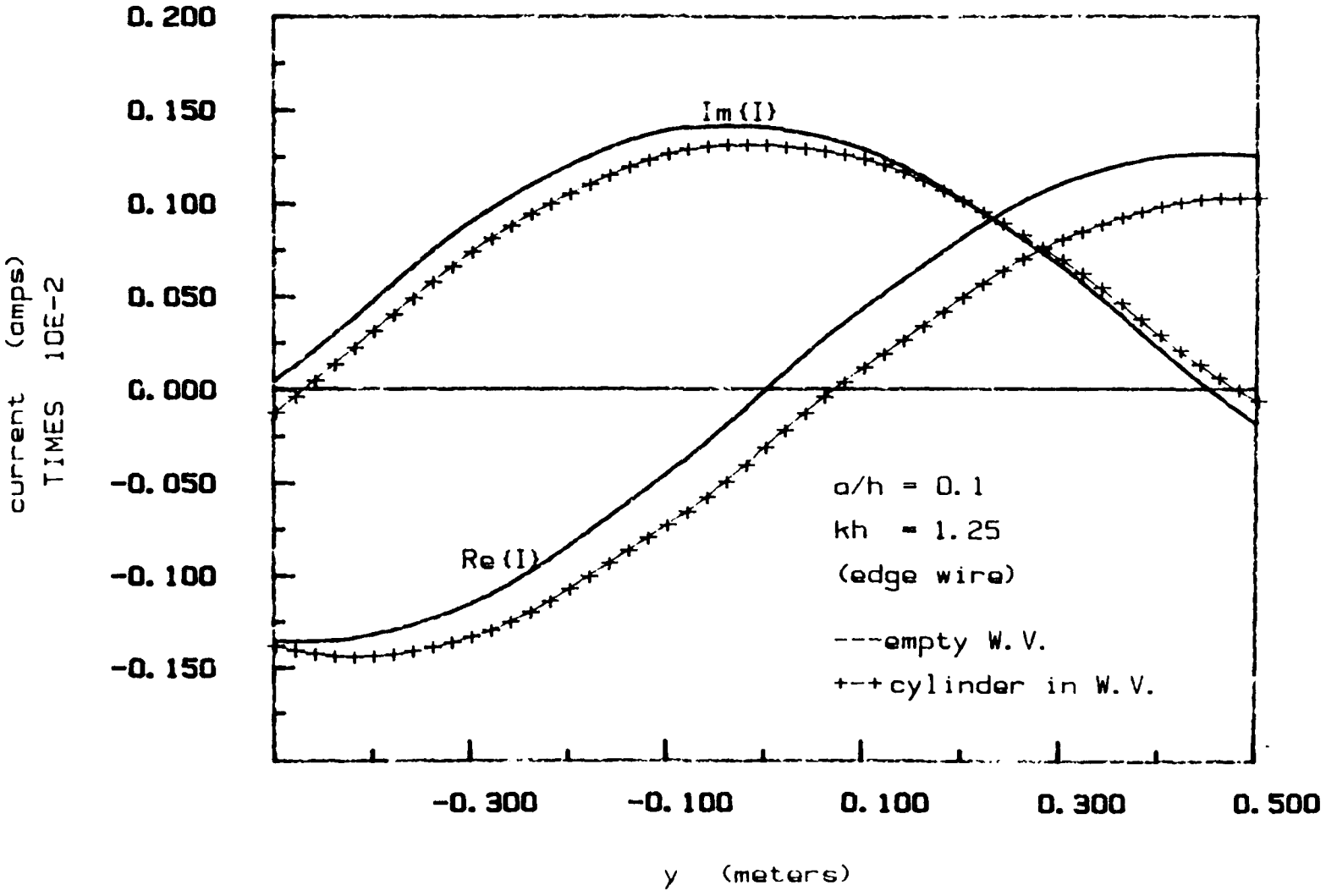

(b) Computed along the edge wire (x = 0.076 meters).

Figure 49. (Cont'd).

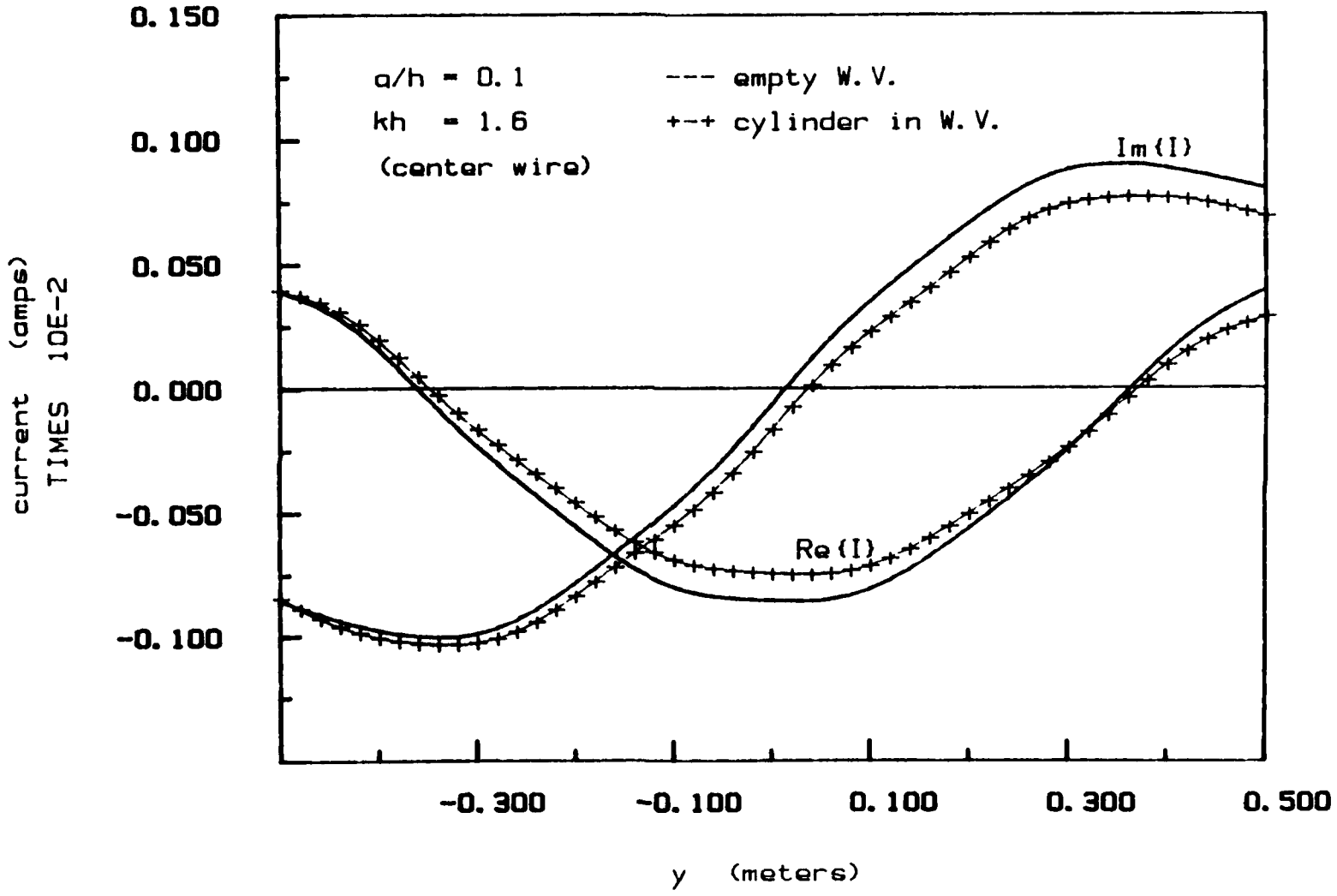

(a) Computed along the center wire (x = 0.076 meters).

Figure 50. Currents computed on the surface of the conducting plates of the EMP simulator in the parallel-plate region: for an empty working volume, and with the cylinder in the working volume (a/h = 0.1, kh = 1.6).

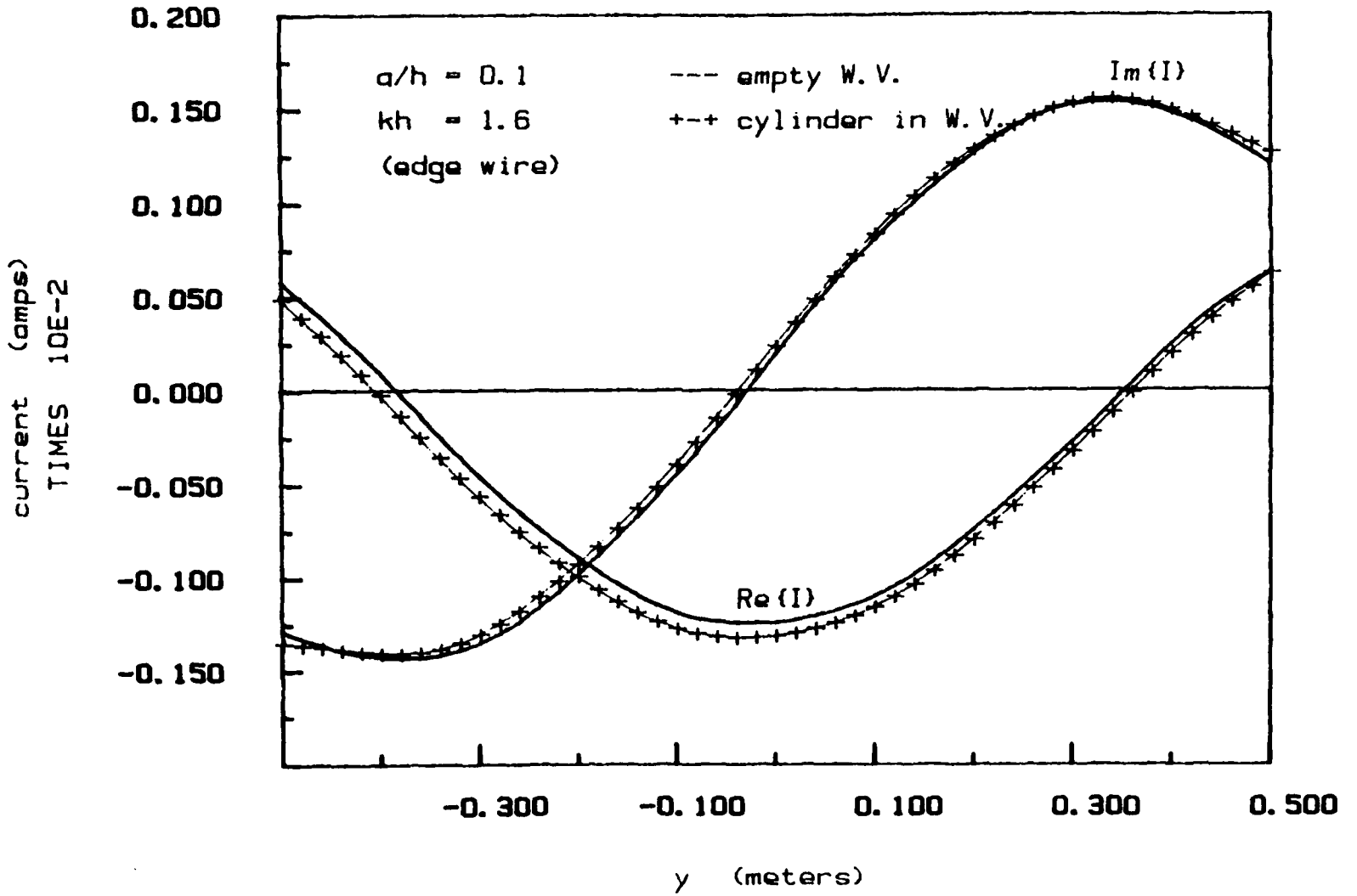

(b) Computed along the edge wire (x = 0.076 meters).

Figure 50. (Cont'd).

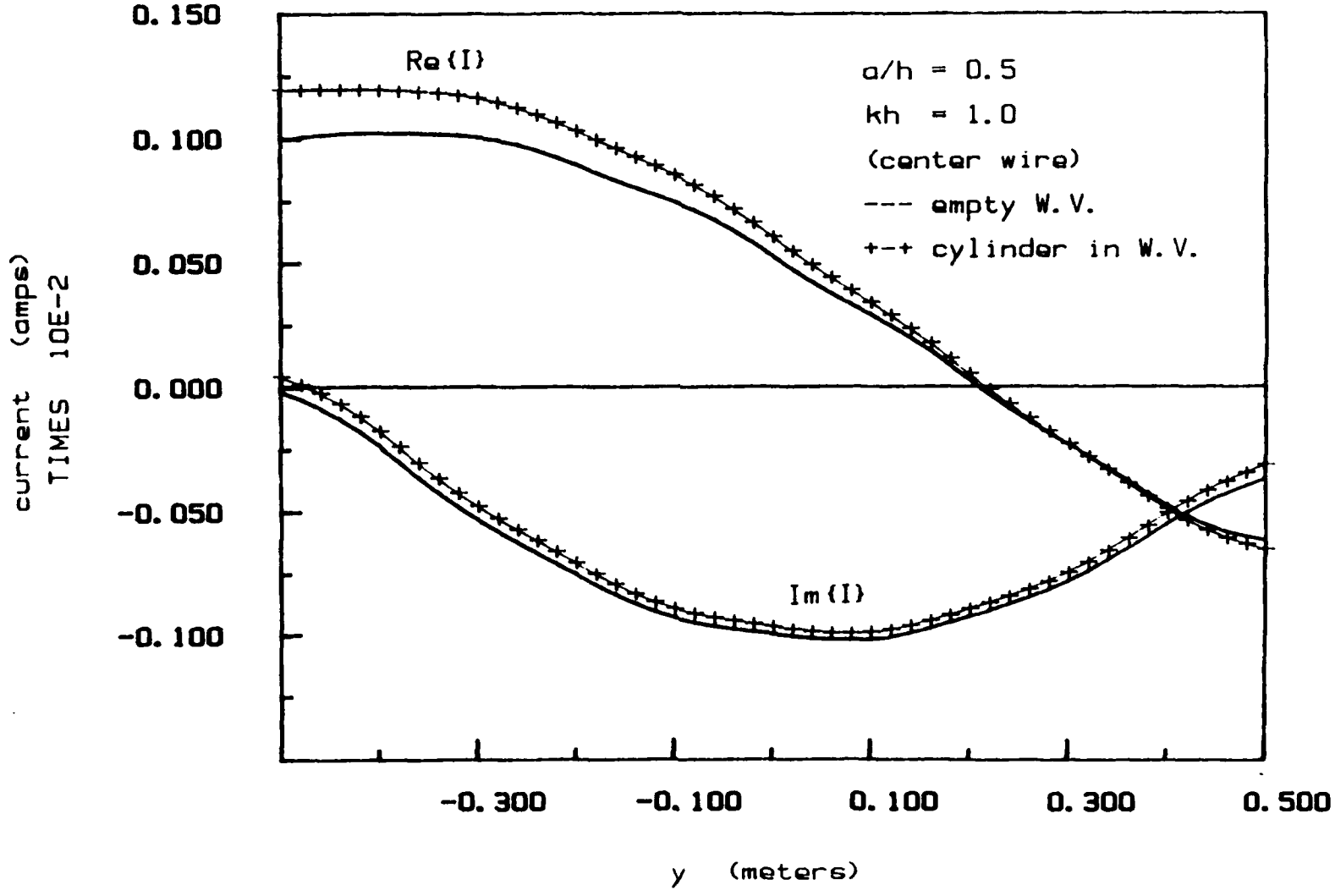

(a) Computed along the center wire (x = 0.076 m).

Figure 51. Currents computed on the surface of the conducting plates of the EMP simulator in the parallel-plate region: for an empty working volume, and with the cylinder in the working volume (a/h = 0.5, kh = 1.0).

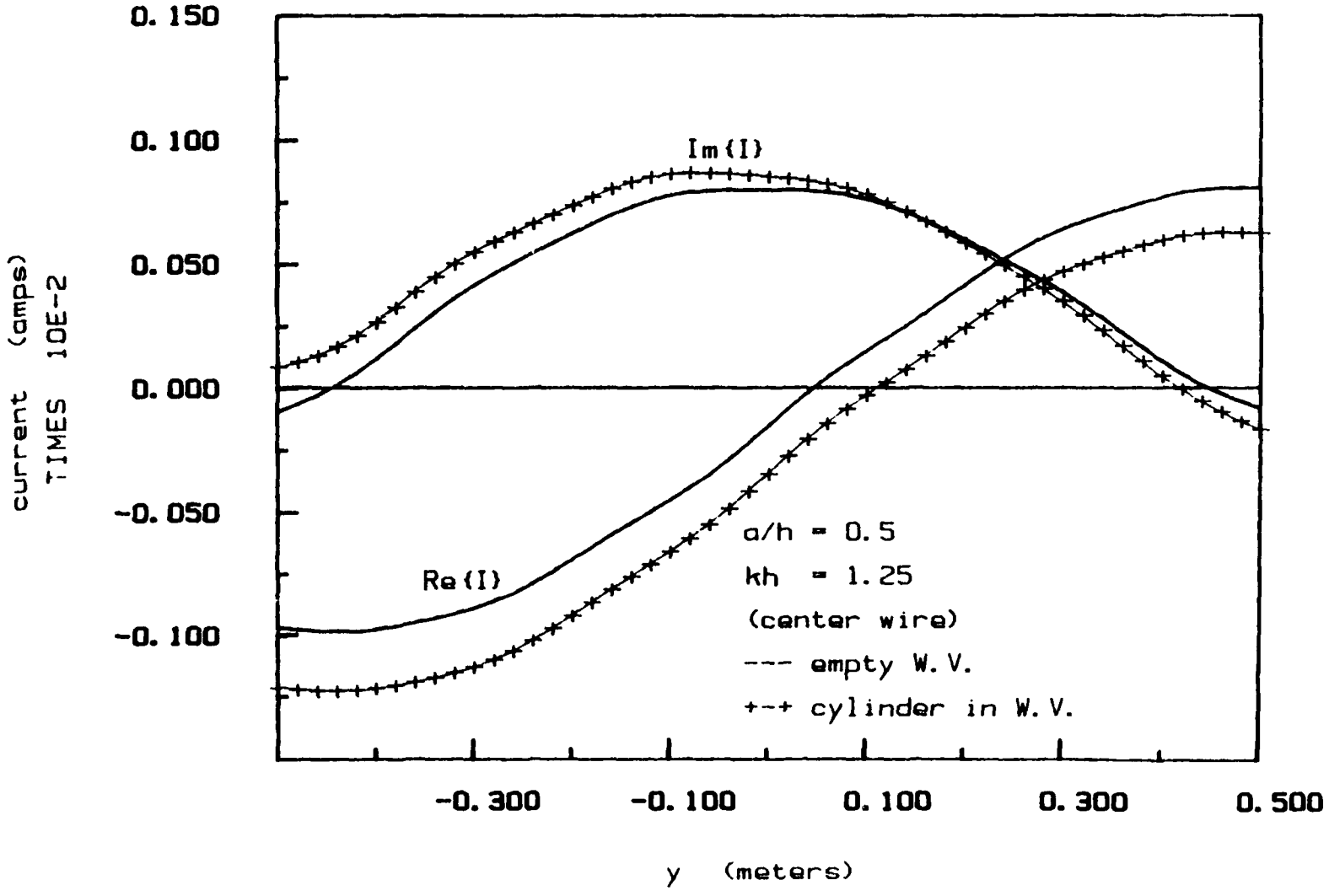

(a) Computed along the center wire (x = 0.076 m).

Figure 52. *Currents computed on the surface of the conducting plates of the EMP simulator in the parallel-plate region: for an empty working volume, and with the cylinder in the working volume (a/h = 0.5, kh = 1.25).*

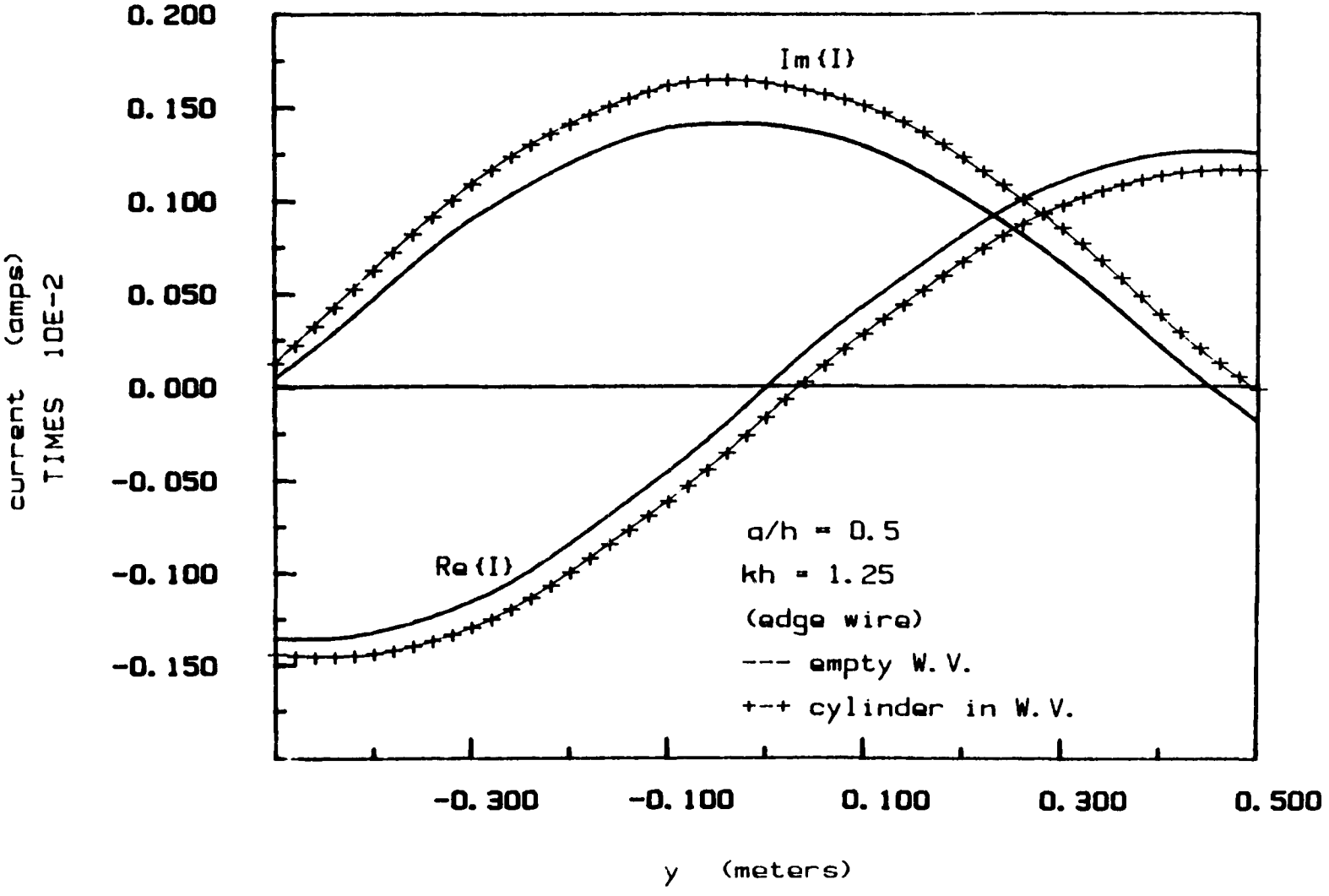

(b) Computed along the edge wire (x = 0.076 meters).

Figure 52. (Cont'd).

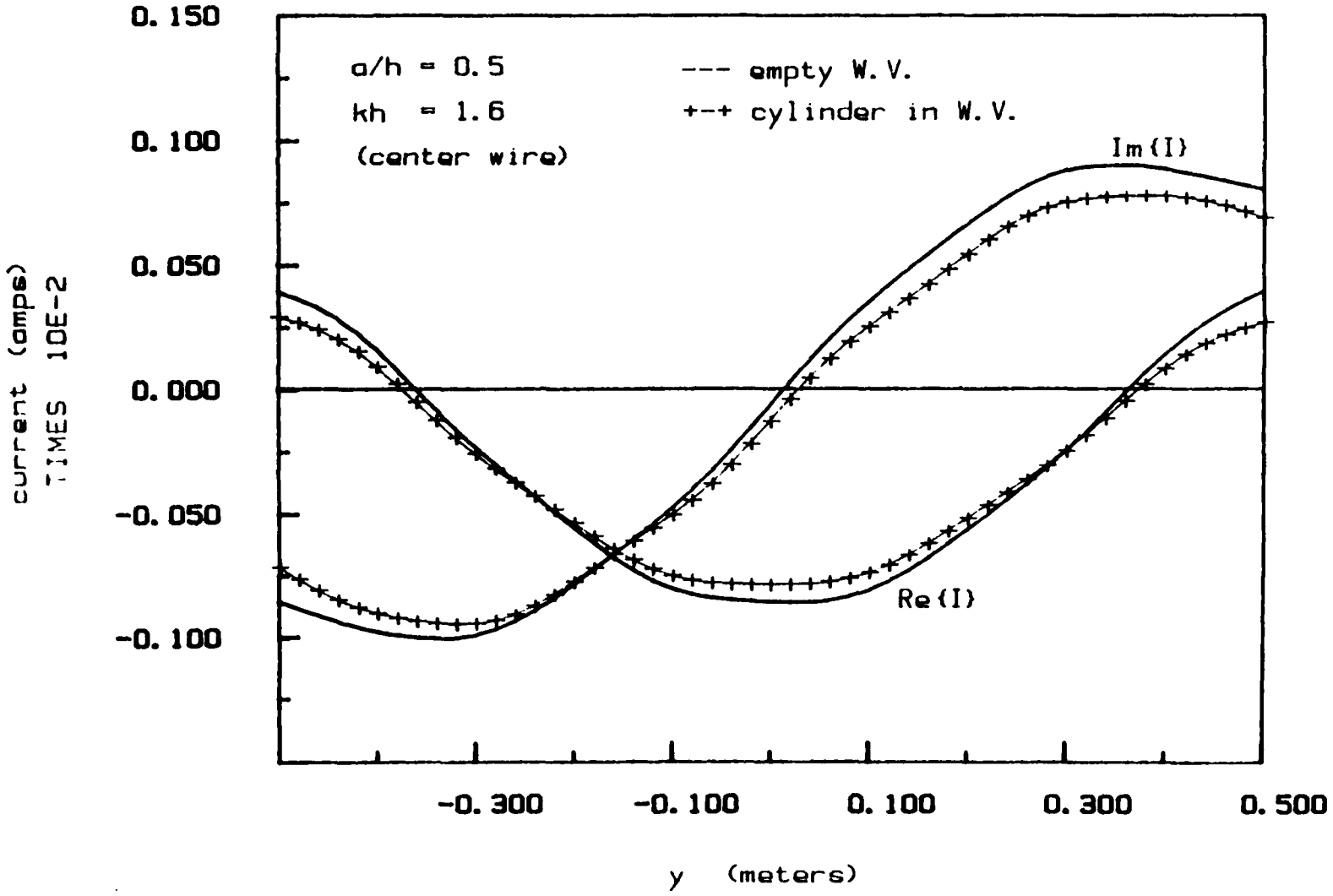

(a) Computed along the center wire (x = 0.076 m).

Figure 53. Currents computed on the surface of the conducting plates of the EMP simulator in the parallel-plate region: for an empty working volume, and with the cylinder in the working volume (a/h = 0.5, kh = 1.6).

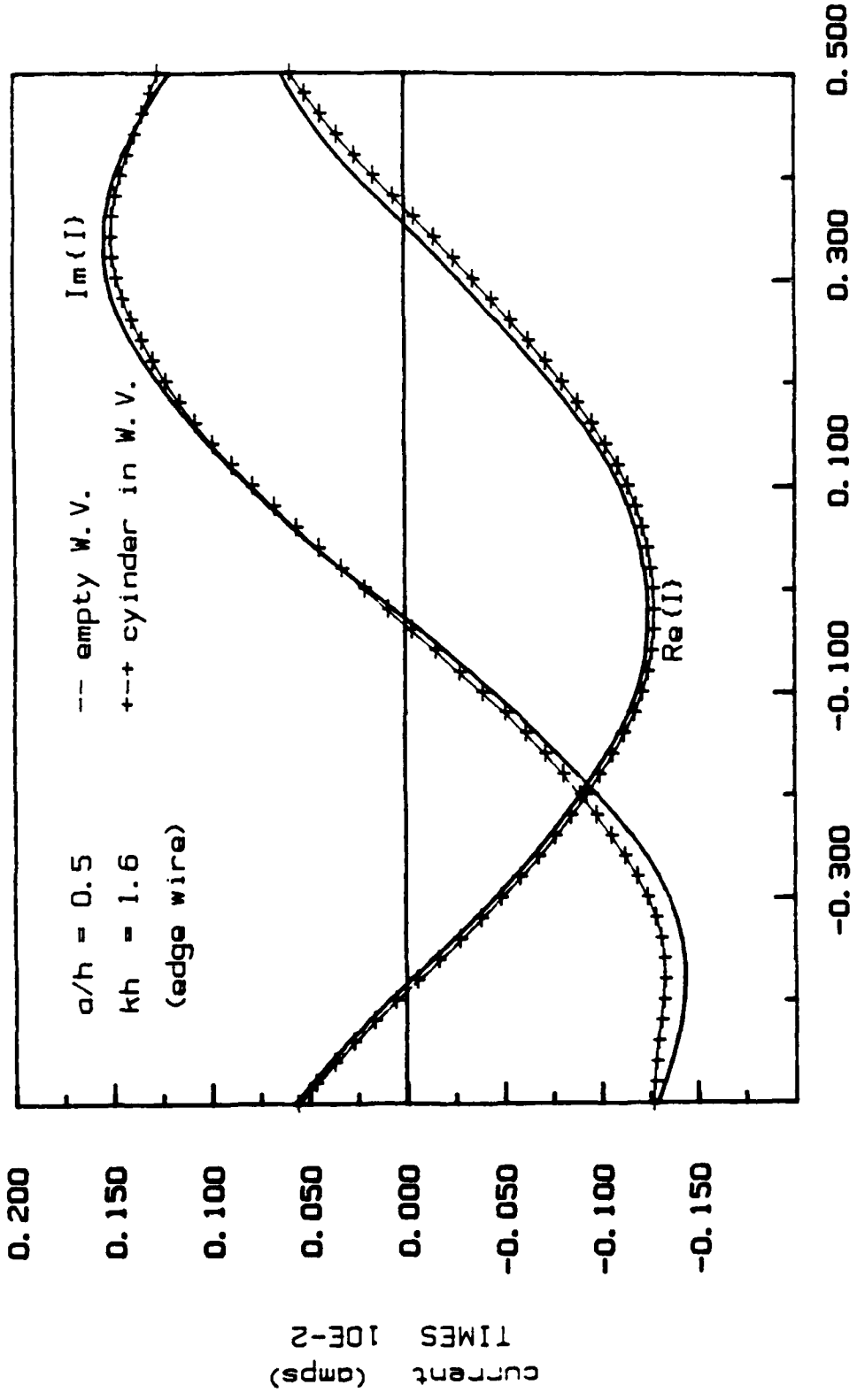

(b) Computed along the edge wire (x = 0.076 meters).

Figure 53. (Cont'd).

5 SUMMARY AND CONCLUSIONS

This study has analyzed the parallel-plate bounded-wave EMP simulator using a dynamic field solution. The parallel-plate simulator consists of a finite-width parallel-plate waveguide that is excited and terminated by conical tapered end-sections. The conducting surfaces of the simulator were modeled by a thin-wire mesh approximation. The NEC was used to solve for the currents induced on the wire mesh due to a continuous wave excitation across the source gap. These results were used to establish the characteristics of the simulator over a broad frequency region. The field distribution within the parallel-plate region was computed and shown to be predominantly TEM with a linearly progressive phase-shift for low frequencies. In the mid-frequency region, where the plate separation becomes comparable to a wavelength, higher order TE and TM modes will propagate. Energy is coupled into these modes due to the mismatch encountered by the quasi-spherical wavefront supported by the conical tapered waveguide when launched into the parallel-plate region, which supports a planar wavefront. The existence of these higher order modes deteriorates the uniformity of the desired field distribution. The deterioration of the uniformity becomes significant near the upper frequency limit of the "simulator bandwidth."

When a test object is placed within the simulator, there will be an interaction between them. If this "simulator-obstacle" interaction is significant, the currents measured experimentally could differ greatly from those produced by an actual EMP exposure. An investigation of the mechanisms contributing to the simulator-obstacle interaction revealed that the interaction was primarily a function of: (1) mutual coupling, (2) field fringing, and (3) multiple reflections. A numerical model was devised to analyse this problem using a thin-wire mesh approximation of the conducting surfaces of the parallel-plate simulator and the obstacle. The currents induced on a cylindrical tube were presented and compared to the currents induced on the cylinder when illuminated by a TEM plane wave in free space. The tube was placed perpendicularly to the plates and the largest deviation of currents occurred near the lowest resonant frequency of the cylinder. At higher frequencies, other deviations in the currents were also noted. This was primarly due to nonuniformities in the fields produced by the presence of propagating higher order modes.

The end-sections of the simulator must be gradually tapered so that the simulator has a bandwidth large enough to support the highest frequency component of the transient pulse excitation. Moreover the dimensions of the parallel-plate region must be large enough to support the desired test objects with very little electromagnetic interaction. The largest interaction will be due to mutual coupling between the test object and the parallel-plate waveguide. If the plate separation is chosen such that the ratio of the height of the object to the plate separation is less than 40 percent, the mutual coupling will be negligible. It is also extremely important to maximize the distance between the object and the parallel-plates and/or the ground plane (in an asymmetric case). Nevertheless, it was illustrated that there will be some deviations in the desired response due to nonuniformities in the fields and multiple reflections.

REFERENCES

Baum, Carl E., *A Sloped Admittance Sheet Plus Coplanar Conducting Flanges as a Matched Termination of a Two-Dimensional Parallel-Plate Transmission Line*, Sensor and Simulation Note 95 (Air Force Weapons Laboratory, Kirtland AFB, Albuquerque, NM, 31 December 1969).

Baum, Carl E.,*The Conical Transmission Line as a Wave Launcher and Terminator for a Cylindrical Transmission Line,"* Sensor and Simulation Note 31 (Air Force Weapons Laboratory, 16 January 1967).

Baum, Carl E., "EMP Simulators for Various Types of Nuclear EMP Environments: An Interim Categorization," *IEEE Transactions on Antennas and Propagation*, vol. AP-27 (January 1978), pp. 35-53.

Baum, Carl E., *General Principles for the Design of Atlas I and II, Part III: Additional Considerations for the Design of the Terminations*, Sensor and Simulation Note 145 (Air Force Weapons Laboratory, 3 January 1972).

Baum, Carl E., *Impedance and Field Distributions for Parallel-Plate Transmission Line Simulators*, Sensor and Simulation Note 21 (Air Force Weapons Laboratory, 6 June 1966).

†Baum, Carl E., *Singularity Expansion of Electromagnetic Fields and Potentials Radiated From Antennas or Scattered From Objects in Free Space*, Sensor and Simulation Note 179 (Air Force Weapons Laboratory, May 1973).

Baum, Carl E., D.V. Giri, and R.D. Gonzalez, *Electromagnetic Field Distribution of the TEM Mode in a Symmetrical Two-Parallel-Plate Transmission Line*, Sensor and Simulation Note 219 (Air Force Weapons Laboratory, 1 April 1976).

Brown, T.L., and K.D. Granszow, *A Parameter Study of Two Parallel-Plate Transmission Line Simulators of EMP Sensor and Simulation Note 21*, Sensor and Simulation Note 52 (Air Force Weapons Laboratory, 19 April 1968).

Burke, G.J., and A.J. Poggio, *Numerical Electromagnetics Code (NEC) – Method of Moments*, Technical Document 116, vols. I and II (Naval Ocean Systems Center [NOSC], San Diego, CA, January 1981).

Chen, K., CAPT G. Michaelidis, Carl E. Baum, and D.V. Giri, *ACHATES Design*, ACHATES Memo 1 (Air Force Weapons Laboratory, 5 November 1976).

†Cho, Soon K., and Chiao-Min Chu, *A Parametric Study of Circular Cylinder Within Two Parallel Plates of Finite Width*, Sensor and Simulation Note 174 (Air Force Weapons Laboratory, January 1973).

†Reference sources specifically dealing with simulator-test object interaction are marked with a dagger.

REFERENCES (Cont'd)

Gedney, Stephen D., *A Dynamic Analysis of the Parallel-Plate EMP Simulator Using a Wire Mesh Approximation and the Numerical Electromagnetics Code*, Technical Manuscript M-87/15/ADA-187535 (U.S. Army Construction Engineering Research Laboratory [USACERL], September 1987).

Giri, D.V., et al., *Experimental Investigations Into Higher-Order Mode Effects and Simulator-Object Interaction in Parallel-Plate Transmission-Line Geometries*, Miscellaneous Simulator Memo 11 (Air Force Weapons Laboratory, May 1977).

Giri, D.V., T.K. Liu, F.M. Tesche, and R.W.P. King, *Parallel-Plate Transmission Line Type of EMP Simulators: A Systematic Review and Recommendations*, Sensor and Simulation Note 261 (Air Force Weapons Laboratory, 1 April 1980).

Itoh, T., and R. Mittra, *Analysis of Modes in a Finite-Width Parallel-Plate Waveguide*, Sensor and Simulation Note 208 (Air Force Weapons Laboratory, January 1975).

King, R.W.P., and D.J. Blejer, "The Electromagnetic Field in an EMP Simulator at High Frequency," *IEEE Transactions on Electromagnetic Compatibility*, vol. EMC-21 (August 1979), pp. 263-269.

Krichevsky, V., *Source Excitation of an Open, Parallel-Plate Waveguide, Numerical Results*, Sensor and Simulation Note 254 (Air Force Weapons Laboratory, August 1978).

Lam, J., *Excitation of the Parallel-Plate Section of a Bounded-Wave EMP Simulator by a Conical Transmission Line*, Sensor and Simulation Note 263 (Air Force Weapons Laboratory, 31 May 1979).

†Latham, R.W., *Interaction Between a Cylindrical Test Body and a Parallel-Plate Simulator*, Sensor and Simulation Note 55 (Air Force Weapons Laboratory, November 1976).

†Latham, R.W., and K.S.H. Lee, *Electromagnetic Interaction Between a Cylindrical Post and a Two-Parallel-Plate Simulator, I*, Sensor and Simulation Note 111 (Air Force Weapons Laboratory, July 1970).

†Lee, K.S.H., *Electromagnetic Interaction Between a Cylindrical Post and a Two-Parallel-Plate Simulator, II (A Circular Hole in the Top Plate)*, Sensor and Simulation Note 121 (Air Force Weapons Laboratory, November 1970).

†Lee, K.S.H., *A Vertical Post Inside a Two-Parallel-Plate Simulator*, Sensor and Simulation Note 139 (Air Force Weapons Laboratory, October 1971).

Longmire, C.L., "On the Electromagnetic Pulse Produced by Nuclear Explosions," *IEEE Transactions on Antennas and Propagation*, vol. AP-27 (January 1978), pp. 3-13.

Marcuvitz, N., *Waveguide Handbook* (McGraw-Hill, New York, 1951).

REFERENCES (Cont'd)

†Marin, Lennart, *Application of the Singularity Expansion Method to Scattering From Imperfectly Conducting Bodies and Perfectly Conducting Bodies Within a Parallel-Plate Region*, Sensor and Simulation Note 116 (Air Force Weapons Laboratory, June 1972).

†Marin, Lennart, *A Cylindrical Post Above a Perfectly Conducting Plate, II (Dynamic Case)*, Sensor and Simulation Note 136 (Air Force Weapons Laboratory, August 1971).

†Marin, Lennart, *A Cylindrical Post Above a Perfectly Conducting Plate, I (Static Case)*, Sensor and Simulation Note 134 (Air Force Weapons Laboratory, July 1971).

Marin, Lennart, *Modes on a Finite-Width, Parallel-Plate Simulator, II. Wide Plates*, Sensor and Simulation Note 223 (Air Force Weapons Laboratory, November 1977).

Marin, Lennart, *Modes on a Finite-Width, Parallel-Plate Simulator I. Narrow Plates*, Sensor and Simulation Note 201 (Air Force Weapons Laboratory, September 1974).

Marin, Lennert, and G.C. Lewis, Jr., *Modes on a Finite-Width Parallel-Plate Simulator III. Numerical Results for Modes on Wide Plates*, Sensor and Simulation Note 227 (Air Force Weapons Laboratory, September 1977).

Neureuther, A.R., G.J. Burke, E.K. Miller, and G.M. Pjerrou, "Resonance Region Scatterer Studies by a Rail Line Range," *IEEE Transactions on Antennas and Propagation*, vol. AP-19 (November 1971), pp. 789-792.

Pan, Wei-Yan, "An Experimental Investigation of the Distribution of Current and Charge Induced in a Tubular Conducting Cylinder by an Electromagnetic Pulse," *IEEE Transactions on Electromagnetic Compatibility*, vol. EMC-27 (May 1985), pp. 88-95.

Ricketts, L.W., J.E. Bridges, and J. Miletta, *EMP Radiation and Protective Techniques* (John Wiley and Sons, New York, 1976).

Rushdi, A.M., R.C. Menendez, R. Mittra, and S.W. Lee, "Leaky Modes in Parallel-Plate EMP Simulators," *IEEE Transactions on Electromagnetic Compatibility*, vol. EMC-20 (August 1978), pp. 443-451.

Shen, H.M., and R.W.P. King, "Experimental Investigation of the Rhombic EMP Simulator: Comparison With Theory and Parallel-Plate Simulator," *IEEE Transactions on Electromagnetic Compatibility*, vol. EMC-24 (August 1982), pp. 349-355.

Shen, H.M., and R.W.P. King, "The Rhombic EMP Simulator," *IEEE Transactions on Electromagnetic Compatibility*, vol. EMC-24 (May 1982), pp. 255-265.

†Taylor, C.D., and G.A. Steigerwald, *On the Pulse Excitation of a Cylinder in a Parallel-Plate Waveguide*, Sensor and Simulation Note 99 (Air Force Weapons Laboratory, March 1970).

†Taylor, J.P., "Thin Wire Receiving Antenna in a Parallel-Plate Waveguide," *IEEE Transactions on Antennas and Propagation*, vol. AP-15 (July 1967), pp. 572-574.

REFERENCES (Cont'd)

[†]Tesche, F.M., *On the Behavior of Thin-Wire Scatterers and Antennas Arbitrarily Located Within a Parallel-Plate Region I (The Formulation)*, Sensor and Simulation Note 135 (Air Force Weapons Laboratory, August 1971).

[†]Tesche, F.M., "On the Behavior of Thin-Wire Antennas and Scatterers Arbitrarily Located Within a Parallel-Plate Region," *IEEE Transactions on Antennas and Propagation*, vol. AP-20 (July 1972), pp. 482-486.

[†]Tesche, F.M., "Transient Response of a Thin-Wire Antenna or Scatterer Near a Conducting Ground Plane," *IEEE Transactions on Antennas and Propagation*, vol. AP-22 (March 1974), pp. 352-355.

Tsao, C-H, E. Yung, and R. Mittra, *The Source Excitation of a Finite-Width Parallel-Plate Waveguide*, Sensor and Simulation Note 255 (Air Force Weapons Laboratory, February 1979).

[†]Varvatsis, A.D., and M.I. Sancer, *Electromagnetic Interaction Between a Perfectly Conducting Sphere and a Two-Parallel-Plate Simulator, I (Top Plate Removed)*, Sensor and Simulation Note 140 (Air Force Weapons Laboratory, October 1971).

Wright, David L., *Sloped Parallel Resistive Rod Terminations for Two-Dimensional Parallel-Plate Transmission Lines*, Sensor and Simulation Note 103 (Air Force Weapons Laboratory, 7 May 1970).

Yang, F.C., and K.S.H. Lee, *Impedance of a Two-Conical-Plate Transmission Line*, Sensor and Simulation Note 221 (Air Force Weapons Laboratory, November 1976).

Yang, F.C., and Lennert Marin, *Field Distributions of a Two-Conical-Plate and Curved Cylindrical-Plate Transmission Line*, Sensor and Simulation Note 229 (Air Force Weapons Laboratory, September 1977).

USACERL DISTRIBUTION

Chief of Engineers
ATTN: CEHEC-IM-LH (2)
ATTN: CEHEC-IM-LP (2)
ATTN: CEMP-EE
ATTN: CERD-L

CEHSC 22060
ATTN: CEHSC-PREP

US Army Engineer Districts
ATTN: Library (41)

US Army Engr Divisions
ATTN: Library (14)

DNA ATTN: NADS 20305

INSCOM - Ch, Instl. Div.
Vint Hill Farms Station 22186
ATTN: IAV-DEH
Arlington Hall Station 22212
ATTN: Engr & Hsg Div

SHAPE 09055
ATTN: Survivability Sect. CCB-OPS
ATTN: Infrastructure Branch, LANDA

Fort Belvoir, VA
ATTN: CECC-R 22060

US Army White Sands Missile Range 88002
ATTN: STEWS-TE-NO-EMP

ADEA Fort Lewis 98433
ATTN: AFVO-RA-EN

Natick R&D Ctr 01760
ATTN: STRNC-VE

Harry Diamond Labs 20783
ATTN: DELHD-NW-E
ATTN: DELHD-NW-EA
ATTN: DELHD-NW-EC
ATTN: DELHD-NW-ED
ATTN: DELHD-NW-EE

Naval Air Systems Command
ATTN: Library

Hanscom AFB 01731
ATTN: HQ AFSC
ATTN: ESDA/AVMS

Kirtland AFB 01731
ATTN: AFWL/DES
ATTN: AFWL/DYC
ATTN: AFWL/NTCA

Wright-Patterson AFB 45433
ATTN: ASD/ENAMA
ATTN: AFWAL/MILSE

Naval Civil Engr Lab
ATTN: Library 93041
ATTN: Code L08A
ATTN: Code L72
ATTN: Code L33

Naval Sea Systems Command
ATTN: PMS-423

USACC Ft Huachuca 85613
ATTN: USAI SEIC AT ASBI-SST

Defense Nuclear Agency
ATTN: DNA-RAEE
ATTN: DNA-RAEV

Tyndall AFB, FL 32403
AFESC/Engineering & Service Lab

Nat'l Institute of Standards & Tech 20899

US Government Printing Office 20401
Receiving/Depository Section (2)

Defense Technical Info. Center 22304
ATTN: DTIC-FAB (2)